Stony Brook University

NMR Investigation of Organic Phosphorus in Calcite

A Thesis Presented

by

Zelong Zhang

to

The Graduate School

in Partial Fulfillment of the

Requirements

for the Degree of

Master of Science

in

GEOSCIENCES

Stony Brook University

May 2014

Stony Brook University

The Graduate School

Zelong Zhang

We, the thesis committee for the above candidate for the

Master of Science degree, hereby recommend

acceptance of this thesis.

Dr. Brian. L. Phillips – Thesis Advisor
Professor, Department of Geosciences

Dr. Troy Rasbury – Chairperson of Defense
Associate Professor, Department of Geosciences

Dr. Richard J. Reeder
Professor, Department of Geosciences

This thesis is accepted by the Graduate School

Charles Taber
Dean of the Graduate School

Abstract of the Thesis

NMR Investigation of Organic Phosphorus in Calcite

by

ZELONG ZHANG

Master of Science

in

GEOSCIENCES

Stony Brook University

2014

The interaction between calcite and dissolved organic phosphate is important to biomineral and geochemical systems. Organic molecules and phosphates can be adsorbed to the calcite surface and incorporated as impurities in the matrix during crystal growth. Although ^{31}P NMR spectroscopy has been extensively used to study the nature of P in a wide variety of natural samples, a lack of understanding of spectroscopic characteristics of organic P occluded in calcite hinders NMR application in this area. Here, a methodology based on ^{31}P NMR is proposed to help determine the speciation of P at low concentrations in calcite based on spectroscopic characteristics of organophosphoesters coprecipitated with calcite, and succeeded in characterizing the organic P occluded in a natural calcite sample, calcitic moonmilk.

By dissolving in the ^{13}C-enriched carbonate (anion) syringe an amount sufficient to yield a Ca:P ratio of approximately 1000:1, we succeeded in coprecipitating various phosphoesters (e.g. monoesters and diesters) with calcite in seeded constant-rate-of-addition experiment. ^{31}P NMR experiments such as $^{31}P\{^{1}H\}$ CP/MAS (cross polarization under magic-angle spinning condition) and $^{1}H\rightarrow^{31}P\{^{13}C\}$ CP/ REDOR (rotation-echo double resonance) were carried out to study the chemical environment of phosphorus in the coprecipitate samples. In all cases, we find minor differences in the $^{31}P\{^{1}H\}$ CP NMR spectra between the organic phosphates and their corresponding coprecipitates, demonstrating that the molecules remain intact during precipitation. Detailed analysis of the chemical shift and chemical shift anisotropy ($\Delta\delta$) revealed systematic differences among the coprecipitates. None of the coprecipitate chemical shifts overlap that for inorganic orthophosphate coprecipitated with calcite. The differences in $\Delta\delta$ values can differentiate monoester from diester in coprecipitates based on whether $\Delta\delta$ exhibits a positive or negative value, which can be easily recognized in the SSB pattern. For monoesters,

compared to the first SSB(+) on the left side of central band, the intensity of the first SSB(−) on the right side is larger for each monoester coprecipitate and smaller for each diester coprecipitate. $^{31}P\{^{13}C\}$ REDOR experiments of all coprecipitates exhibit strong dephasing signal, demonstrating multiple $^{31}P - ^{13}C$ pairs within about 4 Å distances and hence that these P-esters are occluded in the calcite structure. The ^{31}P NMR spectra present here reveal significant differences (e.g. chemical shift, chemical shift anisotropy, spinning sidebands) between different phosphate esters occlude in calcite structure, providing a spectroscopic method to determine the speciation of phosphorus at low-concentration in carbonate minerals.

Moonmilk samples obtained from cave Coel Zel à, Italy were bleached to remove extra-crystalline organic matter. CP/MAS (cross polarization under magic angle spinning conditions) was exclusively applied to obtain the NMR signals of ^{31}P and ^{13}C from these moonmilk samples, considering the anticipated low concentration of P in moonmilk and low abundance of ^{13}C in nature. XRD revealed that these moonmilk samples are composed dominantly of calcite. ^{31}P spectra of moonmilk samples significantly resembles that of a well characterized stalagmite calcite and orthophosphate/calcite coprecipitate, which suggests that the main P content is inorganic and present as structural defects. The dominant peak ($\delta_{P\text{-}31}$=3.45 ppm) is somewhat larger in peak width (FWHM about 5.2 ppm) and value of the chemical shift anisotropy ($\Delta\delta$ around −40 ppm) than that of orthophosphate defect, indicating that the inorganic P appears to be non-protonated and structurally distorted. Detailed analysis revealed that a small ^{31}P resonance $\delta_{P\text{-}31}$ at −2.0 ppm exhibits significant spinning sideband effect, which can be attributed to organic phosphate. Substantial ^{13}C resonances from carbon-bearing groups other than calcite carbonate confirms that these moonmilk samples contain organic matter, mainly fatty acids. Taken together, ^{31}P and ^{13}C CP/MAS reveal that rich organic matter, minor inorganic phosphate, and trace amount of organophosphate present in the moonmilk calcite as structural defects. Most significantly, even though the P speciation in moonmilk closely resembles stalagmite calcite, monetite is absent in moonmilk due to the Ca^{2+} deficiency caused by organic compounds.

This study demonstrates the advantage of using solid-state NMR spectroscopy in characterizing organic phosphates in calcite mineral particular at low phosphorus concentrations, and provides a valuable methodology and data that complement previous studies on carbonate minerals and biomineralization.

Table of Contents

List of Figures

List of Tables

List of Abbreviations

2D: Two-dimensional

ACC: Amorphous Calcium Carbonate

ADC: Analog to Digital Converter

CP: Cross Polarization

CP/MAS: Cross Polarization/ Magic-angle Spinning technique

CP/REDOR: Cross Polarization/ Rotational-echo Double-resonance

CSA: Chemical Shift Anisotropy

BET: Brunauer–Emmett–Teller

DCP: Dicalcium Phosphate

DGA: 2,3-Diphospho-D-glyceric Acid Pentasodium Salt

DGP: D-(−)-3-Phosphoglyceric Acid Disodium Salt

EDTPH: Ethylenediamine - N, N, N', N'- tetrakis (methylenephopshonic acid)

FWHM: Full Width at Half Maximum

FID: Free Induction Decay

FT-IR: Fourier Transform Infrared Spectroscopy

GPA: β-Glycerol Phosphate Disodium Salt Pentahydrate

HetCor: Heteronuclear Correction

IHP: Myo-inositol Hexaphosphate

LTA: Lipoteichoic Acid

NMR: Nuclear Magnetic Resonance

o.d.: Outside Diameter

OrthoP: Orthophosphate

PGA: D-(−)-3-Phosphoglyceric Acid Disodium Salt

PPA: Phosphoenolpyruvic Acid Trisodium Salt Heptahydrate

ppm: Parts Per Million

REDOR: Rotational-Echo Double-Resonance

SEM/EDX: Scanning Electron Microscopy/ Energy Dispersive X-ray Spectroscopy

SP: Single Pulse

SSB: Spinning Sideband

UV-Vis: Ultraviolet–visible spectroscopy

Acknowledgments

Many people have in some way contributed to this thesis, including my family members, faculty in the Department of Geosciences, my colleagues, and my friends. I thank them for their advice and support.

First, I would like to thank Professor Brian L. Phillips for being my advisor and providing significant support throughout my research work and thesis preparation. His advice has gone beyond the limit of academia and influence many other aspects of my life. Meanwhile, I would like to thank my supportive wife. Without her encouragement, I would never have been able to spend hours on writing each day. I also want to thank Dr. Andrew Ilott for his assistance with NMR instrumentation in Chemistry Building, and Dr. James Marecek for his maintenance of NMR facilities. Many thanks go to Dr. Yan-Yan Hu, Dr. Olivera Zivkovic, and other members of the research group lead by Professor Clare P. Grey in Department of Chemistry for sharing their NMR experience. All these people have helped enrich my research experience in ways I could never have imagined. In addition, moonmilk samples and the site information in my study are provided by Dr. Silvia Frisia and Dr. Andrea Borsato. XRD data of moonmilk are collected by my fellow, John Vaughn. Professor Martin Schoonen offered the access to his laboratory facilities, allowing me to perform BET and UV-Vis analysis. I would like to acknowledge all the students working in the laboratories of geosciences. They provide me with technical help, as well as much-needed breaks from the technical work.

And finally, I would like to thank everyone in the Department of Geosciences in Stony Brook University for their work and support on my study.

I. Introduction: Interaction between Phosphate and Calcite

1.1 Phosphate and Calcite

The interaction between phosphate and calcite mineral is important to biomineralization and low temperature geochemical processes. Phosphate is an essential nutrient for life and often the limiting nutrient in nature. Calcite is a common biomineral and a geologically abundant mineral especially in low temperature settings such as spelethoms in karst caves. Phosphate can be strongly bonded to the calcite surface (Geffroy et al., 1999) and incorporated as an impurity in the matrix during crystal growth(Geffroy et al., 1999; Mason et al., 2007). It is also widely studied that phosphate can inhibit the crystal growth of calcite (Dekanel and Morse, 1978; Freeman and Rowell, 1981; Giannimaras and Koutsoukos, 1987; Griffin and Jurinak, 1974; House and Donaldson, 1986; Kamiya et al., 2004; So et al., 2011, 2012; Suzuki et al., 1986). Phosphate content of calcite can reveal valuable information regarding the conditions present during formation of calcite, such as the seasonality of calcite precipitation (Huang et al., 2001). Although it is possible to measure P-content of calcite at high spatial resolution (Baldini et al., 2007; Borsato et al., 2007; Fairchild et al., 2001; Frisia et al., 2012; Garcia-Anton et al., 2011; Huang et al., 2001; Mason et al., 2007a; Pogson et al., 2011; Treble et al., 2005), it is difficult to determine the nature of P, which could be present in several different forms such as inorganic orthophosphates, organic phosphates, and other phosphate minerals. To use P content as a paleoenvironmental indicator requires knowledge about the nature of the phosphorus. Therefore, it is important to develop methods to determine the form of P in the calcite, which is the purpose of this study.

1.1.1 Organic Phosphate Ester

Phosphorus is an essential element for life. Phosphodiesters link the mononucleotide units that enable the formation of the long chain of DNA (Deoxyribonucleic acid) and RNA (Ribonucleic acid), which store almost all the genetic information. Adenosine triphosphate (ATP) and its dephosphorylated adenosine diphosphate (ADP) are essential for metabolism. Their reversible conversion allows energy transportation within cells for metabolism. Hydroxylapatite, $Ca_{10}(PO_4)_6(OH)_2$, a phosphorus-rich mineral comprises almost 60% of bone and 70% of teeth of vertebrate animals (Smil, 2000). Phospholipids are a group of lipids that are a major component of cells as they form bilayers that constitute the membrane of almost all living organisms and many viruses (van Meer et al., 2008). Typically, phospholipids are composed of a phosphate group, two alcohols, and one or two fatty acids.

With an average concentration of 0.1 % by mass, phosphorus is the eleventh most abundant element in the Earth's crust (Klein et al., 1993). Elemental phosphorus, including white phosphorus and red phosphorus, has very high reactivity under normal conditions. Phosphorus can never be present in nature as a free element. It is present in inorganic forms within minerals and organic phosphate derivatives in rock and soils. Phosphorus in the crust primarily exists in calcium phosphate minerals and is usually present in poorly soluble forms. Apatite group

minerals, $Ca_5(PO_4)_3(F, Cl, OH)$, contain over 95% of the phosphorus in Earth's crust (Klein et al., 1993).

Phosphate is commonly a limiting nutrient in terrestrial systems. Only a small fraction of phosphate in the soil is readily available to plants. Soluble phosphates released from rock weathering can be rapidly turned into insoluble forms in soil (Khasawneh et al., 1980). The insoluble ferric and calcium phosphates in rocks and on mineral surfaces as adsorbates are the largest natural phosphate reservoirs in soils. Phosphate is also added to soil as artificial fertilizers. In addition, some phosphorus deposited in deep oceans is brought to soil cycle by tectonic uplift (Figure 1.1). The phosphorus distribution in soil is controlled by both geochemical and biological processes. The primary geochemical reservoir of phosphorus is supplied by the weathering of calcium phosphate minerals. Geochemical processes are determined by soil properties (resulting from pedogenesis of parent material) and local climate (Cross and Schlesinger, 1995). Biological communities, such as bacteria, fungi, and plants, affect the phosphorus distribution through microbial decomposition, immobilization, biomineralization, and subsequently plant uptake (Cross and Schlesinger, 1995).

In many aquatic systems, the scarcity of phosphate is even greater. The upward flowing of nutrients including phosphorus is restricted by the thermal stratification of water bodies which consist of a warm shallow surface layer (epilimnion) and cooler deep layers (hypolimnion) lying beneath. The phosphorus released from dead sinking phytoplankton can be recycled as much as the amount that bacteria are able to promptly decompose within the epilimnion. Although phosphorus recycling is rapid in aquatic system, phosphorus is often the limiting nutrient for biota. Accidental excessive P input can change water bodies first from oligotrophic (low nutrient level) to mesotrophic (moderate nutrient level) and eventually from mesotrophic to eutrophic (high nutrient level) or hypereutrophic (extremely high nutrient level).

In addition, there are significant anthropogenic interferences in the phosphorus cycle, which can be divided into three major categories. 1) Deforestation and urbanization accelerate erosion and runoff. 2) Traditional and modern agricultural farming utilizes fertilizer that contains soluble inorganic phosphate and recycles organic waste. 3) Human waste water such as sewage contains phosphate detergents is often untreated and can be released to the environment (Smil, 2000).

1.1.2 Calcite

Calcite is the most stable and predominate form of calcium carbonate mineral at ambient conditions. It is a typical constituent of the marine shell biomaterial (Schmahl et al., 2012) and sedimentary rocks. For example, limestone, mostly composed of the mineral calcite, is a sedimentary rock largely formed from the shells of deceased marine biota. In karst caves, it is present as stalagmites and stalactites. Due to its stability and predominance, calcite is particularly useful in paleoenvironment studies because it can contain several records such as oxygen and carbon isotopes, ratios of trace elements, and even biomarkers.

For biomineralization processes of calcite formation, there are two fundamentally different groups in terms of biological control factors of mineralization: biologically induced and biological controlled mineralization.

Biologically induced mineralization of calcite occurs as a result of interactions between bioactivities and environment. Bacteria often act as an agent for calcite nucleation and subsequent mineral growth. The biological system favors calcite precipitation in an indirect way through metabolic processes of the organism which mediates the pH, pCO_2, and composition of the environment. The biological system has little control in the composition and habit of calcite precipitated (Dove, 2003). Biologically induced calcite has been utilized in the remediation and prevention of concrete cracks and biogrout (Al-Thawadi, 2011; Barkouki et al., 2011; Chou et al., 2011; DeJong et al., 2006; DeJong et al., 2010; Rong et al., 2011; van Paassen et al., 2010; Whiffin et al., 2007) and possibly the sequestration of radionuclides and heavy metals (Curti, 1999; Fujita et al., 2004; Pingitore and Eastman, 1986; Zachara et al., 1991). The induced mineral precipitation binds the sands together by contact at particle level, which strengthens the stiffness of the soil. The particular precipitation process is called microbiologically induced calcite precipitation. It is a biogeochemical process within the soil matrix that surface bacteria catalyze the reaction network to induce calcium carbonate precipitation by acting as nucleation sites for calcite and by producing alkaline conditions which promote precipitation (Mortensen et al., 2011).

In biologically controlled mineralization of calcite, microbial activities direct the nucleation, growth, morphology, and location of the calcite deposited. Biologically controlled mineralization mostly occurs in an isolated environment. The processes of this type can be categorized by the location of mineralization site with respect to the causative cells such as extracellular, intercellular, and intracellular mineralization (Dove, 2003). One example of intercellular mineralization is found in calcareous algae. Calcareous algae nucleate and grow calcite with an orientation that is perpendicular to the cell surface, which eventually fill the intercellular space with calcite (Weiner and Dove, 2003). Intracellular mineralization was discovered in haptophyte algae. A single crystal of calcite is preassembled intracellularly into a coccolith structure, a unicellular exoskeleton of minute calcite plates, before passing the mature sheath through the cell membrane (Young and Henriksen, 2003). However, in some cases, mineral formation begins inside the cell and then proceeds outside.

1.1.3 Interaction between Phosphate and Calcite

The interaction between phosphate and calcite is important to many terrestrial and aquatic geochemical processes. For example, coprecipitation during seeded calcite crystallization and absorption on calcite surface can effectively remove phosphate in eutrophic waters and recover phosphate from waste waters (Gunawan et al., 2010; Karageorgiou et al., 2007; Liu et al., 2012; Song et al., 2006). Since phosphate can be adsorbed by calcite at a low concentration (Gunawan et al., 2010), typically <20 μmol/L (Liu et al., 2012), it is possible at low concentrations for phosphate to become incorporated in the calcite matrix as an impurity during crystal growth. Recent research has revealed that phosphorus recorded in calcite speleothems (Fairchild et al., 2006; Fairchild and Treble, 2009; Huang et al., 2001), calcite sediment (Otsuki and Wetzel, 1972), and sea animal shells (Becker et al., 2005) can serve as a proxy to reflect primary

productivity, enabling the reconstruction of paleoenvironments. Since most elements circulating in nature commonly occur in inorganic forms, organic matter including organophosphate attracts limited attention in the study of adsorption and coprecipitation.

1.1.4 Previous Study of Interaction between Calcite Surface and Organic Phosphorus

Several experiments have been reported that organic phosphates can be effectively retained by calcite surfaces. In these studies, the adsorption experiments utilized calcite suspension to absorb organic phosphate. The uptake of added organic phosphate of varied concentration yields an adsorption isotherm. Consequently, the maximal amount of phosphate absorbed on the calcite surface can be extrapolated from the isotherm curves. In terms of surface adsorption on calcite, some organic phosphates such as phytate and polyphosphate show stronger adsorption than inorganic phosphates such as orthophosphate (Celi et al., 2000; Sawada et al., 2003).

Celi et al. (2000) studied the adsorption of phytic acid, myo-inositol hexaphosphate (IHP), on calcite. Calcite from limestone was ground to less than 2 μm in diameter. Its specific surface area was 2.8 m^2/g. 3.5mL of calcite suspension was added to an equal volume of P-containing solutions at a selected concentrations ranging from 0 to 0.015M at pH 8.3. After shaking for 24 h at room temperature in the dark, samples were centrifuged and filtered through 0.25 μm Millipore membranes. The uptake of phosphate was determined by deducting the phosphate concentration measured in the initial solutions from that of the filtrate solution. Adsorption isotherms were obtained based on the concentration of adsorbed P and final pH of reacted solution of each sample. The IHP isotherm indicated calcite can retain up to 17.8 μmol · m^{-2} IHP, significantly higher than the maximal amount of sorbed orthophosphate, 1.4 μmol · m^{-2}. This indicated that the IHP uptake involves multiple processes. The IHP can complex calcium and form Ca-phytate species (Ca_1-IHP and Ca_2-IHP), whereas Ca_3-IHP could precipitate at any pH. In addition, the association constant value for the Ca-IHP complexes is 7 $\times 10^3$ and suggests that IHP at pH 8.3 can complex calcium ion even at low concentration, removing it from the calcite and favoring calcite dissolution. FT-IR spectra showed that bands at 1127 and 990 cm^{-1} appeared on both IHP-calcite and IHP. In the same positions two sharp peaks occurred on the difference spectrum (IHP − calcite minus calcite). These IR spectra confirmed no acid dissociation of IHP at pH 8.3. In conclusion, the interaction between IHP and calcite involves adsorption, precipitation of calcium salt, and subsequently calcite dissolution even at the lowest concentration of IHP (Celi et al., 2000).

Another study focused on the adsorption of organic polyphosphate on calcite surfaces. The organic polyphosphate is ethylenediamine - N, N, N', N'- methylene phosphonic acid (EDTPH) labelled with ^{14}C and ^{32}P. The experiments were undertaken in a temperature-controlled vessel at 25 °. The calcite suspension was adjusted to pH 9.0 by NaOH and the calcium concentration 5.0×10^{-4} to 5.01×10^{-3} mol·L^{-1} by addition of calcium chloride. The reaction was monitored by pH electrode and ion analyzer. The reaction solution re-equilibrated with calcium carbonate to minimize the change of surface conditions for the calcite crystals. With the calcite added, the calcite suspension was equilibrated for 30min and a small portion of EDTPH was added in which pH and calcium concentration were adjusted to those of the calcite suspension. After being shaken for 30min, the mixture solution was filtered through a 0.2 μm

cellulose nitrate membrane filter. Then, the radioactivity of the filtrate was measured to calculate the concentration of EDTPH remaining in solution. Likewise, the concentration of EDTPH adsorbed on the calcite solid was measured by dissolving the filtered calcite solid in hydrochloric acid and measuring the radioactivity of the resulting solution. The results show that at low concentration 0.32 $\mu mol \cdot L^{-1}$ 100% EDTPH was removed from solution, whereas the fraction of orthophosphate and triphosphate are much smaller at similar concentration. The result indicates the adsorption of EDTPH is much stronger than for both orthophosphate and triphosphate (Sawada et al., 2003). Therefore, a strong adsorption on the calcite surface is possible for organophosphate at low concentration.

These studies employed measurement of sorption isotherms, which is an effective method for extrapolating the concentration of surface adsorbates on calcium carbonate mineral at equilibrium conditions and estimating the maximum sorption capacity. However, understanding the uptake mechanism is difficult without information on the chemical nature of phosphate speciation in the mineral. Some structural information can be revealed by many methods including infrared spectroscopy, scanning electron microscopy, and X-ray scattering with synchrotron radiation. However, understanding the chemical nature of interactions requires structural information on the relationship between sorbate and mineral in detail. Such direct information is usually hard to obtain from most analytical instruments, but development of advanced solid-state NMR techniques has made it possible in some cases.

1.2 Solid-State NMR Spectroscopy

Nuclear Magnetic Resonance (NMR) is a physical phenomenon based on the change of orientation of nuclear magnetic moments in a magnetic field. Being immersed in a static magnetic field, nuclei of certain atoms can adsorb and reemit electromagnetic radiation to generate a second oscillating magnetic field, depending on the nuclear magnetic properties.

According to quantum mechanics, a nucleus of overall spin I would have $2I+1$ possible orientations, as is shown in Figure1.2. Thus, nuclei with an overall spin $I = 1/2$, such as ^{1}H, ^{13}C, and ^{31}P studied in this thesis, has two possible orientations, as shown in Table 1.2. When an external magnetic field is applied to these nuclei, their magnetic orientation would split into two different energy levels. This is called the Zeeman effect. The splitting between the nuclear spin levels is referred as the Zeeman splitting. The level lower in energy is more populated in nuclei than the higher energy level, as described by the Boltzmann distribution. It is possible to excite nuclei in the lower energy level into the higher level by electromagnetic radiation of certain frequency. The radiation frequency is determined by the energy difference of these two levels. The energy difference is determined by the strength of the magnetic field applied (B_0) and magnetic properties of the target nuclei. The difference in energy is

$$\Delta E = \gamma h B_0 / 2\pi,$$

where the proportionality constant γ is called the gyromagnetic ratio. Different isotopes have different gyromagnetic ratios, as is shown in Table 1.2; h is the Planck constant; B_0 is the strength of magnetic field in the unit of tesla, T.

There are only two energy levels for a single nucleus with spin I =1/2, which can be labelled with the magnetic quantum number *m* having values m = ±1/2. These two energy levels, E_α and E_β, are:

$$E_\alpha = + \tfrac{1}{2} h \nu_0 \text{ and } E_\beta = - \tfrac{1}{2} h \nu_0,$$

where ν_0 is the Larmor frequency of one spin. Apparently, the energies E_m only depend on m:

$$E_m = - m h \nu_0$$

Where the Larmor frequency (ν_0) depends on the gyromagnetic ratio γ and the strength of applied magnetic field B_0:

$$\nu_0 = B_0 \gamma / 2\pi$$

A typical NMR spectrometer is capable of: (1) polarizing the nuclear spins to yield a net nuclear magnetic moment; (2) rotating the spin polarization with radio frequency to produce transverse nuclear spin magnetization; (3) detecting the intensity and frequency of the small oscillating electric current induced by the transverse magnetization as it rotates around B_0.

Solid-state NMR Spectroscopy is a powerful non-destructive and analytical technique that takes advantage of NMR phenomena to ascertain structural information of target nuclei. It is possible to obtain structural information of molecules ranging from small inorganic molecules to large proteins as well as solids and to provide complete analysis of the entire spectrum.

1.2.1 ^{31}P NMR

Phosphorus possesses a natural isotopic abundance 100% in ^{31}P, a nucleus with relatively high γ, and nuclear spin of half integer (*I*=1/2), as is shown in Table 1.2. All the phosphorus species in natural sample are able to be detected by NMR. The isotope abundance and nuclear spin make ^{31}P NMR spectroscopy a very powerful technique to study P-bearing materials. Since calcium phosphate is widely found in the biominerals of vertebrates, ^{31}P NMR is a common technique for the studies of bone and teeth. ^{31}P NMR has been used to characterize calcium phosphate phases, such as hydroxylapatite, octacalcium phosphate, brushite, and amorphous calcium carbonate (Cade-Menun, 2005; Tsai and Chan, 2011). According to a comprehensive review by Kolodziejski, ^{31}P NMR studies on biomineralization are mostly concentrated on bone and related model compounds (Kolodziejski, 2005). ^{31}P NMR has been extensively applied to distinguish protonated from unprotonated phosphate groups in synthetic crystalline calcium phosphate (Tsai and Chan, 2011). Increasing protonation of the phosphate group tends to decrease the isotropic chemical shift as well as chemical shift anisotropy (see below), which results in the increase of spinning sideband intensities (Hinedi et al., 1992). In biological applications, ^{31}P NMR is largely used in characterizing phospholipid bilayers and membranes (Schiller and Arnold, 2002).

1.2.2 NMR Signal

The NMR signal is a free induction decay (FID), which is an oscillating decaying radiofrequency signal arising from relaxation of the induced transverse magnetization that emerges from the NMR probe (Figure 1.3). FID is a time-domain signal. After being digitized and Fourier transformed, the FID is converted into the frequency spectrum. The frequency of different NMR signals is dependent on the external magnetic field strength. Since no two magnets have exactly the same magnetic field, resonance frequencies would vary accordingly. To make the NMR spectrum and signal location comparable between different NMR analyses, the NMR result is reported in a spectrum as a chemical shift relative to a reference signal from an agreed upon reference compound. For example, the reference compound of ^{31}P NMR is 85% H_3PO_4 (Harris et al., 2002). Assuming the frequency of the target signal is ν and the frequency of H_3PO_4 is ν_{ref}, the chemical shift δ, which will be discussed in the following, of the target signal is calculated by the equation below and reported as a relative frequency in parts per million (ppm).

$$\delta = 10^6 \times (\nu - \nu_{ref}) / \nu_{ref} \text{ (ppm)}$$

1.2.3 Chemical Shift and Chemical Shift Anisotropy

The electrons in the molecules and solids can cause fluctuation of local magnetic fields on a submolecular distance scale. Any change in the electronic environment results in slightly different magnetic fields experienced by nuclei at two sites in the same molecule. For instance, the magnetic field experienced by the protons located in the benzene ring of hydroxybenzene is different from the proton in the hydroxyl group -OH. This phenomenon is called the chemical shift. The nature of the chemical shift is a two-step process: First, the external magnetic field induces the currents in the electron clouds; then, the circulating currents generate an induced magnetic field at the nucleus, altering the frequency.

Chemical shifts are very sensitive to the electronic environment of a nucleus and can serve as a fingerprint of structural/ chemical environments. Major factors that influence chemical shift are electron density, electronegativity of neighboring groups, coordination number, and anisotropic induced magnetic field effects. Electron density shields a nucleus from the external magnetic field. An electronegative atom would reduce the electron density of neighboring nuclei, which means the nuclei are deshielded. Anisotropic induced magnetic field effects are the result a local induced magnetic field of nucleus due to the electron currents. This can be paramagnetic when the induced magnetic field parallels to the applied external magnetic fields or diamagnetic when they are anti-parallel. Chemical shifts δ are small numbers, which are typically described in ppm.

The chemical shift arises because the induced magnetic field at a nucleus is different than the external field applied to the sample. The magnetic field experienced by the nucleus depends on the orientation of the molecule relative to the external field. The variation of chemical shift with orientation is called chemical shift anisotropy (CSA). The change is very small but sufficient to be detected by NMR. The size of the CSA is described by a tensor $\boldsymbol{\delta}$, which mathematically represents by a second rank tensor.

$$\delta = \begin{pmatrix} \delta_{x,x} & \delta_{x,y} & \delta_{x,z} \\ \delta_{y,x} & \delta_{y,y} & \delta_{y,z} \\ \delta_{z,x} & \delta_{z,y} & \delta_{z,z} \end{pmatrix}$$

where the x, y, and z represents the principal axes. For example, $\delta_{x,y}$ gives the size of the extra field in the x-direction which results from a field being applied in the y-direction. These second rank tensors depend on the electronic properties and symmetry of the molecule. In solution NMR, the chemical shift observed is the average chemical shift as the result of rapid molecular tumbling averaging over all possible orientations.

The measured chemical shift tensors can be fully described by the three principal components and three eigenvectors representing the orientation of the principal axes. The principal components are labelled according to the IUPAC (Harris et al., 2002):

$$\delta_{11} \geq \delta_{22} \geq \delta_{33}$$

$$\delta_{iso} = (\delta_{11} + \delta_{22} + \delta_{33}) / 3$$

$$\Omega = \delta_{11} - \delta_{22} \geq 0$$

$$\kappa = 3 (\delta_{22} - \delta_{iso}) / \Omega$$

where δ_{11} represents to the direction of least shielding, with the highest frequency, while δ_{33} corresponds to the direction of highest shielding, with the lowest frequency. The isotropic chemical shift (δ_{iso}) is the average value of the principal tensor elements. The span (Ω) represents the maximum width of the powder pattern. And skew (κ) measures the amount and orientation of the asymmetry of the tensor.

The second rank tensor (3 by 3 matrix) can also be described by the Haeberlen–Mehring–Spiess convention using the principal components δ_{XX} , δ_{YY}, δ_{ZZ} where

$$| \delta_{iso} - \delta_{ZZ} | \geq | \delta_{iso} - \delta_{XX} | \geq | \delta_{iso} - \delta_{YY} |$$

$$\delta_{iso} = (\delta_{XX} + \delta_{YY} + \delta_{ZZ}) / 3$$

$$\delta = \delta_{ZZ} - \delta_{iso}$$

$$\Delta\delta = \delta_{Z,Z} - (\delta_{XX} + \delta_{YY}) /2 = 3\delta /2$$

$$\eta = (\delta_{YY} - \delta_{XX}) / \delta$$

$$1 \geq \eta \geq 0$$

where the anisotropy ($\Delta\delta$) describes the largest differentiation from the spectral center of gravity center. The asymmetry (η) describes the deviation from an axially symmetric tensor. If the atom position has 3-fold or higher rotational symmetry, the tensor is symmetric which makes ($\delta_{Y,Y} - \delta_{X,X}$) to be zero as well as asymmetry ($\eta = 0$).

1.2.4 Dipolar Coupling

The dipolar coupling or dipole - dipole coupling is a mutual interaction between the nuclear spins. Each nuclear spin has a magnetic moment that produces a magnetic field at the position of the other spin. The two nuclear spins mutually experience their induced magnetic fields, as is shown in Figure 1.4, which can add to or subtract from the applied magnetic field (B_0). The dipole – dipole coupling may be either intramolecular or intermolecular and involve same nuclei (homonuclear) or different nuclei (heteronuclear).

The dipolar coupling is very useful for the study of molecular structure since it depends only on the known physical constants and internuclear distance. The dipolar coupling constant ($b_{j,k}$) is given by:

$$b_{j,k} = -(\mu_0/4\pi)(\gamma_j \gamma_k \hbar / r^3_{j,k})$$

where $\mu_0 = 4\pi \times 10^{-7}$ Hm^{-1} is the magnetic constant or vacuum permeability in SI units , γ_j and γ_k are the gyromagnetic ratio of spin j and spin k, $\hbar = 1.055 \times 10^{-34}$ Js is the reduced Planck constant equal to $h/2\pi$, and $r_{j,k}$ is distance between these two spins in meters.

Dipolar coupling provides a direct spectroscopic probe of the estimate the internuclear distance, allowing one to determine the molecular geometry and detect spatial proximity of nuclei. In solid-state NMR, most spectroscopic experiments implement MAS to achieve a higher resolution of the spectrum, which also averages out the dipolar coupling. However, there are many methods that can measure the dipolar coupling while still benefiting from MAS, such as cross polarization and rotational-echo double resonance.

1.2.5 Magic Angle Spinning

Magic Angle Spinning (MAS) is a technique commonly used in solid-state NMR spectroscopy. Spinning a sample around an axis inclined at the magic angle (54.74^o) with respect to the direction of the magnetic field can narrow the normally broad lines resulting from variation of frequency with orientation. Anisotropic interactions such as CSA and dipolar coupling cause the NMR frequency to vary with orientation in the magnetic field, yielding broad peaks for polycrystalline solids. Narrow lines from MAS enhance the spectrum resolution to achieve a better identification in spectral analysis.

In solution NMR, the rapid molecular tumbling about all possible directions averages out major interactions including chemical shift anisotropy, dipolar coupling, and quadrupolar coupling partially, which depend on the orientation of the interaction tensor with the external magnetic field. MAS, spinning the sample at the magic angle, can mimic the orientation averaging in solution to average the dipolar coupling to zero. The chemical shift anisotropy and quadrupolar interaction are also partially averaged. MAS gives rise to a main peak at the isotropic value (δ_{iso}) and spinning sidebands spaced at the spinning frequency, which can be useful for measuring the CSA of the target nuclei.

The physical spinning of the sample is driven by an air turbine, which can achieve rates in the 1 – 50 kHz range. The sample containers are cylindrical rotors and axially symmetric about the rotation axis.

1.2.6 Single Pulse

Single pulse (SP) is the most basic operation of all NMR experiments. The one pulse experiment is capable of detecting all forms of a particular nuclide in the sample. It is possible to quantify the proportions of each species if the magnetization is allowed to fully relax between each acquisition. The SP spectrum is acquired through a 90 °or shorter pulse, which rotates the net magnetic moment away from magnetic field generating the transverse magnetization that is detected.

As is show in Figure 1.5, single pulse experiment consists of a single RF pulse on a single channel, and followed by signal acquisition. There are four events in this sequence (Levitt, 2001).

1. Initialization. Before the experiment, the workstation computer sends instruction to program the pulse and adjunct facilities, such as the radio frequency (RF) synthesizer and analog to digital converters (ADC).
2. Excitation. The pulse program executes a time sequence of instruction to set the phase of the RF synthesizer and initializes the pulse. An RF pulse arrives in the probe from amplifier, resonates in the tuned circuit of the probe, and excites the sample with a RF field that oscillates close the Larmor frequency of target nuclear isotope.
3. Detection. After the pulse switched off, the NMR signal is ready to detect once the pulse energy is dissipated in the circuit. The nuclear spin magnetization oscillates in the probe circuit, which results in an RF signal (the FID). Then, the signal is amplified by the preamplifier, converted in frequency by the quadrature receiver, and eventually stored in the computer as a digitized complex signal. The complex signal allows positive and negative frequency shifts to be distinguished and is generated by shifting the phase of the receiver.
4. Processing and display. The digital signal is processed by various mathematical operations. The most important one is the Fourier transformation. Fourier transformation converts the NMR signal into an NMR frequency spectrum, which transforms the NMR data from a function of time to a function of frequency.

1.2.7 Cross Polarization

Cross polarization (CP) from abundant spins, such as ^{1}H, to dilute spins, such as ^{31}P, is a double resonance technique to enhance the sensitivity of the dilute spins and qualitatively measure the dipole coupling between heteronuclei. CP overcomes two common problems in the solid-state NMR. The first problem is the solid-state NMR of dilute nuclei suffers from low signal intensity, particularly when the nuclei also have low gyromagnetic ratio. The second one is relaxation time of dilute nuclei of ½ spin are typically long due to the weak heteronuclear dipolar coupling and absence of strong homonuclear dipolar interaction.

CP, often combined with MAS, takes advantage of the fact that many dilute and abundant nuclei are in close proximity in solids. To enable the polarization transfer, for instance, from ^{1}H to ^{31}P, the magnetization of spins must fulfill the Hartmann-Hahn condition:

$$\gamma_H B_H = \gamma_P B_P$$

$$(\gamma_H = 26.753; \gamma_P = 10.840)$$

where the B_H is the amplitude of the 'lock' pulse of the ^1H spins. B_P is the amplitude of the pulse applied to the ^{31}P spins. γ_H and γ_P are the gyromagnetic ratios of ^1H and ^{31}P, respectively.

As shown in Figure 1.6, a typical $^{31}P\{^1H\}CP$ consist of three events. First, a 90 ° excitation pulse is applied along the x axis of the rotating frame on the indirect ^1H channel. Then the phase of the indirect channel excitation changes to the y-axis to lock the transverse magnetization, while the spin of observed nucleus ^{31}P is locked by implementing a simultaneous contact pulse along the y axis to the observed channel of ^{31}P. If the transverse precession rates of the directly and the indirectly observed nuclei are equal, which means the amplitudes of pulses satisfy the Hartmann – Hahn condition, CP can induce magnetization transfer via dipole coupling between ^1H and ^{31}P.

CP is able to 1) increase the signal of observed nucleus, such as ^{31}P NMR signal by a ratio up to $\gamma_{H\,/}\,\gamma_P$; 2) shorten the repetition interval since the relaxation time of ^1H is much shorter than for ^{31}P; and 3) select signal of ^{31}P that is close to the ^1H. CP is sensitive to internuclear distances of molecules or functional groups involved. CP provides a very useful approach in structural characterization by establishing the connectivity between coupled nuclei and monitoring molecular dynamics in solids.

1.2.8 Rotational-Echo Double-Resonance

The rotational-echo double-resonance experiment measures the dipolar coupling between a heteronuclear spin pair (e.g. $^{31}P - ^{13}C$) during the MAS experiment (Gullion and Schaefer, 1989). The REDOR experiment typically prepares the observed magnetization using CP, and thus requires a three channel (HXY) solid state NMR spectrometer and a triple resonance probe (HXY).

The REDOR experiment consists of two separate NMR experiments, as is shown in Figure 1.7. The first one is a standard spin-echo on the observe channel. The second is the same spin-echo on the observe channel, while a series of 180 °pulses are applied on the indirect channel that reintroduce heteronuclear $^{31}P - ^{13}C$ dipolar coupling. The signal from the second experiment is reduced compared to the first spin-echo by an amount that depends on the strength of the $^{31}P - ^{13}C$ dipole coupling and the length of the spin-echo experiment (dephasing time). The $^{31}P - ^{13}C$ internuclear distance must be shorter than about 4 Å to observe a REDOR effect.

1.3 Previous NMR Studies of Phosphate and Organics in the Calcite

Interaction between two dissimilar organic and inorganic phases of atomic scale is extremely difficult to study by diffraction techniques. Lee et al (1995) proposed NMR as a helpful adjunct to X-ray diffraction (XRD) in ascertaining the trace of organics in fossil bone (Lee et al., 1995). This fossil bone was examined by XRD and NMR spectroscopy. The NMR results not only revealed two mineral components that were confirmed by XRD data, but also

detected organic components of small quantities which XRD failed to. De Reggi et al. (1998) deployed high-resolution NMR to determine the structural information of pancreatic stone protein in the *in vitro* incorporation of calcium into $CaCO_3$ crystal (De Reggi et al., 1998). The phosphorus distribution in calcite speleothem was studied using ^{31}P solid-state NMR, which suggested strong affinity of phosphates for calcite surfaces, a similarity in the inorganic phosphorus distribution of natural calcite to that of a more rapidly crystallized synthetic sample (Mason et al., 2006), and that P can form calcium phosphate surface precipitates on calcite (Mason et al., 2007).

Several solid-state NMR techniques have been developed to study the interaction between organics and calcite. Cross polarization magic angle spinning such as $^{13}C\{^{1}H\}$ CP/ MAS has been used to indicate the strong affinity of polyamides for calcite surfaces (Ueyama et al., 1998) as one additional ^{13}C signal peak was observed from calcite grown in the presence of polyamide, which was attributed to the carboxylate group of polyamide coprecipitated in calcite. Two-dimensional (2D) $^{13}C\{^{1}H\}$ Heteronuclear Correction (HetCor) has successfully determined the incorporation of citrate in calcite (Phillips et al., 2005) due to the strong HetCor signal, which was caused by the close proximity of between ^{13}C from calcite carbonate groups and ^{1}H from citrate. Rotational-echo double-resonance such as $^{13}C\{^{31}P\}$ and $^{13}C\{^{15}N\}$ REDOR experiments were carried out to determine the spatial distance between resonating nuclei P and N from incorporated moieties and carbon from calcite grown in a ^{13}C- and ^{15}N-enriched medium (Gertman et al., 2008). These studies show that double resonance NMR methods can be used to study the relationship between calcite and other substances present during precipitation or sorption.

^{31}P solid-state NMR spectroscopy is widely used in the studies of biomineralization, because calcium phosphate is commonly found in the biomineral of vertebrates, particularly in bone and teeth (Tsai and Chan, 2011). The highly complex hierarchical structures of bones and teeth contain different P species such as protonated orthophosphate and unprotonated orthophosphate. ^{31}P chemical shifts are the most helpful information for the characterization of calcium phosphates. The chemical shift anisotropy is also helpful because it is sensitive to the symmetry of the electronic environment of P. The more protonated phosphates have larger value of ^{31}P CSA because of the larger distortion of the electronic environment. Therefore, it is possible to obtain structural information from ^{31}P solid-state NMR in ascertaining the nature of the interaction between organic phosphate and calcite. In this study, I apply ^{31}P NMR methods to determine the characteristics of organophosphates coprecipitated with calcite.

1.4 Figures

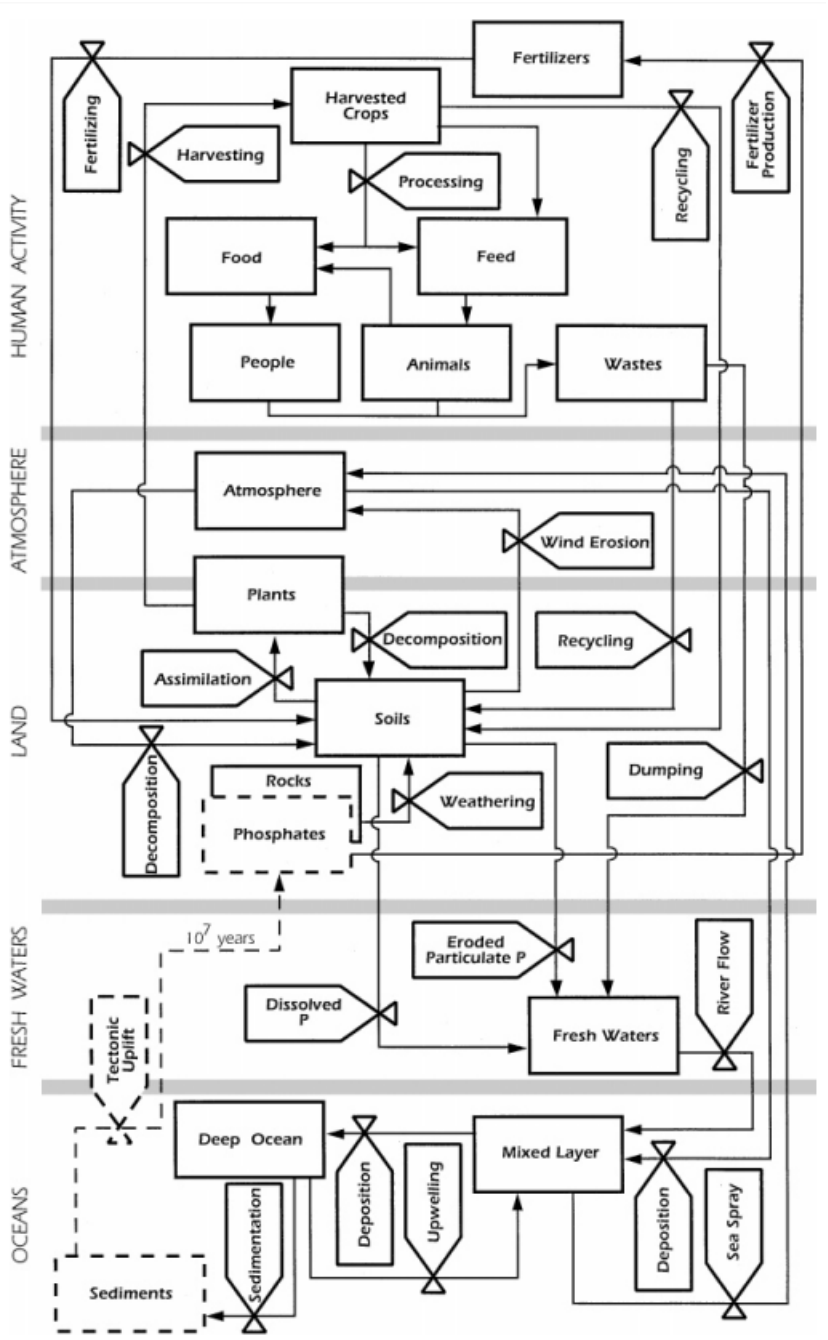

Figure 1.1 Global Phosphorus Cycle (V. Smil, 2000)

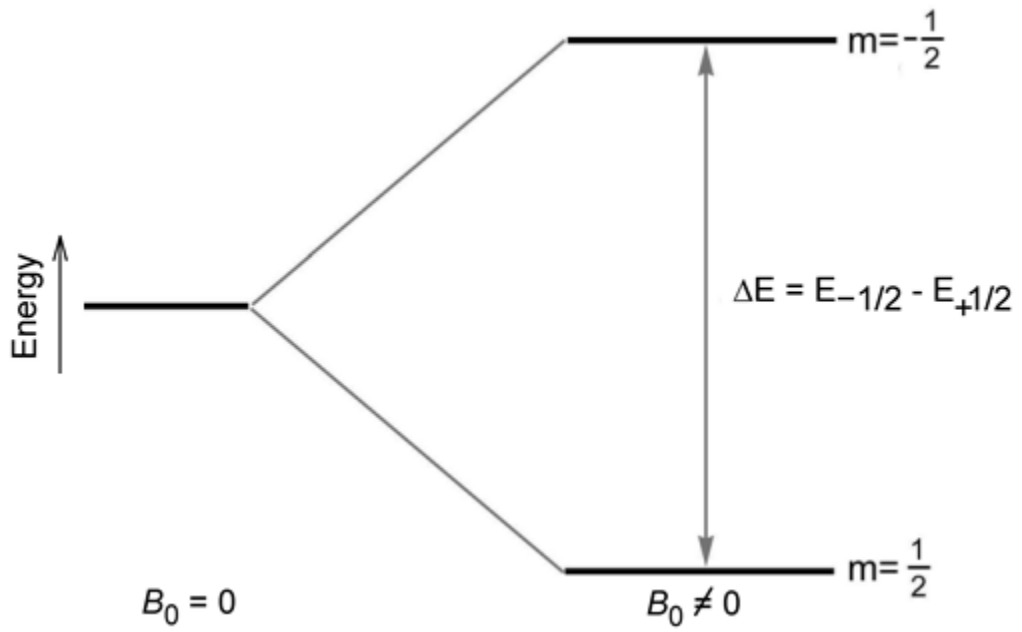

Figure 1.2 Splitting of nuclei spin states in an external magnetic field for a nucleus having spin I = ½.

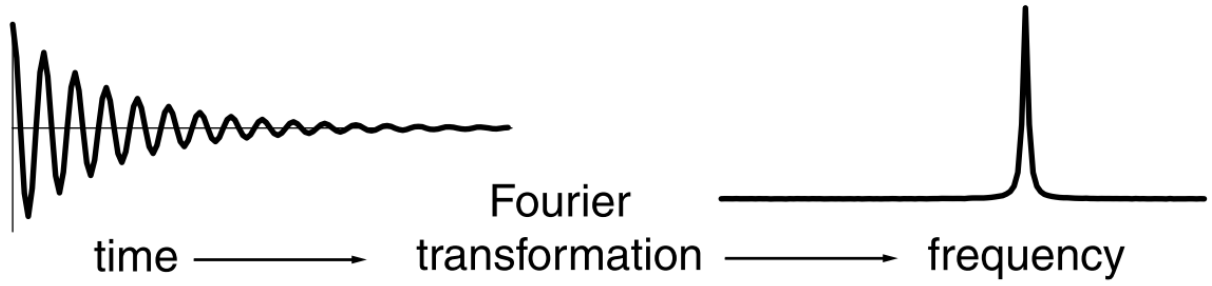

Figure 1.3 Fourier Transformation of signal: from free induction decay (time domain) to spectrum (frequency domain) via Fourier transform (Keeler, 2010)

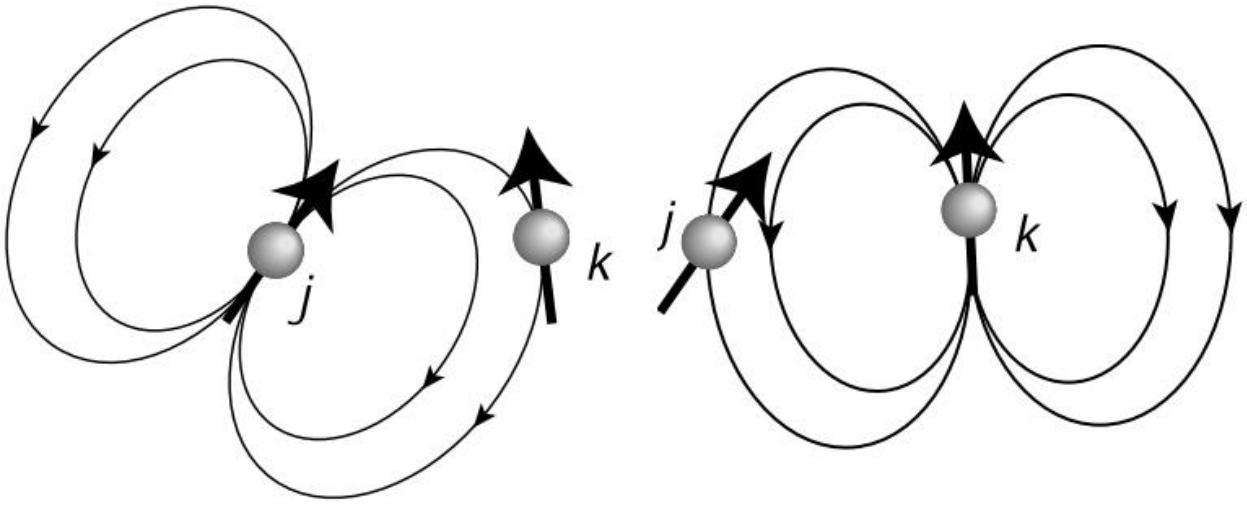

Figure 1.4 The dipole – dipole interaction. In an external magnetic field, spin J will generate an induced magnetic field at the site of spin k (Left), while the spin J also experiences the magnetic field induced by spin k (Right). The dipole – dipole interaction is mutual (Levitt, 2001).

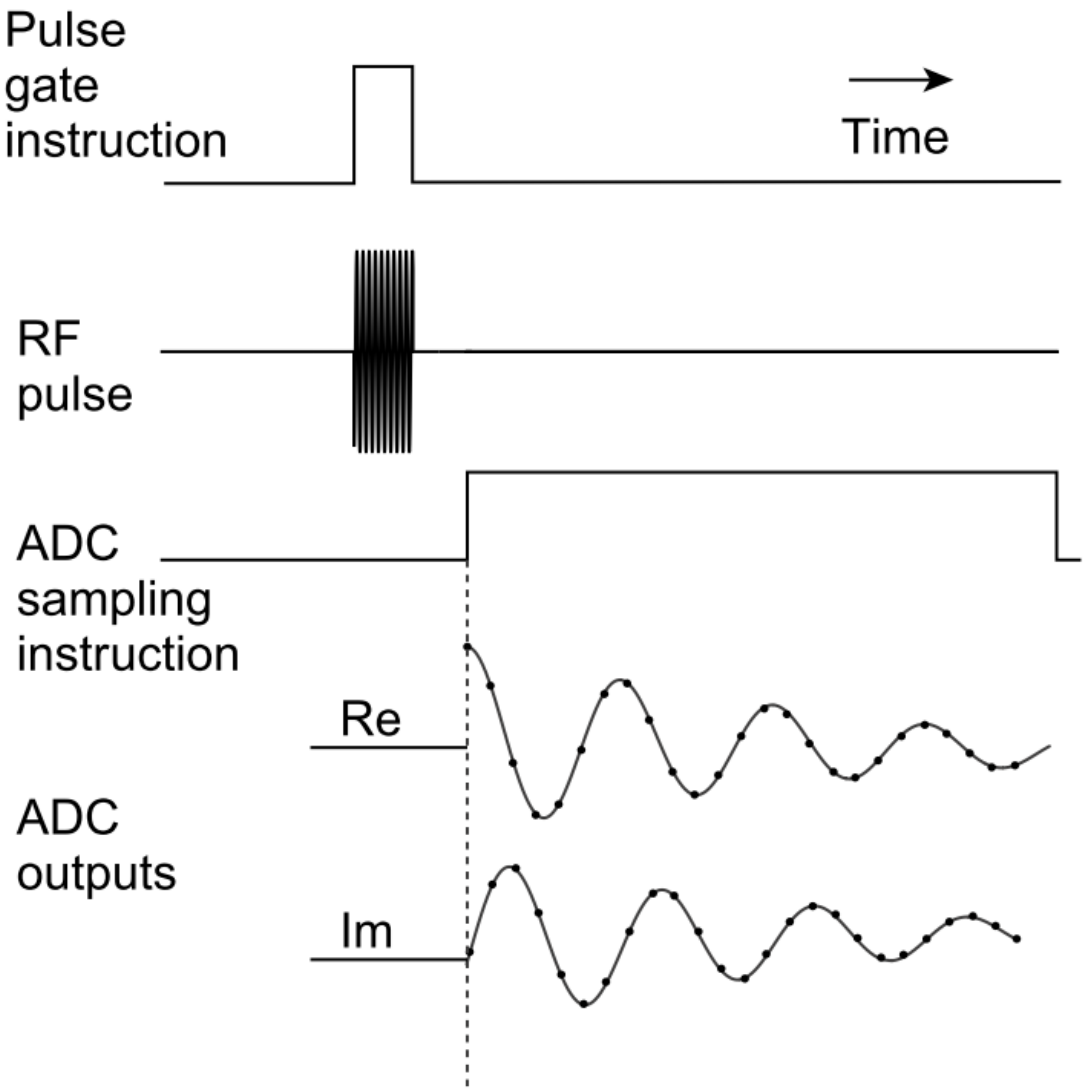

Figure 1.5 Timing sequence for a simple single pulse experiment (Levitt, 2001). From top to bottom, the first three events are 1) initialization, 2) excitation, and 3) detection. The fourth and final step is 4) processing and display, which includes Fourier transformation in Figure 1.3.

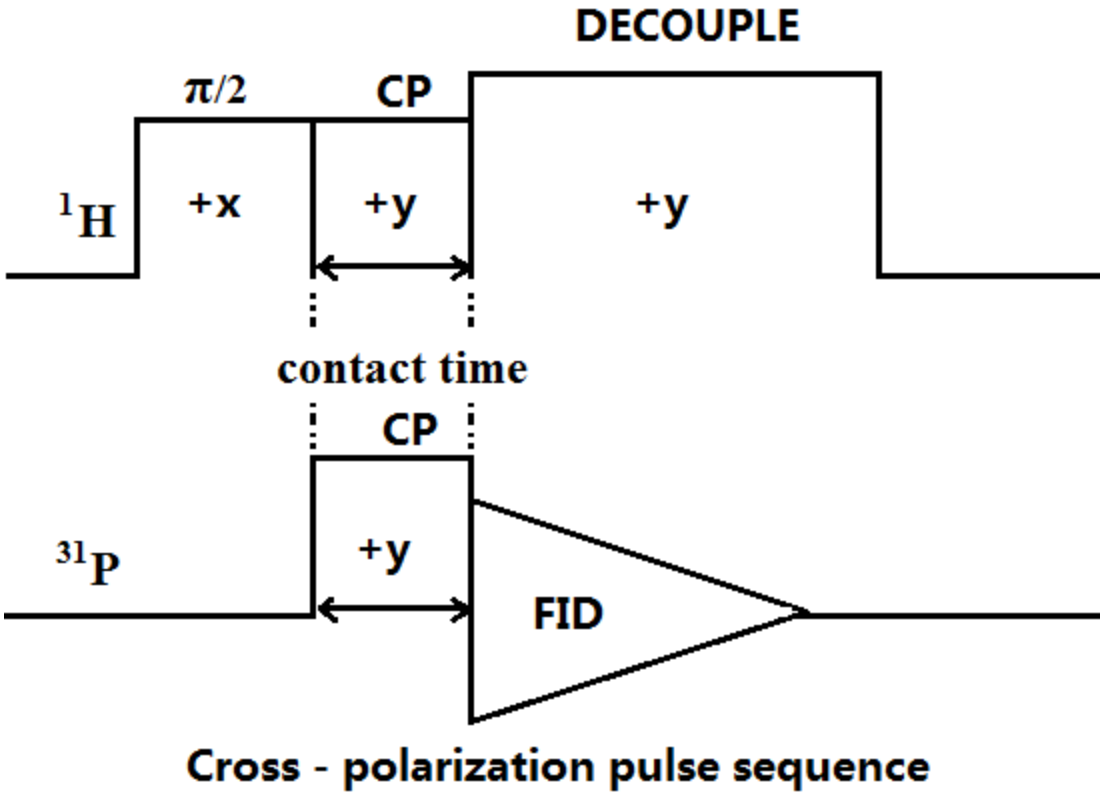

Figure 1.6 Cross-polarization pulse sequence (Kolodziejski and Klinowski, 2002). A π/2 pulse is applied to the spin ^{1}H, and follows with a long spin locking pulse of B_H. At the same time, a long pulse of B_P is applied to the spin ^{31}P. This time period, during which CP takes place, is called the contact time. Finally, the FID of ^{31}P NMR is observed after the RF applied to ^{31}P channel switched off.

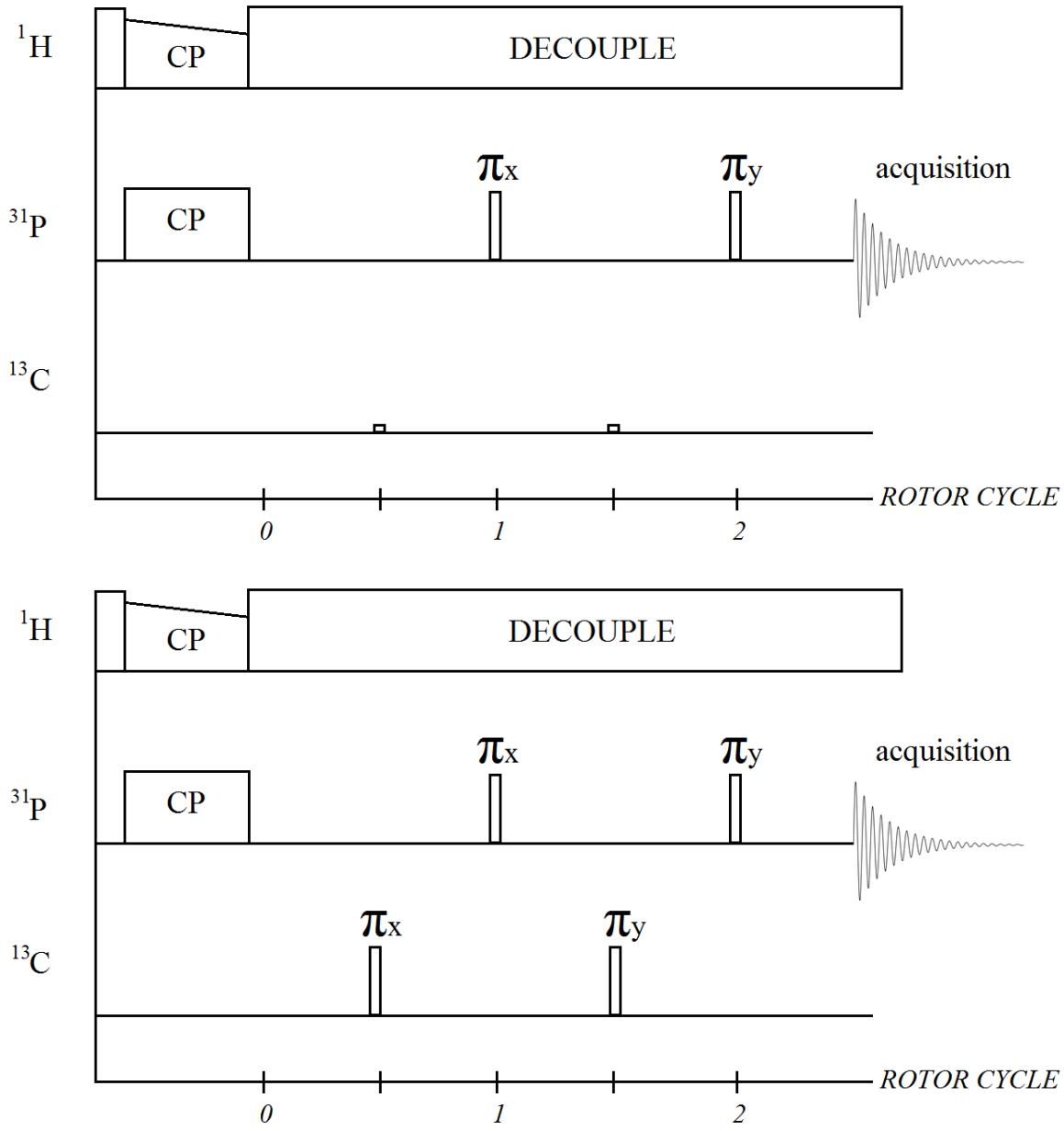

Figure 1.7 $^{31}P\{^{13}C\}$ REDOR pulse sequence of two-rotor-cycle. Each sequence consists of two parts. The first part is the standard spin-echo of ^{31}P NMR. The second one is same for the observe channel ^{31}P, while a series of π pulses are deployed on the ^{13}C indirect channel (Gullion and Schaefer, 1989).

1.5 Tables

Table 1.1 Major biosphere reservoirs of phosphorus (V. Smil, 2000)

P Reservoirs	Total Storage (Mt P)
Ocean	93000
Surface	8000
Deep	85000
Soils	40–50
Inorganic P	35–40
Organic P	5–10
Phytomass	570–625
Terrestrial	500–550
Marine	70–75
Zoomass	30–50
Anthropomass	3

Table 1.2 Magnetic properties of selected nuclei which are of geochemical interest in NMR.

Isotope	Natural % Abundance	Spin (I)	Magnetic Moment (μ)*	Magnetogyric Ratio (γ)†
^{1}H	99.9844	1/2	2.7927	26.753
^{2}H	0.0156	1	0.8574	4,107
^{11}B	81.17	3/2	2.6880	--
^{13}C	1.108	1/2	0.7022	6,728
^{17}O	0.037	5/2	-1.8930	-3,628
^{19}F	100.0	1/2	2.6273	25,179
^{29}Si	4.700	1/2	-0.5555	-5,319
^{31}P	100.0	1/2	1.1305	10,840

* **μ** in units of nuclear magnetons = $5.05078 \cdot 10^{-27}$ JT^{-1}

† γ in units of 10^{7}rad T^{-1} sec^{-1}

1.6 Reference

Al-Thawadi, S.M. (2011) Ureolytic bacteria and calcium carbonate formation as a mechanism of strength enhancement of sand. *J. Adv. Sci. Eng. Res.* **1**(1), 98-114.

Baldini, J.U.L., McDermott, F. and Fairchild, I.J. (2007) Structure of the 8200-year cold event revealed by a speleothem trace element record (Retraction of vol 296, pg 2203, 2002). *Science* **317**(5839), 748-748.

Barkouki, T., Martinez, B., Mortensen, B., Weathers, T., De Jong, J., Ginn, T., Spycher, N., Smith, R. and Fujita, Y. (2011) Forward and inverse bio-geochemical modeling of microbially induced calcite precipitation in half-meter column experiments. *Transport. Porous Med.* **90**(1), 23-39.

Becker, A., Ziegler, A. and Epple, M. (2005) The mineral phase in the cuticles of two species of Crustacea consists of magnesium calcite, amorphous calcium carbonate, and amorphous calcium phosphate. *Dalton Trans.*10), 1814-1820.

Borsato, A., Frisia, S., Fairchild, I.J., Somogyi, A. and Susini, J. (2007) Trace element distribution in annual stalagmite laminae mapped by micrometer-resolution X-ray fluorescence: Implications for incorporation of environmentally significant species. *Geochim. Cosmochim. Ac.* **71**(6), 1494-1512.

Cade-Menun, B.J. (2005) Characterizing phosphorus in environmental and agricultural samples by P-31 nuclear magnetic resonance spectroscopy. **66**(2), 359-371.

Celi, L., Lamacchia, S. and Barberis, E. (2000) Interaction of inositol phosphate with calcite. *Nutr. Cycl. Agroecosyst.* **57**(3), 271-277.

Chou, C.-W., Seagren, E.A., Aydilek, A.H. and Lai, M. (2011) Biocalcification of sand through ureolysis. *J. Geotech. Geoenviron.* **137**(12), 1179-1189.

Cross, A.F. and Schlesinger, W.H. (1995) A literature review and evaluation of the. Hedley fractionation: Applications to the biogeochemical cycle of soil phosphorus in natural ecosystems. **64**(3-4), 197-214.

Curti, E. (1999) Coprecipitation of radionuclides with calcite: estimation of partition coefficients based on a review of laboratory investigations and geochemical data. *Appl. Geochem.* **14**(4), 433-445.

De Reggi, M., Gharib, B., Patard, L. and Stoven, V. (1998) Lithostathine, the presumed pancreatic stone inhibitor, does not interact specifically with calcium carbonate crystals. *J. Biol. Chem.* **273**(9), 4967-4971.

DeJong, J.T., Fritzges, M.B. and Nüsslein, K. (2006) Microbially induced cementation to control sand response to undrained shear. *J. Geotech. Geoenviron.* **132**(11), 1381-1392.

DeJong, J.T., Mortensen, B.M., Martinez, B.C. and Nelson, D.C. (2010) Bio-mediated soil improvement. *Ecol. Eng.* **36**(2), 197-210.

Dekanel, J. and Morse, J.W. (1978) The chemistry of orthophosphate uptake from seawater on to calcite and aragonite. *Geochim. Cosmochim. Ac.* **42**(9), 1335-1340.

Dove, P.M.D.Y.J.W.S.M.S.o.A. (2003) *Biomineralization*. Mineralogical Society of America, Washington, DC.

Fairchild, I.J., Baker, A., Borsato, A., Frisia, S., Hinton, R.W., McDermott, F. and Tooth, A.F. (2001) Annual to sub-annual resolution of multiple trace-element trends in speleothems. *J. Geol. Soc. London* **158**, 831-841.

Fairchild, I.J., Smith, C.L., Baker, A., Fuller, L., Spötl, C., Mattey, D. and McDermott, F. (2006) Modification and preservation of environmental signals in speleothems. *Earth-Sci. Rev.* **75**(1), 105-153.

Fairchild, I.J. and Treble, P.C. (2009) Trace elements in speleothems as recorders of environmental change. *Quaternary Sci. Rev.* **28**(5-6), 449-468.

Freeman, J.S. and Rowell, D.L. (1981) The adsorption and precipitation of phosphate onto calcite. *J. Soil Sci.* **32**(1), 75-84.

Frisia, S., Borsato, A., Drysdale, R.N., Paul, B., Greig, A. and Cotte, M. (2012) A re-evaluation of the palaeoclimatic significance of phosphorus variability in speleothems revealed by high-resolution synchrotron micro XRF mapping. *Clim. Past.* **8**(6), 2039-2051.

Fujita, Y., Redden, G.D., Ingram, J.C., Cortez, M.M., Ferris, F.G. and Smith, R.W. (2004) Strontium incorporation into calcite generated by bacterial ureolysis. *Geochim. Cosmochim. Ac.* **68**(15), 3261-3270.

Garcia-Anton, E., Cuezva, S., Fernandez-Cortes, A., Cuevas-Gonzalez, J., Munoz-Cervera, M.C., Benavente, D., Sanchez-Moral, S. and Canaveras, J.C. (2011) Mineral-Variations Study of Canelobre Cave Phosphate Stalactites by Raman and Luminescence Methods. *Spectr. Lett.* **44**(7-8), 539-542.

Geffroy, C., Foissy, A., Persello, J. and Cabane, B. (1999) Surface complexation of calcite by carboxylates in water. *J. Colloid. Interf. Sci.* **211**(1), 45-53.

Gertman, R., Ben Shir, I., Kababya, S. and Schmidt, A. (2008) In situ observation of the internal structure and composition of biomineralized Emiliania huxleyi calcite by solid-state NMR spectroscopy. *J. Am. Chem. Soc.* **130**(40), 13425-13432.

Giannimaras, E.K. and Koutsoukos, P.G. (1987) The crystallization of calcite in the precence of orthophosphate. *J. Colloid. Interf. Sci.* **116**(2), 423-430.
Griffin, R.A. and Jurinak, J.J. (1974) Kinetics of the Phosphate Interaction with Calcite. *Soil Sci. Soc. Am. J.* **38**(1), 75-79.
Gullion, T. and Schaefer, J. (1989) Rotational-echo double-resonance NMR. *J. Magn. Reson.* **81**(1), 196-200.
Gunawan, E.K., Warmadewanthi and Liu, J.C. (2010) Removal of phosphate and fluoride from optoelectronic wastewater by calcite. *Int. J. Environ. Tech. Manag.* **12**(2-4), 308-321.
Harris, R.K., Becker, E.D., Cabral de Menezes, S.M., Goodfellow, R. and Granger, P. (2002) NMR nomenclature: nuclear spin properties and conventions for chemical shifts. IUPAC Recommendations 2001. International Union of Pure and Applied Chemistry. Physical Chemistry Division. Commission on Molecular Structure and Spectroscopy. *Magn. Reson. Chem.* **40**(7), 489-505.
Hinedi, Z.R., Goldberg, S., Chang, A.C. and Yesinowski, J.P. (1992) A P-31 and H-1 MAS NMR study of phosphate sorption onto calcium carbonate. *J. Colloid. Interf. Sci.* **152**(1), 141-160.
House, W.A. and Donaldson, L. (1986) Adsorption and coprecipitation of phosphate on calcite. *J. Colloid. Interf. Sci.* **112**(2), 309-324.
Huang, Y., Fairchild, I.J., Borsato, A., Frisia, S., Cassidy, N.J., McDermott, F. and Hawkesworth, C.J. (2001) Seasonal variations in Sr, Mg and P in modern speleothems (Grotta di Ernesto, Italy). *Chem. Geol.* **175**(3), 429-448.
Kamiya, M., Hatta, J., Shimada, E., Ikuma, Y., Yoshimura, M. and Monma, H. (2004) AFM analysis of initial stage of reaction between calcite and phosphate. *Mat. Sci. Eng. B-solid.* **111**(2-3), 226-231.
Karageorgiou, K., Paschalis, M. and Anastassakis, G.N. (2007) Removal of phosphate species from solution by adsorption onto calcite used as natural adsorbent. *J. Hazard. Mater.* **139**(3), 447-452.
Keeler, J. (2010) *Understanding NMR spectroscopy*. John Wiley and Sons, Chichester, U.K.
Khasawneh, F.E., Sample, E. and Kamprath, E. (1980) *The role of phosphorus in agriculture*. American Society of Agronomy, Crop Science Society of America, Soil Science Society of America. Madison, Wisconsin.
Klein, C., Hurlbut, C.S. and Dana, J.D. (1993) *Manual of mineralogy*. Wiley, New York.
Kolodziejski, W. (2005) Solid-state NMR studies of bone, in: Klinowski, J. (Ed.), *New Techniques in Solid-State Nmr*. Springer-Verlag Berlin, Berlin, 235-270.
Kolodziejski, W. and Klinowski, J. (2002) Kinetics of cross-polarization in solid-state NMR: A guide for chemists. *Chem. Rev.* **102**(3), 613-628.
Lee, A.P., Klinowski, J. and Marseglia, E.A. (1995) Application of nuclear magnetic resonance spectroscopy to bone diagenesis. *J. Archaeol. Sci.* **22**(2), 257-262.
Levitt, M.H. (2001) *Spin dynamics : basics of nuclear magnetic resonance*. John Wiley & Sons, Chichester; New York.
Liu, Y., Sheng, X., Dong, Y.H. and Ma, Y.J. (2012) Removal of high-concentration phosphate by calcite: Effect of sulfate and pH. *Desalination* **289**, 66-71.
Mason, H.E., Frisia, S., Tang, Y., Reeder, R.J. and Phillips, B.L. (2007) Phosphorus speciation in calcite speleothems determined from solid-state NMR spectroscopy. *Earth Planet. Sci. Lett.* **254**(3-4), 313-322.
Mason, H.E., Hausner, D., Frisia, S., Tang, Y., Reeder, R.J., Strongin, D.R. and Phillips, B.L. (2006) Phosphorus distribution in calcite speleothems from solid-state NMR and AFM. *Geochim. Cosmochim. Ac.* **70**(18), A399-A399.
Mortensen, B., Haber, M., DeJong, J., Caslake, L. and Nelson, D. (2011) Effects of environmental factors on microbial induced calcium carbonate precipitation. *J. Appl. Microbiol.* **111**(2), 338-349.
Otsuki, A. and Wetzel, R.G. (1972) Coprecipitation of phosphate with carbonates in a marl-lake. *Limnol. Oceanogr.* **17**(5), 763-767.
Phillips, B.L., Lee, Y.J. and Reeder, R.J. (2005) Organic coprecipitates with calcite: NMR spectroscopic evidence. *Eviron. Sci. Technol.* **39**(12), 4533-4539.
Pingitore, N.E. and Eastman, M.P. (1986) The coprecipitation of Sr2+ with calcite at 25 ℃ and 1 atm. *Geochim. Cosmochim. Ac.* **50**(10), 2195-2203.
Pogson, R.E., Osborne, R.A.L., Colchester, D.M. and Cendon, D.I. (2011) Sulfate and phosphate speleothem at Jenolan caves, New South Wales, Australia. *Acta Carsologica* **40**(2), 239-254.
Rong, H., Qian, C. and Wang, R. (2011) A cementation method of loose particles based on microbe-based cement. *Sci. China Ser. E.* **54**(7), 1722-1729.
Sawada, K., Abdel-Aal, N., Sekino, H. and Satoh, K. (2003) Adsorption of inorganic phosphates and organic polyphosphonate on calcite. *Dalton Trans.*3), 342-347.

Schiller, J. and Arnold, K. (2002) Application of high resolution ^{31}P NMR spectroscopy to the characterization of the phospholipid composition of tissues and body fluids - a methodological review. *Med. Sci. Monitor* **8**(11), 205-222.

Schmahl, W.W., Griesshaber, E., Kelm, K., Goetz, A., Jordan, G., Ball, A., Xu, D.Y., Merkel, C. and Brand, U. (2012) Hierarchical structure of marine shell biomaterials: biomechanical functionalization of calcite by brachiopods. *Z. Kristall.* **227**(11), 793-804.

Smil, V. (2000) Phosphorus in the environment: natural flows and human interferences. **25**(1), 53-88.

So, H.U., Postma, D., Jakobsen, R. and Larsen, F. (2011) Sorption of phosphate onto calcite; results from batch experiments and surface complexation modeling. *Geochim. Cosmochim. Ac.* **75**(10), 2911-2923.

So, H.U., Postma, D., Jakobsen, R. and Larsen, F. (2012) Competitive adsorption of arsenate and phosphate onto calcite; experimental results and modeling with CCM and CD-MUSIC. *Geochim. Cosmochim. Ac.* **93**, 1-13.

Song, Y.H., Weidler, P.G., Berg, U., Nuesch, R. and Donnert, D. (2006) Calcite-seeded crystallization of calcium phosphate for phosphorus recovery. *Chemosphere* **63**(2), 236-243.

Suzuki, T., Inomata, S. and Sawada, K. (1986) Adsorption of phosphate on calcite. *J. Chem. Soc. Faraday T. 1*. **82**, 1733-1743.

Treble, P.C., Chappell, J. and Shelley, J.M.G. (2005) Complex speleothem growth processes revealed by trace element mapping and scanning electron microscopy of annual layers. *Geochim. Cosmochim. Ac.* **69**(20), 4855-4863.

Tsai, T.W.T. and Chan, J.C.C. (2011) Recent Progress in the Solid-State NMR Studies of Biomineralization. *Annu. Rep. NMR Spectrosc.* **73**, 1-61.

Ueyama, N., Hosoi, T., Yamada, Y., Doi, M., Okamura, T.-a. and Nakamura, A. (1998) Calcium Complexes of Carboxylate-Containing Polyamide with Sterically Disposed NH --- O Hydrogen Bond: Detection of the Polyamide in Calcium Carbonate by ^{13}C Cross-Polarization/Magic Angle Spinning Spectra. *Macromolecules* **31**(21), 7119-7126.

van Meer, G., Voelker, D.R. and Feigenson, G.W. (2008) Membrane lipids: where they are and how they behave. *Nat. Rev. Mol. Cell Biol.* **9**(2), 112-124.

van Paassen, L.A., Ghose, R., van der Linden, T.J., van der Star, W.R. and van Loosdrecht, M.C. (2010) Quantifying biomediated ground improvement by ureolysis: large-scale biogrout experiment. *J. Geotech. Geoenviron.* **136**(12), 1721-1728.

Weiner, S. and Dove, P.M. (2003) An overview of biomineralization processes and the problem of the vital effect, in: Dove, P.M., DeYoreo, J.J., Weiner, S. (Eds.), *Biomineralization*. Mineralogical Soc America, Washington, 1-29.

Whiffin, V.S., van Paassen, L.A. and Harkes, M.P. (2007) Microbial carbonate precipitation as a soil improvement technique. *Geomicrobiol. J.* **24**(5), 417-423.

Young, J.R. and Henriksen, K. (2003) Biomineralization within vesicles: The calcite of coccoliths, in: Dove, P.M., DeYoreo, J.J., Weiner, S. (Eds.), *Biomineralization*. Mineralogical Soc Amer, Chantilly, 189-215.

Zachara, J., Cowan, C. and Resch, C. (1991) Sorption of divalent metals on calcite. *Geochim. Cosmochim. Ac.* **55**(6), 1549-1562.

II. NMR Investigation of Organic Phosphoesters Coprecipitated with Calcite

2.1 Introduction

The interaction between calcite and dissolved organophosphate is important to biomineral and geochemical systems. Organic molecules and phosphates can be adsorbed to the calcite surface and incorporated as impurities in the matrix during crystal growth. Although phosphate in nature is commonly found in inorganic forms, recent progress in phosphorus study has brought organic phosphate to the spotlight. Increasing anthropogenic interference releases substantial amount of organic phosphate to the phosphorus cycle, which may contribute to eutrophication (Correll, 1998). Phosphorus biomarkers preserved in speleothems can reflect paleotemperature, which allows the reconstruction of paleoclimate at high resolution (Blyth et al., 2008). Calcite is often used as a natural sorbent to treat eutrophic waters (Murphy et al., 1988). The growing calcite can record phosphate variation to reflect environmental change. For instance, a discontinuity in a homogeneous lacustrine sediment caused by a laminated calcite sequence might indicate eutrophication event in the past (de Vicente et al., 2006). In recent studies of speleothems, the phosphate distribution has been recognized to indicate paleotemperature variation, and subsequently enables the reconstruction of paleoenvironment (Fairchild et al., 2006; Fairchild and Treble, 2009; Huang et al., 2001).

2.1.1 Calcite

Calcite is thermodynamically the most stable polymorph of calcium carbonate at Earth's surface conditions. It is also a common biomineral formed by organisms such as coccolithophores, brachiopods, and mollusks (Lowenstam and Weiner, 1989). Calcite can adsorb small organic molecules, such as citrate (Phillips et al., 2005), phytic acid (Celi et al., 2000), and polyphosphate (Sawada et al., 2003). Traces of organic P in solution can inhibit the crystallization of calcium carbonate by selective adsorption or poisoning of the growth sites (kinks) of calcite surfaces (Meyer, 1984; Reddy and Nancollas, 1973; Sawada et al., 2003). Calcite surface morphology can be influenced by low-molecular-weight organic additives (Meldrum and Hyde, 2001). Organic compounds such as phosphonic, citric, and malic acid can promote crystal aggregation along specific orientation by binding to specific faces of calcite (Didymus et al., 1993).

2.1.2 Phosphate esters

Phosphate esters, also known as organophosphates, consist of phosphate groups having ester linkages (e.g. monoester, diester), which play crucial roles in the living world (Westheimer, 1987). Adenosine triphosphate (ATP), creatine phosphate, and phosphoenolpyruvate are the principal components of biochemical energy cycles. The genetic materials DNA and RNA are phosphodiesters. Organic phosphates, particularly those contained

in genetic material, are relatively stable and resistant to hydrolysis (Westheimer, 1987). Organophosphates are also the basis of many insecticides, herbicides, and nerve gas. Organic phosphate pool has been discovered in sediments particularly in lake and marine systems (Benitez-Nelson, 2000; Degroot and Golterman, 1993; Filippelli, 2011; Follmi, 1996; Wang et al., 2007).

2.1.3 Interaction of calcite and organics

Some organic matter, such as soil extract, malic acid, and citric acid, can inhibit calcite precipitation and dissolution (Amrhein and Suarez, 1987; Lin et al., 2005; Meldrum and Hyde, 2001). Glycerolphosphate was reported as to be an inhibitor at a concentration of 16 μM in calcite crystallization experiments (Reddy, 1977). However, some organic macromolecules, such as the polyanion of L-aspartic acid and organic-matrix protein extracted from shells of *Mytilus californianus,* can induce calcite precipitation (Sethmann et al., 2005; Tiano, 1995). Adsorption of organic ligands on mineral surfaces can either enhance the dissolution rate of the mineral in undersaturated solution or inhibit the precipitation of mineral in supersaturated solution (Furrer and Stumm, 1986). Recent studies have demonstrated that dissolved organics (e.g. carboxylate, citrate, polyamide) can be strongly bonded to surfaces of calcium carbonates (Geffroy et al., 1999; Phillips et al., 2005; Ueyama et al., 1998). Subsequently, such adsorbates can be coprecipitated with the growing calcite (Phillips et al., 2005), for example, by the surface entrapment process (Watson, 2004). At low concentrations an insufficient amount of organics is available to block potential sites of crystal growth. Therefore, at sufficiently low concentration the incorporation of organics during crystallization might be enabled.

2.1.4 Previous Study

Many analytical methods have contributed to the research of organic interactions with calcite. Early studies were focused on the adsorption of organics on calcite surfaces and the interference from their interaction in aquatic geochemistry (Celi et al., 2000; Celi et al., 1999; Sawada et al., 2003), due to its importance to water remediation and soil fertilization. With the development of analytical technology, calcite morphology imaging at the nanoscale can be obtained from atomic force microscopy (AFM). Together with scanning electron microscopy (SEM), they can detect the change of calcite morphology in the presence of dissolved organic molecules, which continually provide inspiration for biomaterial engineering (Matsuya et al., 2006; Merkel et al., 2009; Mirtchi et al., 1990, 1991; Monchau et al., 2013; Ruiz-Agudo et al., 2010; Sethmann et al., 2005; Tas, 2007, 2008). To understand the chemical nature of the interaction between organic and mineral, synchrotron X-ray spectroscopy is extensively implemented to obtain the structural information, possibly to the atomic-level. However, it is a technical challenge for most scattering and spectroscopic techniques to provide accurate information of (i) structures of amorphous polymers and macromolecules (Gullion and Schaefer, 1989) and (ii) intracrystalline defects involving light elements (Feng et al., 2008). To better

understand the structural information for the interface of organic and mineral (e.g. internuclear distance and chemical bonding), it is favorable to apply nuclear magnetic resonance spectroscopy to enable direct detection of the chemical environment of nuclei. The following is a snapshot of NMR methodology that has recently been applied to study the interaction of organics with calcite.

Ueyama et al. (1998) employed $^{13}C\{^{1}H\}$ CP-MAS (Cross Polarization combined with Magic Angle Spinning) solid-state NMR spectroscopy to observe a polyamide in calcite (Ueyama et al., 1998). Phillips et al. (2005) utilized $^{13}C\{^{1}H\}$ CP-MAS and 2D $^{13}C\{^{1}H\}$ HetCor (Heteronuclear Correction) solid-state NMR spectroscopy to determine the citrate incorporation in calcite (Phillips et al., 2005). Feng et al. (2008) implemented $^{13}C\{^{1}H\}$ CP/MAS and ^{2}H SP/MAS to advance the research on citrate coprecipitation with calcite through measuring the heteronuclear distances and characterizing the structural defect of large intracrystalline citrate (Feng et al., 2008). Gertman et al. (2008) carried out the direct ^{13}C excitation echo (DE), $^{13}C\{^{31}P\}$ REDOR, and $^{13}C\{^{15}N\}$ REDOR to examine the internal structure and composition of biomineralized calcite (Gertman et al., 2008). These studies showed that solid-state NMR can provide important structural information about organic molecules in calcite.

The speciation of incorporated organophosphate as a biomarker in the biomineralized calcite lattice has been discussed for a long time (Banfield et al., 2005; Banfield and Nealson, 1997; Dove et al., 2003). The presence of biomarkers during the biomineralization has also been found, typically given by methods such as chromatography and mass spectrometry (Xie et al., 2005; Xie et al., 2003), which consume and disintegrate the samples. The *in situ* information, e.g. structural defect and spatial distribution, is inevitably lost. Though X-ray scattering and spectroscopic methods provide non-destructive solution for structural characterization, they encounter technical challenges in obtaining interatomic information at low concentrations of P. Solid-state NMR spectroscopy is a feasible solution to address those issues. ^{31}P is the only natural isotope of phosphorus (^{31}P 100%). The signal of all phosphorus species can be detected with NMR. Thus, ^{31}P NMR spectroscopy is advantageous to characterize phosphorus and has been used extensively to study the nature of P in a wide range of natural samples including agricultural soil, marine sediment, biomass, mineral, and colloids suspended in water (Cade-Menun, 2005; Gröger et al., 2009; Iuga et al., 2006; Pettersson, 2001). Mainly because of the low natural concentration of P and broad peaks in solid-state spectra (due to the chemical shift anisotropy), most studies utilized solution NMR to study extracts of solid samples, of which the P content can be concentrated after extraction. Cade-Menun (2005) compared the ^{31}P NMR spectra of algal samples and its extract obtained with solid-state and solution NMR respectively, and demonstrated the advantage of solution state NMR in peak identification and quantification (Cade-Menun, 2005). However, preparing extracts of solid sample requires various extractants to solubilize different concentration and forms of P, which consumes large amount of samples and pose risk of altering the phosphorus environment (e.g. hydrolysis) (Turner et al., 2005). On the contrary, solid-state NMR characterization requires a small volume of sample with minimal

preparation or alteration. Therefore, ^{31}P solid-state NMR is preferable to study solid samples as long as sufficient amount of P content is present. Mason et al. (2006) applied ^{31}P solid-state NMR (e.g. direct and indirect excitation) to study P content in calcitic speleothem samples. Comparing the NMR spectra yielded from a synthetic calcite coprecipitated with inorganic orthophosphate, Mason et al. (2006) determined that the main P content in speleothem samples is inorganic, which are present as structural defects in calcite (Mason et al., 2007). However, current understanding about the organic P occluded in minerals (e.g. calcite) is limited as its ^{31}P NMR spectroscopic characteristics is unclear, which constrains the application of NMR in this area. Here, a methodology based on ^{31}P NMR spectroscopy is proposed to help determine the speciation of P *in situ* at low-concentration in calcite based on the spectroscopic characteristics of organophosphoesters coprecipitated with calcite.

2.2 Materials and Methods

2.2.1 Materials

A series of commercially available organophosphates able to form bilayers or containing large amount of hydroxyl groups are deliberately chosen for preparing the calcite/ P-ester coprecipitates, as detailed in Table 2.1. These molecules contain several different types of functional groups in addition to phosphate that could interact favorably with the calcite surface, such as hydroxyl and carboxyl groups. In aqueous solution, lipid, such as stearic acid, can electrostatically entrap Ca^{2+} ions into its bilayer film (Damle et al., 2002). Hydroxyl species (e.g. OH, $-O^-$) in aqueous solution can bond to Ca^{2+} ions and form a monolayer adsorbed on a stoichiometric calcite surface (Fenter et al., 2000).

- Glycerolphosphate (GPA) was obtained as its sodium salt: β-Glycerol phosphate disodium salt pentahydrate (Pfaltz & Bauer). The sodium salt of GPA ester with the formula $C_3H_7Na_2O_6P$ is a P-monoester attached to a glycerol group. As shown in Figure 2.1, the functional groups that may contribute to adsorption are the phosphate groups, two sodium bonded oxygens (-ONa), and the glycerol group with two hydroxyls. The -ONa groups in aqueous solution will be ionized to form organophosphate ions $[-O]^-$, which are stronger than hydroxyls -OH in terms of electronegativity.
- Lipoteichoic acid (LTA) is a bacterial cell wall polymer extracted form a Gram-positive bacterium staphylococcus aureus (InvivoGen). As shown in Figure 2.1, LTA is an amphiphilic molecule consists of a lipid tail connected to a disaccharide D-glucose head group and a negatively charged, hydrophilic teichoic acid chain. The teichoic acid chain is a polyphosphodiester with repeated units decorated with D-alanine, glucosamine, and hydroxyl groups. These D-alanine functional groups enable LTA to adhere to a variety of materials including metal oxide surfaces (Wickham and Rice, 2008). The lipid tail with two fatty acid chains acts as the hydrophobic head, while the rest functional components of LTA including the disaccharide head group and the teichoic acid chain attached are

functioning as a hydrophilic tail. Therefore, LTA can form bilayer film in aqueous solution.

- Diphosphoglycerate (DGA) was obtained as its sodium salt: 2, 3-Diphospho-D-glyceric acid pentasodium salt (Sigma-Aldrich) with the formula $C_4H_5Na_5O_{10}P_2$. As shown in Figure 2.1, DGA is a P-monoester that consists of two phosphates connected via a glycerate group. The functional groups for DGA adsorption are two phosphate groups each with two sodium bonded oxygens (−ONa) and a glycerate group with sodium carboxyl group (−COONa). In terms of electronegativity, -COONa group is much stronger than –ONa.
- Distearoyl phosphoglycerol (DGP) was obtained as its sodium salt of 1, 2-Distearoyl-sn-glycero-3-phospho-rac-(1-glycerol) (Sigma-Aldrich) with the formula $C_{42}H_{82}NaO_{10}P$. As shown in Figure 2.1, DGP is a P-diester that has a long lipid tail and a phosphoglycerol. DGP contains a lipid tail with two stearyl groups, one phosphate group bonded to sodium (-ONa), and one glycerol group with two hydroxyls (-OH). The stearyl groups, each of which has an 18-carbon chain of saturated fatty acid, give DGP a relatively large molecular weight 801 g/mol, over two times larger than the other organophosphates studied. It is expected that DGP has relatively low solubility. To ensure no ester precipitated prior to the coprecipitation, the amount of DGP used in the synthesis was much less than for the other coprecipitates.
- Phosphoglycerate (PGA) was obtained as its sodium salt: D-(-)-3-Phosphoglyceric acid disodium salt (Sigma-Aldrich). As shown in Figure 2.1, the P-monoester is the sodium salt of 3-phsphoglyceric acid. PGA consists of a phosphate group and a glycerate group bearing a hydroxyl (-OH) and carboxyl (-COONa).
- Phosphoenolpyruvate (PPA) was obtained as its sodium salt: Phosphoenolpyruvic acid trisodium salt heptahydrate (Alfa Aesar). As shown in Figure 2.1, PPA is a monoester bearing a phosphate group and acrylic acid group with a carboxyl (-COONa). PPA is a metabolite that has been identified in biogenic amorphous calcium carbonate (Akiva-Tal et al., 2011).

2.2.2 Synthesis

Coprecipitates of calcite with organophosphates were synthesized according to a modified seeded constant-addition method. This method is well-established for preparing coprecipitates of dissolved ions with calcite at ambient conditions (Reeder et al., 2000; Shaojun and Mucci, 1993; Tesoriero and Pankow, 1996). Illustrated in Figure 2.2, the synthesis requires a constantly stirring initial solution in a reaction vessel (Pyrex beakers 1L volume) and two different solutions in syringes (Becton Dickinson syringe 100 mL). All solutions were prepared with deionized water. The initial solution contains 700 mL water, 0.8401 g ^{13}C-enriched $NaHCO_3$ (Aldrich), and 1.5 mL of a 60 g/L pre-equilibrated calcite suspension as nucleation seeds prepared from 5μm calcite particles (Alfa Aesar). The first syringe solution contained

0.1mol/L $CaCl_2$, and the second one 0.1mol/L ^{13}C-enriched $NaHCO_3$ plus the organic phosphate as detailed in Table 2.2. The main reaction is best described as:

$$Ca^{2+} + 2HCO_3^- = CaCO_3\,(s) + CO_2\,(g) + H_2O$$

The pH of all solution was adjusted with NaOH and HCl to 8.2 ±0.5, which is the pH of saturated calcite solution equilibrated with air, assessed by VMINTEQ. To minimize the loss of ^{13}C in HCO_3^- during the reaction, $NaHCO_3$ was added to the second syringe solution after the solution was adjusted to basic ($pH \geq 7$). After adding $NaHCO_3$, this syringe solution was adjusted to a pH 8.2.

Both syringe solutions were pumped simultaneously into the reaction vessel at a constant rate of 150 μL/min through check valves. Total reaction time was 540 minutes (9 hours) with consumption of 81 mL solution from each syringe. The coprecipitate was collected through a 0.2 μm membrane filter and rinsed by water. Once collected, the solid coprecipitate was air-dried and stored at −18°C to resist biodegradation.

Inorganic phosphate ions can be incorporated in the calcite surface without forming calcium phosphate phase at low P concentration, typically < 20 $\mu mol \cdot L^{-1}$ (Hinedi et al., 1992a; Plant and House, 2002). However, high phosphorus concentrations (e.g. 50 − 500 $\mu mol \cdot L^{-1}$) promote the precipitation of calcium phosphate phases on the calcite surface, whereas no coprecipitation occurs (Plant and House, 2002). To enable organophosphate coprecipitate with calcite, typical concentration of P dissolved is 9.4 $\mu mol \cdot L^{-1}$ in the reacted solution.

Once the coprecipitation experiment is completed, the reaction vessel will contain 862 mL solution, which consists of the 700 mL initial solution plus two syringe solutions of 81 mL each. To allow the P concentration to be 9.4 $\mu mol \cdot L^{-1}$ in the final reacted solution, the P concentration in the syringe is 100 $\mu mol \cdot L^{-1}$, which results in a typical 1000:1 ratio of Ca/P in the syringe solutions. The target stoichiometric amount of phosphorus is

$$251.1\ \mu g = 81\ mL \times 100\ \mu mol \cdot L^{-1} \times 31\ g \cdot mol^{-1},$$

while the stoichiometric amount of calcium carbonate precipitated is

$$0.81\ g = 81\ mL \times 0.1\ mol \cdot L^{-1} \times 100\ g \cdot mol^{-1}.$$

If assuming all the reaction are stoichiometric, including calcium carbonate precipitation (0.81 g $CaCO_3$) and complete phosphate coprecipitation (251.1×10^{-6} g in phosphorus), the stoichiometric concentration of phosphorus in the solid yielded (0.81 g calcite/phosphate coprecipitate and the 0.09 g calcite seed) is

$$279\ ppm = 251.1 \times 10^{-6}\ g\ /\ (0.81\ g + 0.09\ g) = 279 \times 10^{-6}.$$

The actual estimated P concentrations for each coprecipitate sample are listed in Table 2.2. However, DGP has a low solubility. Experiment for DGP at 1000:1 Ca:P ratio resulted in a

cloudy syringe solution, indicating incomplete dissolution. Reduced concentration of DGP was pumped in to ensure all DGP was fully dissolved in the syringe solution (Table 2.2). The DGP final solution contained 12.8 μm DGP with a Ca/P ratio of 7800:1 in the syringe solutions. The stoichiometric concentration of DGP phosphorus in the solid yielded is 39.7 ppm. The calcite/GPA coprecipitate was prepared with a higher P concentration of 500 $\mu mol \cdot L^{-1}$ in the syringe, resulting in a P concentration 47 $\mu mol \cdot L^{-1}$ in the final reacted solution. The stoichiometric concentration of GPA phosphorus in the solid yielded is 1550 ppm.

2.2.3 NMR

Solid-state NMR experiments were carried out on two spectrometers: a 400 MHz Varian Inova and a 500 MHz three-channel Varian Infinity Plus.

2.2.3.1 CP/MAS

Cross polarization (CP) under the magic-angle spinning (MAS) condition is an effective and ubiquitous technique to study the chemical environment of phosphate. CP can enhance the signal of ^{31}P nuclei by magnetization transfer from ^{1}H, and reduce experimental repetition time to a few seconds. These effects allow ^{31}P spectra to be obtained at low P content. Most $^{31}P\{^{1}H\}$ CP/ MAS experiments were performed on the 400MHz spectrometer. Samples were spun at rates of 3 kHz and 5 kHz if packed in 7.5 mm (o.d.) rotors. Samples packed in 3.2 mm (o.d.) rotors were spun at rates of 5 kHz and 8 kHz. CP/ MAS experiments were generally conducted with 2 ms $^{1}H \rightarrow {}^{31}P$ contact time with a linear ramp of the ^{31}P transverse field. The operating frequencies for ^{31}P and ^{1}H were respectively 161.87 MHz and 399.8 MHz.

2.2.3.2 REDOR

The rotation-echo double-resonance (REDOR) technique was employed to characterize the interaction of the phosphate ester with the coprecipitate crystalline inorganic matrix. $^{31}P\{^{13}C\}$ REDOR is a dipolar recoupling technique that enables the measurement of ^{31}P - ^{13}C dipolar coupling, which is a sensitive function of internuclear distance. The natural abundance of ^{13}C is 1.1%, which could not yield sufficient ^{13}C REDOR signal in this study. Synthesis of ^{13}C enriched calcite in the coprecipitates would greatly increase the REDOR decoupling signal of ^{13}C only from calcite carbonate groups, which makes REDOR feasible to study the calcite/phosphate coprecipitates without effects from C in the organophosphate molecules.

The $^{1}H \rightarrow {}^{31}P\{^{13}C\}$ CP/ REDOR data were collected on the 500 MHz three-channel spectrometer at a spinning rates of 8000 ± 10 Hz. Samples were contained in 4 mm (o.d.) rotors. The REDOR experiments used $^{1}H \rightarrow {}^{31}P$ CP to generate the initial ^{31}P signal, and then applied various ^{13}C dephasing periods ranging from 0.25 to 64 ms. The operating frequencies were

125.7MHz, 202.3MHz, and 499.8MHz for ^{13}C, ^{31}P, and ^{1}H respectively. Typical acquisition conditions include 5 μs ^{1}H 90^{o} pulse, 2 ms $^{1}H \rightarrow ^{31}P$ contact time, 8 μs ^{13}C 180^{o} dephasing pulses, 10 μs ^{31}P re-focusing pulses, and 1 s relaxation delay for 20,000 – 80,000 acquisitions.

2.2.4 SEM/EDX

A LEO Gemini 1550 scanning electron microscope equipped with an EDX (energy dispersive X-ray spectroscopy) detector was used to examine three coprecipitate samples: P-monoester GPA/calcite coprecipitate, P-diester LTA/calcite coprecipitate, and blank/calcite precipitate. The blank/calcite precipitate was prepared with the identical method as other calcite/P coprecipitates, as described in the section 2.2.2, except that no phosphate was added to the syringe solution. Sample powder mounted on the specimen stub was adhered by an electrically conductive double-side tape to perform SEM imaging. Samples were bombarded with a focused beam of electrons, and emitted X-rays. EDX makes use of the X-ray spectrum to analyze the element distribution present in the solid sample surface. In principle, the EDX detector is sensitive to elements from atomic number 4 (Be) to 92 (U). The tape used to adhere samples powder would introduce a very low phosphorus signal in the EDX spectrum. In EDX analysis, detection limits are typically about 0.1% or 1000 ppm, which is much higher than 279 ppm the stoichiometric concentration of phosphate in the calcite precipitate.

2.2.5 BET

Multi-point BET surface area analysis was performed by the Quantachrome NOVA Surface Area Analyzer located in the Aqueous Geochemistry Laboratory of Prof. Martin Schoonen. Two synthetic samples, calcite/GPA coprecipitate, and a blank/calcite precipitate, were studied to obtain information about their specific surface area.

2.2.6 UV-Vis

Ultraviolet–visible spectroscopy (UV-Vis) was applied in an attempt to measure the phosphorus concentration in coprecipitate growth solution. A spectrophotometer (Hach DR/4000 U) located in the Aqueous Geochemistry Laboratory was employed. Samples were collected before, during, and after the coprecipitate experiments, which were filtered with syringe filters (Millipore, 0.2 μm pore size).

2.3 Results

All $^{31}P\{^{1}H\}$CP/MAS spectra of phosphate esters and their corresponding coprecipitates show a relatively broad central band and strong spinning sideband (SSB) effect. Chemical environments of ^{31}P in both organic phosphates and corresponding calcite/Phosphate coprecipitates can be reflected by the measurable and informative NMR parameters such as chemical shift, chemical shift anisotropy, and line widths. All calcite/P-ester coprecipitates yield

strong $^{31}P\{^{13}C\}$ REDOR signals. $^{31}P\{^{13}C\}$ REDOR experiments were performed with and without dephasing pulses to quantify the extent of the dephasing effect. The proportion of dephasing can determine the average value for the dipolar coupling strength, which can be correlated to the internuclear distance between ^{31}P and ^{13}C in the solid samples. Additional analyses such as BET and SEM/EDX were carried out to characterize the solid sample after NMR experiments.

2.3.1 $^{31}P\{^{1}H\}$ CP/MAS

The $^{31}P\{^{1}H\}$ CP/MAS spectra of the phosphoester salts and their calcite coprecipitates are compared in Figures 2.3 – 2.8 and the chemical shift (δ_{iso}) and peak widths summarized in Table 2.3. Figure 2.3 illustrates the $^{31}P\{^{1}H\}$CP/MAS spectra of the sodium salt of GPA ester and calcite/GPA coprecipitate. Two spectra of sodium salt of GPA ester were collected at spinning rates of 3 kHz and 5 kHz. The chemical shifts of sodium salt of GPA ester, given by the position of the central peak, are 6.5 ppm average from 6.4 ppm and 6.6 ppm for the 3 kHz and 5 kHz spectra. These two spectra for the sodium salt of GPA ester have line width (full width at half-maximum; FWHM) of 8.2 and 5.7 ppm, respectively. For the calcite/GPA coprecipitate, two spectra, at spinning rates of 5 kHz and 8 kHz, were collected, indicating one resonance with a chemical shift at 0.7 ppm (5.9 ppm FHWM) and 1.1 ppm (3.7 ppm FHWM), respectively (Table 2.3).

As shown in Figure 2.4, $^{31}P\{^{1}H\}$CP/MAS of the LTA ester and calcite/LTA coprecipitate were collected at several spinning rates. Two spectra of the LTA ester were collected at spinning rates of 5 kHz and 8 kHz. The central peak appears at −4.2 ppm (8.3 ppm FWHM) and −3.9ppm (7.2 ppm FWHM) in the 5 kHz and 8 kHz spectra indicating the chemical shift of LTA ester is −4.1 ppm, from the average of the peak position values. But the difference between the two values is within uncertainty, considering the large peak widths. The spectra of the calcite/LTA coprecipitate, taken at 3 kHz, 5 kHz and 8 kHz, indicate one resonance at −0.8 ppm (7.6 ppm FWHM), −1.5 ppm (8.7 ppm FWHM), and -1.4 ppm (7.0 ppm FWHM), respectively. Large valves in FWHM bring large uncertainty in chemical shift for each spectrum. Additionally, low signal to noise ratio (S/N) of the 3 kHz coprecipitate spectrum further increased the spectral data uncertainty. Considering the smaller uncertainty due to the relatively higher S/N and smaller FWHM from 5 kHz spectrum, a chemical shift of −1.5 ppm in the 5 kHz spectrum is assigned to calcite/LTA coprecipitate.

As shown in Figure 2.5, ^{31}P CP/MAS spectra of the sodium salt of the DGA ester taken at spinning rates of 3 kHz and 5 kHz both show one central peak at 6.4 ppm (5.6 and 6.0 ppm FWHM for 3 kHz and 5 kHz, respectively), whereas the spectra of the calcite/DGA coprecipitate collected at different spinning rates show one resonance with a chemical shift at 1.7ppm, averaged from 2.0 ppm (5.2 ppm FWHM) , 1.7 ppm (5.7 ppm FWHM), and 1.5 ppm (5.2 ppm FWHM) from central peaks at 3 kHz, 5 kHz and 8 kHz, respectively. Considering the

large FWHM, the difference in chemical shift between coprecipitate spectra is within uncertainty.

As shown in Figure 2.6, ^{31}P CP/MAS spectra for the sodium salt of DGP were collected at spinning rates of 3 kHz and 5 kHz, while the CP/MAS spectra for the calcite/DGP coprecipitate were collected at spinning rates of 3 kHz, 5 kHz, and 8 kHz. All spectra show multiple small peaks are shouldering one dominant peak. The 3 kHz spectrum of the sodium salt of the DGP ester shows one main peak at 1.8 ppm (3.8 ppm FWHM) and two small peaks at 6.4 ppm (2.5 ppm FWHM) and −2.3 ppm (3.0 ppm FWHM), while the 5 kHz spectrum shows three central peaks at 5.2 ppm (1.7 ppm FWHM), 0.8 ppm (2.0 ppm FWHM), and 0.8 ppm (4.8 ppm FWHM). Although multiple central peaks were observed in the coprecipitate sample, only the dominate peak was measurable in the coprecipitate spectra due to the large FHWM of peaks and low S/N of spectra. The calcite/DGP coprecipitate yielded a resonance with chemical shift at −1.8 ppm (7.1 ppm FWHM), −2.7 ppm (FWHM 7.8 ppm) , and −2.4 ppm (FWHM 8.3 ppm) from spectra taken at 3kHz, 5kHz, and 8kHz spinning rates, respectively. The chemical shift of coprecipitate is taken to be −2.6 ppm, averaged from 5 kHz and 8 kHz spectra, considering the poor S/N of the 3 kHz spectrum. For comparison, the chemical shift of P was referred to the main peak as it was the only peak measurable on coprecipitate spectra. The chemical shift of DGP ester, given by the position of dominate peak, is 1.3 ppm average from the 1.8 ppm of 3 kHz and 0.8 ppm of 5 kHz (Table 2.3).

As shown in Figure 2.7, ^{31}P CP/MAS of the sodium salt of the PGA ester were collected at spinning rates of 3 kHz and 5 kHz. The chemical shift of PGA ester is 2.9 ppm, averaged from the central peak at 3.0 ppm (FWHM 6.7 ppm) in the 3 kHz spectrum and the central peak at 2.8 ppm (FWHM 5.8 ppm) at 5 kHz. The three spectra obtained for the calcite/PGA coprecipitate show one resonance with a chemical shift at 1.8 ppm, averaged from central peaks at 1.7 ppm (FWHM 4.0 ppm), 1.8 ppm (FWHM 4.5 ppm), and 1.8 ppm (3.8 ppm) in the 3 kHz, 5 kHz, and 8 kHz spectra, respectively (Table 2.3).

As shown in Figure 2.8, the ^{31}P CP/MAS spectra of the sodium salt of the PPA ester show a resonance with a chemical shift at 3.3 ppm, average from peak positions at 3.6 ppm (5.9 ppm FWHM) and 2.9 ppm (6.5 ppm FWHM) under 3 kHz and 5 kHz, respectively. The spectra for calcite/PPA coprecipitate show a resonance with a chemical shift at −2.1 ppm, average from peak positions at −2.0 ppm (2.9 ppm FWHM) and −2.2 ppm (3.7 ppm FWHM) from the 3 kHz and 5 kHz spectra, respectively. The coprecipitate also shows a small additional peak near 2.7 ppm (most evident in the 5 kHz data) that suggests a small amount of the ester hydrolyzed during the experiment.

The isotropic chemical shift (δ_{iso}) for P esters in coprecipitates has narrow range −2.7 to 2.0 ppm; different from that of inorganic phosphates (e.g. orthophosphate) over +3 ppm. In addition, δ_{iso} of P in coprecipitates ranges from −2.2 to 2.0 ppm for P monoesters and −2.7 to

−0.8 ppm for P diester, respectively. Hence, there is no systematic difference between monoester and diester of P.

However, the isotropic chemical shift of phosphorus in calcite/P coprecipitates deviates systematically from P ester salts. For instance, the deviation $\Delta\delta_{iso}$ is – 5.8 ppm of phosphorus site during the GPA coprecipitation, given that the chemical shift 6.5 ppm of GPA ester and 0.7 ppm of calcite/GPA coprecipitate.

$$\Delta\delta_{iso} = \delta_{iso} \text{ (calcite/GPA coprecipitate)} - \delta_{iso} \text{ (GPA ester)}$$

$$= 0.7 \text{ ppm} - 6.5 \text{ ppm} = -5.9 \text{ ppm}$$

Likewise, $\Delta\delta_{iso}$ for LTA coprecipitation is +2.6 ppm, based on the −4.1 ppm of LTA ester and −1.5 ppm of calcite/LTA coprecipitate; $\Delta\delta_{iso}$ for DGA coprecipitation is −4.7 ppm, based on the 6.4 ppm of DGA ester and 1.7 ppm of calcite/DGA coprecipitate; $\Delta\delta_{iso}$ for DGP coprecipitation is −3.6 ppm, based on the 1.3 ppm of DGP ester and −2.3ppm of calcite/DGP coprecipitate; $\Delta\delta_{iso}$ for PGA coprecipitation is −1.1 ppm, based on the 2.9 ppm of PGA ester and 1.8 ppm of calcite/PGA coprecipitate; $\Delta\delta_{iso}$ for PPA coprecipitation is −5.7 ppm, based on the 3.6 ppm of PPA ester and −2.1 ppm from calcite/PPA coprecipitate (Table 2.5). It appears that $\Delta\delta_{iso}$ depends on forms of ester. Accordingly, P esters in this study can be classified into four categories: (i) esters (e.g. DGA, GPA, and PPA) contain two −ONa groups adjacent to phosphate group, which gives a $\Delta\delta_{iso}$ ranges from −5.9 to −4.4 ppm; (ii) ester (e.g. PGA) contains one −ONa group and one −OH group, which gives a $\Delta\delta_{iso}$ ranges from −1.3 to −1.0 ppm; (iii) ester (e.g. LTA) contains one −OH group, which gives $\Delta\delta_{iso}$ ranges from +2.5 to +2.7 ppm; (iv) ester (e.g. DGP) contains one −ONa group, which gives $\Delta\delta_{iso}$ ranges from −3.6 to −3.5 ppm. Each −OH group gives $\Delta\delta_{iso}$ +2.6±0.1 ppm, while each –ONa group contributes −2.9±0.5 ppm of $\Delta\delta_{iso}$. As a consequence, P ester with one −ONa group and one −OH group would be expected to give a $\Delta\delta_{iso}$ = −0.6±0.3 ppm, proximate to $\Delta\delta_{iso}$ of the PGA ester.

2.3.2 ^{31}P Chemical Shift Anisotropy

The chemical shift anisotropy (CSA) is the full tensor values of the chemical shift characterized by three principal components. For ^{31}P in phosphate, the anisotropy parameter ($\Delta\delta$) is a highly useful indicator of chemical environment. It is defined as the largest deviation in chemical shift from the isotropic value, the mean value of the three principal components of the chemical shift tensor. The ^{31}P CSA is sensitive to the symmetry of the electronic environment of the resonating nucleus (Tsai and Chan, 2011). For instance, the more protonated phosphates have larger ^{31}P $\Delta\delta$ because of the larger distortion of the electronic environment, which results a larger deviation from tetrahedral symmetry (Collin, 1966; Turner et al., 1986). The three tensor principal components (δ_{ii}, i=1,2,3) can be calculated from the intensity of the spinning sidebands and the isotropic chemical shift by adopting the method of Herzfeld and Berger (Herzfeld and Berger, 1980). With the convention:

$$\delta_{11} \geq \delta_{22} \geq \delta_{33}$$

From these values the anisotropy can be calculated from:

$$\Delta\delta = \delta_{33} - \tfrac{1}{2} \cdot (\delta_{11} + \delta_{22})$$

The isotropic chemical shift (δiso), which is the position of the central peak, is the average value:

$$\delta_{iso} = 1/3 \cdot (\delta_{11} + \delta_{22} + \delta_{33})$$

All spectra were processed by NMRFIT 5.1, a Lorentzian-Gaussian curve fitting program, to obtain the value of integrated peak intensity and position for each spinning sideband. Each spectrum was fitted to a sum of Gaussian curves, with the constraint that for each phosphorus site the width of the peaks fit to the sidebands equals the width of the central band. This constraint reduces the number of fitting parameters and ensure physically meaningful fitted intensity values. $^{31}P\{^{1}H\}$ CP/MAS spectra of all the samples, including salts of the phosphate esters and their calcite coprecipitates, exhibit strong spinning sidebands (SSB) and a broad sideband envelope indicating significant ^{31}P CSA. The experimentally obtained spectral data are listed in Table 2.3 and 2.4. The CSA of GPA ester (sodium salt) is $\Delta\delta$ = +90 and +103 measured from the 3 kHz and 5 kHz spectrum, respectively, while the CSA of calcite/GPA coprecipitate is $\Delta\delta$ = +105 from 5 kHz spectrum. The sodium salt of the LTA ester has a CSA of $\Delta\delta$ = −156 measured (5 kHz), while the CSA of the calcite/LTA coprecipitate is $\Delta\delta$ = −139 from the 5 kHz spectrum. The CSA of the DGA ester (sodium salt) gives $\Delta\delta$ = +117, averaged from $\Delta\delta$ = +118 (3 kHz) and $\Delta\delta$ = +116 (5 kHz), while the CSA of DGA/calcite yields $\Delta\delta$ = +127 averaged from $\Delta\delta$ = +128 (3 kHz) and +126 (5 kHz). Unlike the other phosphate esters, the DGP ester (sodium salt) yields three central peaks in both the 3 and 5 kHz spectra indicating three phosphorus sites. The main peaks at δ_{iso} = 1.8 ppm (3 kHz) and δ_{iso} = 0.8 ppm (5 kHz) yield $\Delta\delta$ = −171 and −174, respectively. The rest two minor peaks give $\Delta\delta$ = −171 (δ_{iso} = 6.4 ppm) and $\Delta\delta$ = –170 (δ_{iso} = −2.3 ppm) in 3 kHz spectrum and $\Delta\delta$ = −167 (δ_{iso} = 5.2ppm) and $\Delta\delta$ = −154 (δ_{iso} = 0.8 ppm) in 5 kHz spectrum. The spectra of calcite/DGP coprecipitate show one dominant phosphorus site with CSA $\Delta\delta$ = −146 (3 kHz) and −178 (5 kHz). The CSA of the PGA ester (sodium salt) is characterized by $\Delta\delta$ = −126 (3 and 5 kHz), while the CSA of the calcite/PGA coprecipitate gives $\Delta\delta$ = +119, averaged from $\Delta\delta$ = +115 (3 kHz) and +123 (5 kHz). The CSA of PPA (sodium ester) gave an $\Delta\delta$ = +136 (3 and 5 kHz), while the CSA of calcite/PPA coprecipitate is characterized by $\Delta\delta$ = +149, averaged from $\Delta\delta$ = +145 (3 kHz) and +152 (5 kHz).

Notably, the spectra of the DGP ester (sodium salt) show all phosphorus sites share similar CSA value $\Delta\delta$ = −170. All P sites observed in the 3 kHz DGP spectrum show their corresponding $\Delta\delta$ value are nearly identical between the main peak at δ_{iso} = +1.8 ppm with a $\Delta\delta$ = −171 and minor peaks at δ_{iso} = +6.4 and −2.3 ppm with $\Delta\delta$ = −171 and −170, respectively. The main peak of the 5 kHz spectrum at δ_{iso} = +0.8 ppm shows a similar $\Delta\delta$ = −174. The minor peaks

have slightly different Δδ values: Δδ = −167 and −154 at δ_{iso} = +5.2 and +0.8, respectively, Considering the less accurate fitting of 5 kHz spectrum that gives large uncertainty, the differences should be within uncertainty. One minor peak observed in 5 kHz spectrum of DGP ester shares the same chemical shift with the main peak (δ_{iso} = +0.8 ppm), but they are considerably different in CSA. A similar phenomenon was reported in the NMR study of dipalmitoyl lecithin ($C_{40}H_{80}NO_8P$, a phosphodiester similar to DGP $C_{42}H_{82}NaO_{10}P$), of which spectra exhibit different spectral patterns depending upon its water content (Griffin, 1976). DGP ester is originally in a form of lyophilized powder, which is sensitive to moisture and recommended to be stored at −20C^o to store. Collecting NMR data of DGP ester would inevitably expose sample to open air. Noticeably, DGP ester powder became damp and caked while being packed into rotor; even later its particles agglomerated in the rotor and were hard to retrieve after NMR experiment. Conceivably, the water content would be saturated in the DGP ester coprecipitated with calcite under aqueous condition, which was confirmed by the similar spectra of coprecipitate (e.g. 3, 5, 8 kHz in Figure 2.6 and Table 2.3). Although spectra of the calcite/DGP coprecipitate sample appears to show at least two resonances, we are unable to separate these peaks by fitting the curves due to the low S/N ratio and weak signal (low P content in coprecipitate because of the low solubility of DGP). Only a single set of peaks was measured that gives an average Δδ = −162 ppm for the coprecipitate. However, a similar chemical shift of the P resonance indicates a consistent chemical environment of phosphorus nuclei in the coprecipitate. Therefore, we conclude the minor spectral differences in chemical shift and CSA between 3 kHz and 5 kHz spectra of DGP ester reflect different amounts of water content due to its deliquescent behavior.

For the calcite/PGA coprecipitate, the CSA of the P site appears reversed from that in the PGA ester. This is clearly reflected in the difference in appearance of the SSB patterns in Figure 2.7. The PGA ester has a CSA of Δδ = −126, but becomes positive as Δδ = +119 in the coprecipitate. According to MSDS, PGA ester contains one –ONa and one –OH group linking with phosphate. It would be expected that partially protonated PGA ester exhibits a similar NMR characteristics with phosphodiester due to the structural asymmetry, whereas PGA ester in solution would be fully deprotonated like other monoesters. A detailed analysis of the SSB pattern of PGA ester and PGA/calcite coprecipitate confirms the speculation as described in Section 2.4.3

2.3.3 $^{31}P\{^{13}C\}$ REDOR

The $^{31}P\{^{13}C\}$REDOR experiments were performed in two steps. First, a reference spectrum containing signal from all phosphorus species (S_0) is produced without dipolar recoupling. Second, a recoupled spectrum (S) is produced through dipolar recoupling with ^{13}C nuclei by applying 180^o ^{13}C pulses. In the second step, peaks of phosphorus species close to ^{13}C nuclei (within 4 Å) are attenuated compared to the reference spectrum S_0. The amount of attenuation depends on the strength of the dipolar coupling and the length of the dephasing

period, and should approach 100% at long dephasing time for P with several ^{13}C nuclei nearby. The attenuation of spectral peaks in the ^{13}C-recoupled spectrum is quantified by the difference $\Delta S = (S_0 - S)$. In relative terms, the REDOR fraction is used $\Delta S/S_0$ (Table 2.5). Varying the length of the REDOR dipolar evolution period by $n \cdot \tau_{rotor}$, where n is the number of rotor periods and τ_{rotor} is the rotor period, can provide information on the internuclear distance and the strength of dipolar coupling. Dephasing curves for each coprecipitate are shown in Figure 2.9, which are based on the evolution time ($T = \tau_{rotor} \times n$) and the REDOR fraction ($\Delta S/S_0$). All $^{31}P\{^{13}C\}$ REDOR experiments were implemented with 8kHz spinning rate (τ_{rotor} is 0.125 ms).

All calcite/organophosphate coprecipitate samples yielded sufficient REDOR signal in the $^{31}P\{^{13}C\}$REDOR experiments, as shown for typical REDOR sets at intermediate dephasing in Figures 2.10 – 2.15, whereas no REDOR experiments were attempted for the organophosphate esters and salts because of the low natural ^{13}C abundance. Spectral data from REDOR experiments are summarized in Table 2.5 and plotted in Figure 2.9. Notably, small esters such as DGA, GPA, PGA, PPA give similar dephasing effect as orthophosphate in coprecipitate, but build up slower. Little difference (e.g. position and width) was observed between non-dephased spectra (S_0) and difference spectrum ($S_0 - S$) of each coprecipitate. The difference spectrum contains signal only from P in close proximity to carbonate C.

2.3.4 SEM/EDX

The morphology of calcite precipitated with and without organic phosphate was examined by scanning electron microscopy (SEM). SEM micrographs of several samples including calcite/blank precipitate, calcite/GPA coprecipitate, and calcite/LTA coprecipitate are shown in Figure 2.16. To quantify the elements present in the calcite surface energy dispersive x-ray spectroscopy (EDX) has been carried out along with SEM analysis.

The SEM micrographs show calcium carbonate precipitated as crystalline aggregates whose morphology and shape were modified slightly by the presence of phosphate esters (Figure 2.16). All samples appear to be calcite rhombohedra in a wide range of sizes. However, minor morphology changes were found in coprecipitate samples. The calcite/blank experiment yielded pure calcite as rhombohedral crystals shown in Figure 2.16 A) and B), which have smooth (white) faces and clear edges. The calcite/GPA coprecipitate sample in Figure 2.16 C) and D) appears to be calcite rhombohedra with smooth faces but with slightly jagged edges. The calcite/LTA coprecipitate in Figure 2.16 E) and D), however, has a more "corroded" appearance: with jagged edges and coarse (dark) faces. The sizes of aggregated particles in the LTA/calcite sample appears to have a wider range but generally smaller than both the blank/calcite and GPA/calcite sample.

The EDX spectroscopy can show the presence of carbon, calcium, oxygen, and phosphorus in sample. Nearly identical EDX spectra were obtained from all the samples including the pure calcite (Figure 2.17 top) and calcite coprecipitated with phosphate monoester

GPA (Figure 2.17 middle) and diester LTA (Figure 2.17 bottom). The pure calcite sample yielded a small P signal (Figure 2.17 top) as we expected, which arises from phosphorus in the electrically conductive tape. Although coprecipitate samples contain phosphorus, the intensities of their phosphorus signals appear to be the same as the pure calcite, even for the calcite/GPA sample (Figure 2.17 middle) whose stoichiometric amount of P 1395 ppm is slightly higher than the detection limit 1000 ppm of EDX. No difference was detected in the EDX spectra since their distribution patterns of compositional element are the same. The EDX spectra show that organic phosphates are not coating the crystal surfaces and therefore must be occluded in the crystal structures.

2.3.5 BET

Two samples were tested to obtain their specific surface area by BET analysis: a calcite/GPA coprecipitate sample and a calcite/blank precipitate sample prepared with the same experimental method as the coprecipitate but without the presence of phosphate ester in the anion syringe. The result shows specific surface areas of 0.958 m^2/g with correlation coefficient R = 0.994024 for the calcite/GPA coprecipitate and 1.09 m^2/g with R = 0.997962 for the blank sample, which indicates no significant difference with the specific surface area of calcite coprecipitated with the GPA phosphate ester.

2.3.6 UV-Vis

Unlike inorganic phosphates (e.g. orthophosphate), organic phosphates in solution require decomposition of organic compounds, such as by adding potassium persulfate and heating solution, to allow UV-Vis analysis. However, adding persulfate would raise solution pH. Although it is possible to add basic solution, such as NaOH, to offset the increase of solution pH, the volume of solution would inevitably be increased. The additional steps treating organic phosphate would increase the handling error, particularly for the near detection-limit measurements in this study. Alternative methods, such as calibrating the reading by serial dilution of each organophosphate, are not investigated further.

2.4 Discussions

2.4.1 Structural integrity of organophosphates in calcite coprecipitate

Each coprecipitate sample yields signal in ^{31}P CP/ MAS NMR, indicating the solid coprecipitate contained a sufficient amount of phosphate for NMR detection. Comparing the spectra of coprecipitates and their corresponding organophosphate either as a sodium salt or in the acid form, we found a systematically lower chemical shift by several ppm (5.9 to 1.0 ppm) between the sodium salt of P ester and the corresponding calcite coprecipitate, whereas the ^{31}P chemical shift was increased by 2.7 ppm between the acid form of LTA and its corresponding coprecipitate. In general, we found no systematic variations in ^{31}P peak width listed in Table 2.4

between organophosphate and the corresponding coprecipitate. These FWHM values, which are affected by both the strength of $^{31}P - {}^{1}H$ dipolar coupling and heterogeneity of structural environments, are not discussed further. Results for PGA, with one OH and one ONa, were intermediate, showing only a small decrease in chemical shift of about 1 ppm. These findings are similar to trends for orthophosphates where chemical shifts decrease with increasing electronegativity of the cation and protonation, leads to further decrease of several ppm (Turner et al., 1986). This result is consistent with bonding by Ca in the coprecipitates.

In addition, strong intensities of SSBs were observed in all ^{31}P CP spectra of coprecipitates that are similar to those of the ester salts and yield information on chemical shift tensors. In particular we focus on the anisotropy ($\Delta\delta$) of CSA, which reflects the symmetry in the bonding environment of the phosphate group. As shown in Table 2.4, relatively minor differences were found between the $\Delta\delta$ of as-received P esters and the corresponding calcite coprecipitates. The one exception is PGA. The salt of PGA gives a negative $\Delta\delta$ (−126 ppm) that is similar in magnitude to the positive values for the rest monoesters, which ranges from +90 ppm to +136 ppm. For comparison, orthophosphate gives much smaller SSB intensities reflecting its much smaller CSA from a more symmetrical bonding environment (Turner et al., 1986). However, $\Delta\delta$ of PGA coprecipitate (+123 ppm) is within the range for the other monoester coprecipitates (+90 ppm to +152 ppm). This anomaly is likely related to the mono-protonated nature of the Na-salt of PGA. Protonation is known to have a large effect on the ^{31}P CSA (Pourpoint et al., 2007; Rothwell et al., 1980; Turner et al., 1986). Nonetheless, similar values in $\Delta\delta$ for the ester salts and coprecipitates (and magnitude for PGA) suggests that $\Delta\delta$ is mainly influenced by C−O−P bonding environment and provides evidence that organophosphates were incorporated structurally intact in the coprecipitates.

2.4.2 Incorporation of organophosphate in calcite coprecipitate

All coprecipitate samples have yielded dephasing signal in $^{13}P\{^{13}C\}$ REDOR experiments, demonstrating a proximity between ^{31}P and ^{13}C of carbonate groups. Organophosphate ester is the only source of phosphorus in the coprecipitates. Although both organophosphate and calcite contain ^{13}C, they have much different isotopic content. Isotopically normal organophosphate only contains 1.1% ^{13}C in carbon due to its low abundance in nature, while the solid coprecipitates were synthesized with ^{13}C-enriched sodium bicarbonate of 98 atom % ^{13}C. Since at natural abundance the ^{13}C in carbon is too low to yield a detectable REDOR effect on the weak ^{31}P signal (at most, a few % decrease at full dephasing), the REDOR technique can exclusively measure the dipolar coupling between ^{31}P in organophosphate and ^{13}C from calcite carbonate groups. In the REDOR experiments, the $^{31}P - {}^{13}C$ internuclear distances are reflected in the proportion of dephased signal through dipolar coupling. The ^{13}C dephasing pulse in REDOR leads to $^{31}P - {}^{13}C$ dipolar recoupling, which results in a reduction in the intensity of the ^{31}P-observed spectrum. We observed a reduction in the dephased spectrum (S) compared with the spin echo spectrum (S_0) without dephasing pulses (Figures 2.10 − 2.15 and

Table 2.5), which indicates a close proximity between ^{13}C-bearing carbonate and ^{31}P-bearing phosphate (within about 4 Å) (Mason et al., 2011). The observation of such large REDOR fractions requires multiple $^{31}P - ^{13}C$ pairs within such short distances, demonstrating that the organophosphates occur in the structure of the carbonate phase. Substantial extent of dephasing in the REDOR spectra for all coprecipitates including LTA, which has a large molecular weight (1573 $g \cdot mol^{-1}$) and DGP which has long hydrocarbon chains, indicates that all organophosphates in the coprecipitates are structurally incorporated.

Additionally, the collected REDOR data is sufficient to extrapolate the dephasing curves for all calcite/organophosphate coprecipitate (Figure 2.9). In Figure 2.9 and Table 2.5, the varied dephasing time and proportions of dephasing (REDOR fraction, $\Delta S/S_0$) was used to evaluate the $^{31}P - ^{13}C$ dipolar coupling strength, which correlates to the sum of inverse cubed internuclear distance of $^{31}P - ^{13}C$. More ^{13}C nuclei adjacent to ^{13}P and shorter distances of $^{31}P - ^{13}C$ will lead a stronger $^{31}P - ^{13}C$ dipolar coupling, allowing a faster increase of REDOR fraction with evolution time (T). We found that the highest dephasing rates were yielded by the coprecipitates with small organophosphate, whereas those coprecipitates for large P ester such as DGP and LTA yielded lower dephasing rates. The lower dephasing rate for the coprecipitates with large organophosphate indicates fewer neighboring carbonate groups and/ or longer $^{31}P - ^{13}C$ distances.

REDOR data for the organophosphate coprecipitates can be compared to those of orthophosphate/calcite coprecipitate obtained from a previous work in our group (Kubista, 2011). The REDOR dephasing curves for orthophosphate coprecipitate is similar to those samples coprecipitated with small organophosphates such as GPA, DGA, PGA, and PPA, indicating a similar dephasing behavior. The dephasing rate for the orthophosphate coprecipitate is similar to that calculated by Mason et al. (2011) for P surrounded by 6C in a distance of 3.2 Å if phosphate substitutes for a carbonate group in calcite. Similar dephasing behaviors indicates that orthophosphate and small organophosphates act as a structural defect in coprecipitates that occupies environments similar to that of carbonate groups. More structural disruption around a phosphate defect would be expected in order to accommodate the long hydrocarbon chains and bulky structures of LTA and DGP (Figure 2.1), which can be expected to lead to fewer adjacent carbonate (^{13}C) near phosphate and/ or longer $^{31}P - ^{13}C$ distances. Still, LTA and DGP coprecipitates yielded considerable REDOR effects, indicating a close proximity to at least some carbonate groups and hence that they are occluded in the calcite structure.

2.4.3 Spectral differences between coprecipitated P monoesters and diester

^{31}P NMR shows distinct difference in the range of chemical shift anisotropy $\Delta\delta$ between coprecipitated phosphomonoesters and phosphodiesters that could be useful in analysis of natural materials. Significant difference between the monoester and diester coprecipitates was found in the chemical shift anisotropy $\Delta\delta$ of the CSA. The $\Delta\delta$ of coprecipitated monoesters are all positive, ranging in value from +105 to +152 ppm. Conversely, the coprecipitated diesters gave negative values from $\Delta\delta = -178$ to -139 ppm. The differences in $\Delta\delta$ values can differentiate monoester

from diester in coprecipitates based on whether Δδ exhibits a positive or negative value. The difference in Δδ between coprecipitated mono- and diester reflects disparity of local chemical environment and symmetry of phosphate bonded to one or two carbon atoms, since the other oxygens are likely bonded to Ca^{2+}.

Difference in Δδ value between P monoester and diester coprecipitates is easily recognized in the SSB pattern, which would be expected as the Δδ value is measured from the relative intensity of SSBs and the central band. As listed in Table 2.5, the values of the intensity of first SSB on each side of central band demonstrate a systematic difference between coprecipitates based on the P ester type (e.g. monoester, diester). For monoesters, compared to the first SSB(+) on the left side of central band, the intensity of the first SSB(−) on the right side is larger for each monoester coprecipitate and smaller for each diester coprecipitate. Therefore, comparing the relative intensity of the first SSB the chemical shift anisotropy (Δδ) provides a useful method to distinguish between phosphoesters in coprecipitate. This could be useful because 5 kHz is a convenient spinning rate for obtaining spectra for components at low concentration. At this spinning rate, the intensity of the ±1 SSB are comparable to that of the central peak and the distinction between mono- and diesters appears unambiguous.

2.4.4 Spectral differences between organic and inorganic phosphates in calcite

Previous study on inorganic orthophosphate in synthetic and natural calcite shows ^{31}P isotropic chemical shift ranges from 3.1 to 3.6 ppm (Akiva-Tal et al., 2011; Kubista, 2011; Mason et al., 2007), and weak SSBs that are barely noticeable at a 5 kHz spinning rate. The small SSB indicates that chemical shift anisotropy for orthophosphate coprecipitates are nominal, similar to crystalline Ca-orthophosphates in which the PO_4^{3-} group is not protonated (Kubista, 2011; Mason et al., 2007). Comparing with orthophosphate, organophosphates coprecipitated with calcite show a distinct range of the δ_{iso} and Δδ in ^{31}P NMR. As described in Section 2.4.3, the $\delta_{P\text{-}31}$ of these coprecipitated phosphoesters ranges from −2.7 ppm to 2.0 ppm, which does not overlap the value of inorganic orthophosphate coprecipitated with calcium carbonate minerals (e.g. calcite, aragonite) nor with the major peaks observed in the Christmas Island (Kubista, 2011) or alpine speleothem samples (Mason et al., 2007). Although the Δδ values of organic P in coprecipitates varies somewhat, all organophosphates yield CSA in absolute value (range: 105 – 178, Table 2.4), which is much larger than inorganic phosphate in coprecipitate. These Δδ values result in large SSB manifolds in which the intensity of one of the first SSBs is comparable to that of the center band at a 5 kHz spinning rate, in clear contrast to calcite/ orthophosphates.

2.4.5 Additional evidence from surface area analysis and SEM/EDX

No significant difference in specific surface area between calcite and calcite/ organophosphate coprecipitate as measured with the BET gas adsorption method. Furthermore, the surface areas are modest and too low to account for all of the coprecipitated organophosphate

as surface adsorbates. Assuming all phosphate molecules are adsorbed on the calcite surface and calcite is completely precipitated, the calcite/ GPA coprecipitate would bear 41.7 $\mu mol \cdot m^{-2}$ (28 GPA molecules per nm^2). Study on adsorption isotherm of phosphates on calcite surface indicates the maximum adsorption amounts for phytic acid (organic phosphate) and inorganic orthophosphate are 17.8 $\mu mol \cdot m^{-2}$ and 1.4 $\mu mol \cdot m^{-2}$, respectively(Celi et al., 2000). SEM/EDX shows no marked difference in element compositions including phosphorus between coprecipitate and similarly prepared calcite surface, indicating no significant concentration of P at the surface of the coprecipitates. Taken together, the BET and EDX results are consistent with location of much of the coprecipitated P in crystal interiors, rather than on particle surfaces.

Optical information from SEM shows that the bulky diester LTA molecule with long hydrocarbon chains has a stronger influence on calcite morphology than the small monoester GPA, which could be related to the different inhibition effect by organophosphates (Chalmin et al., 2013). During precipitation, adsorbed organophosphate can block the crystal growth sites and inhibit the crystal growth. Larger molecular structure of phosphate (e.g. LTA) brings calcite coprecipitate a stronger structural disruption and more blocked growth sites, leading to fewer ^{13}C carbonate groups neighboring phosphate ^{31}P and possibly longer ^{13}C – ^{31}P distances, which is consistent with the REDOR result. Biominerals usually have distinctive morphology, such as needle-fiber calcite of microbial origin (Verrecchia and Verrecchia, 1994). The fact that organic phosphate alters the calcite morphology supports the general concept that presence of organic molecules including those directly involved in biomineralization, but also other dissolved molecules can alter crystal morphology during crystallization.

2.4.6 Model of organophosphates incorporation in calcite

Chalmin et al. (2013) proposed an insertion mechanism for large organic molecules during calcite precipitation that organic matter humic acid could be entrapped in calcite by the layered structure forming on calcite surface (Chalmin et al., 2013), which can be compared to the present results for the formation of organophosphate/calcite coprecipitate. According to this model, organic matter would preferably adsorb on the positively charged calcite surface due to its numerous negatively charged hydrophilic groups (e.g. hydroxyl, carboxyl, phosphate) (Fenter et al., 2000). Such molecules may also bind aqueous ions such as Ca^{2+} into a dissolved complex (Cotmore et al., 1971), which could be adsorbed and eventually entrapped by 2D-island mono-molecular layers forming on the surface of calcite (Ruiz-Agudo et al., 2011). This insertion behavior was proposed for many other large organic molecules such as amino acids, aminopolyphosphonate benzenepolycarboxylic acid, and polysaccharide in either synthetic or biogenic calcite (Abdel-Aal and Sawada, 2003; Amjad, 1987; Henriksen et al., 2004; Orme et al., 2001), although no direct spectroscopic evidence was presented for intimate association of those molecules with components of the calcite matrix. Therefore, we postulate that incorporation for both organophosphates and inorganic orthophosphate in our study can be described as embedment in the layered structure of calcite coprecipitate.

Accordingly, phosphate was occluded in the structural layers forming on the coprecipitate surface. Intimacy between phosphate group of phosphate and carbonate of structural layers can reasonably be expected to depend on the size and hydrophilic property of the molecule beyond the phosphate group. Compared with phosphomonoesters, the studied phosphodiesters (e.g. DGP, LTA) have much larger molecular structures with lengthy hydrocarbon chains and fewer hydrophilic groups adjacent to phosphate groups, which can deter ^{13}C bearing carbonate to form structural layers in the neighborhood of the phosphate groups. The smaller phosphomonoesters with more hydrophilic groups adjacent to phosphate and much smaller structures more closely resemble the inorganic orthophosphate in ^{31}P chemical environment, causing less disruption to the layered structural layer. As a consequence, the bulky organophosphodiesters bring fewer ^{13}C adjacent to ^{31}P and longer $^{31}P - ^{13}C$ distances, which gives relatively weak $^{31}P - ^{13}C$ dipolar coupling to allow REDOR NMR to differentiate the bulky P diesters from monoesters.

2.5 Conclusion and Perspective

The main contribution of the present study is to provide a methodology for using ^{31}P NMR to obtain structural information of phosphorus present at low concentration in calcite. This study shows conclusively that large organophosphate molecules can be incorporated into calcite with intact structure around the phosphate group and close proximity to carbonate groups of calcite structure, which is consistent with similar investigations studying incorporation of citrate and humic acid in calcite structure (Chalmin et al., 2013; Phillips et al., 2005). The successful coprecipitation of organophosphate with calcite contributes to the understanding that dissolved organic matter can be coprecipitated with calcium carbonate mineral. Calcite precipitated in nature such as speleothem carbonate and palustrine carbonate can include P. Therefore, P detected in carbonate minerals can be present in several different forms and spectroscopic methods are needed to distinguish them. The ^{31}P NMR spectra present here reveal significant differences (e.g. chemical shift, chemical shift anisotropy, spinning sidebands) between different phosphate esters occluded in the calcite structure, providing a spectroscopic method to determine the speciation of low-concentration phosphorus in carbonate minerals.

2.6 Tables

Table 2.1 Organophosphates used in this study including abbreviation, ester type, full name, molecular formula, CAS (Chemical Abstracts Service) serial number, and supplier.

Abbr	Ester	Molecular Formula (with hydrate)	CAS#	Supplier
GPA	Mono-	$C_3H_9Na_2O_6P \cdot 5H_2O$	819-83-0	Pfaltz & Bauer
LTA	Di-	$C_{63}H_{119}N_2O_{36}P_3$	56411-57-5	InvivoGen
DGA	Mono-	$C_3H_3Na_5O_{10}P_2$	102783-53-9	Sigma-Aldrich
DGP	Di-	$C_{42}H_{82}NaO_{10}P$	200800-42-8	Sigma-Aldrich
PGA	Mono-	$C_3H_5Na_2O_7P$	80731-10-8	Sigma-Aldrich
PPA	Mono-	$C_3H_2Na_3O_6P \cdot 5H_2O$	5541-93-5	Alfa Aesar

Table 2.2 Phosphate Preparation for Sample Synthesis
Except for LTA, all the P-esters listed above are in the form of sodium salt.

M.W represents the molecular weight. Me.W stands for the measured weight. Ester (μM) represents the concentration of phosphoester in the syringe solution, while the Phosphorus (μM) represents the total concentration of phosphorus. P/M is the number of phosphorus per phosphoester molecule. Ca:P is the mole ratio for calcium and phosphorus added from syringe solutions. ppm (P) was referred as weight ratio between phosphorus and calcite precipitate which was based on the assumption that cation calcium and anion carbonate were fully reacted to form calcite matrix. 1 μM=1×10^{-6} mol/L; 1$\mu g_{(P)}$ /g represents 1 μg phosphorus in 1 gram calcite.

	M.W(g/mol)	Me.W(g)	Ester	P/M	Phosphorus	Ca:P	$\mu g_{(P)}$/g
GPA	306.12	0.0153	499.8 μM	1	499.8 μM	200: 1	155×10
LTA	1572.68	0.005	31.8 μM	3	95.4 μM	1000:1	296
DGA	375.95	0.00189	50.3 μM	2	101 μM	1000:1	313
DGP	801.66	0.001025	12.8 μM	1	12.8 μM	7800:1	39.7
PGA	230.02	0.00229	99.6 μM	1	99.6 μM	1000:1	309
PPA	360.09	0.0032	88.9 μM	1	88.9 μM	1100:1	276

Table 2.3 Peak positions (δ_{iso}) and widths (FWHM), and differences (e.g. $\Delta\delta_{iso}$, ΔFWHM) between $^{31}P\{^{1}H\}$CP/MAS NMR spectra for the organophosphate salt and its calcite coprecipitate. Difference in FWHM between organophosphate and its coprecipitate is calculated by ΔFWHM = FWHM(δ_P, coprecipitate) – FWHM (δ_P, organophosphate). Estimated uncertainties are given as the error in the last digit.

[1]Due to the interference of the overlapping sidebands in coprecipitates (Figure 2.4 & 2.6), value of peak width may be not accurate and $\Delta\delta_{iso}$ is measured according to the [2]dominant peak.
[3]As described in Table 2.4, spectra of DGP and its coprecipitate show multiple overlapping resonances. These resonances consist of one dominant peak and shouldering weak peaks, making it too complicated to separate them. Therefore, those resonances were measured as one peak, which considerably increased the uncertainty of FWHM values.
*Because of the reasons[1,3] listed above, these values are omitted and excluded in the discussion.

Organophosphate (spinning rate)	δ_{iso} (ppm)	FWHM (ppm)	coprecipitate (spinning rate)	δ_{iso} (ppm)	FWHM (ppm)	$\Delta\delta_{iso}$ (ppm)	ΔFWHM (ppm)
GPA			calcite/ GPA				
(3 kHz)	6.4(4)	8.2(4)	(3 kHz)				
(5 kHz)	6.6(2)	5.7(2)	(5 kHz)	0.7(4)	5.9(3)	-5.9	0.2
(8 kHz)			(8 kHz)	1.1(3)	3.7(2)		
LTA			calcite/ LTA				
(3 kHz)			(3 kHz) [1]	-0.8(9)	7.6(2)		
(5 kHz)	−4.2(5)	8.3(3)	(5 kHz)	-1.5(5)	8.7(3)	2.7	0.5
(8 kHz)	−3.9(3)	7.2(2)	(8 kHz)	-1.4(5)	7.0(1)	2.5	-0.2
DGA			calcite/ DGA				
(3 kHz)	6.4(3)	5.6(2)	(3 kHz)	2.0(5)	5.2(2)	-4.4	-0.4
(5 kHz)	6.4(3)	6.0(1)	(5 kHz)	1.7(3)	5.7(2)	-4.7	-0.3
(8 kHz)			(8 kHz)	1.5(3)	5.2(1)		
DGP			calcite/ DGP[3]				
(3 kHz)	6.4(4)	2.5(3)	(3 kHz)	-1.8(9)	7.1(5)[1]	-3.6[2]	*
	1.8(3)[2]	3.8(2)					
	-2.3(4)	3.0(4)					
(5 kHz)	5.2(3)	1.7(2)	(5 kHz)	-2.7(8)	7.8(5)[1]	-3.5[2]	*
	0.8(3)[2]	2.0(1)					
	0.8(5)	4.8(4)					
(8 kHz)			(8 kHz)	-2.4(8)	8.3(4)		
PGA			calcite/ PGA				
(3 kHz)	3.0(3)	6.7(3)	(3 kHz)	1.7(3)	4.0(2)	-1.3	-2.7
(5 kHz)	2.8(2)	5.8(2)	(5 kHz)	1.8(2)	4.5(3)	-1.0	-1.3
(8 kHz)			(8 kHz)	1.8(4)	3.8(2)		
PPA			calcite/ PPA				
(3 kHz)	3.6(5)	5.9(3)	(3 kHz)	-2.0(6)	2.9(2)	-5.6	-3.0
(5 kHz)	2.9(5)	6.5(2)	(5 kHz)	-2.2(7)	3.7(1)	-5.1	-2.8
(8 kHz)			(8 kHz)				

Table 2.4 Spectral characteristics of P-esters and P-ester/calcite coprecipitates from ^{31}P {^{1}H} CP/MAS spectra at different spinning rates. Uncertainties are given as the error in the last digit. 3k, 5k,and 8k represent spinning rates of 3, 5, and 8 kHz, respectively. [1]Spectra of DGP/calcite coprecipitate show multiple overlapping peaks in a relatively low S/N of signal, which makes it difficult to analyze NMR characteristics for each peak individually. Only information of the dominant peak is listed below.

	Intensity of spinning sideband (SSB) and central band in %															Chemical shift tensor information				
	SSB +7	SSB +6	SSB +5	SSB +4	SSB +3	SSB +2	SSB +1	central	SSB -1	SSB -2	SSB -3	SSB -4	SSB -5	SSB -6	SSB -7	δ_{iso} (ppm)	D11	D22	D33	Δδ
GPA 3k				2.6	4.4	13.0	9.2	23.5	36.9	8.2	2.2					+6.4(5)	68(8)	−24(6)	−24(3)	+92(10)
GPA 5k						6.0	14.5	48.2	28.0	3.3						+6.6(3)	75(4)	−19(3)	−36(2)	+103(5)
GPA (Avg)																+6.5	71.5	−21.5	−30	+97
GPA/calcite 5k					2.4	7.8	15.0	44.7	26.0	4.0						+0.7(5)	71(5)	−19(4)	−50(2)	+105(7)
GPA/calcite 8k						5.2	11.2	62.2	18.9	2.4						+1.1(3)				
GPA/calcite (Avg)																+0.9	71	−19	−50	+105
LTA 5 k					3.6	12.1	31.0	21.0	15.2	12.5	4.6					−4.2(5)	78(4)	18(2)	−108(2)	−156(5)
LTA 8 k						4.4	27.1	44.9	16.8	6.8						−3.9(3)				
LTA (Avg)																−4.1	78	18	−108	−156
LTA/calcite 5k					3.0	8.9	29.3	25.9	16.4	12.1	04.4					−1.5(5)	73(4)	17(3)	−94(2)	−139(5)
LTA/calcite 8k						4.8	27.0	43.1	17.0	8.1						−1.4(5)				
LTA/calcite (Avg)																−1.5	73	17	−94	−139
DGA 3k		0.17	0.97	3.4	7.6	14.4	7.4	15.3	29.0	16.5	4.1	1.0				+6.4(3)	85(3)	−18(2)	−47(2)	+118(4)
DGA 5 k				0.27	1.5	9.2	14.7	38.9	30.0	4.7	0.72					+6.4(3)	84(2)	−20(2)	−45(1)	+116(3)
DGA (Avg)																+6.4	84	−19	−46	+117
DGA/calcite 3k			1.6	4.1	7.3	12.5	6.8	15.1	25.2	19.3	6.4	1.6				+2.0(5)	87(5)	−23(4)	−58(2)	+128(6)
DGA/calcite 5k				0.51	2.8	10.6	14.0	34.1	30.8	6.1	1.1					+1.7(3)	86(3)	−40(2)	−40(1)	+126(4)
DGA/calcite 8k						4.5	12.1	62.6	19.2	1.6						+1.5(3)				
DGA/calcite (Avg)																+1.7	86	−32	−49	+127
DGP 3k			0.1	0.4	1.0	1.4	1.4	1.0	0.8	0.6	0.7	0.7	0.5	0.3	0.1	+6.4(4)	93(4)	34(2)	−17(1)	−171(5)
			1.4	**4.1**	**7.8**	**10.2**	**9.3**	**8.5**	**6.4**	**3.3**	**5.9**	**4.6**	**3.4**	**1.5**	**0.7**	**+1.8(3)**	**91(2)**	**26(2)**	**−112(1)**	**−171(2)**
			0.5	1.2	2.6	4.6	2.6	2.8	1.9	1.8	2.2	2.1	1.2	0.5	0.0	−2.3(4)	81(5)	28(4)	−116(2)	−170(6)
DGP 5k					0.4	1.6	4.4	2.4	1.4	1.6	0.8	0.1				+5.2(3)	80(3)	41(2)	−106(1)	−167(4)
					2.6	**8.3**	**18.1**	**10.3**	**7.8**	**8.3**	**3.8**	**1.3**				**+0.8(3)**	**90(2)**	**28(1)**	**−116(1)**	**−174(2)**
					0.2	2.4	7.7	6.1	3.6	3.6	2.5	0.6				+0.8(5)	80(4)	24(3)	−102(2)	−154(5)
DGP (Avg)																+1.3	90	27	−114	−172
DGP/calcite 3k[1]				4.8	11.2	16.9	16.1	14.5	9.7	7.6	12.1	7.1				−1.8(9)	79(9)	15(8)	−68(6)	−146(14)
DGP/calcite 5k[1]					2.8	14.0	26.8	18.9	12.1	16.0	7.0	2.3				−2.7(8)	90(7)	23(8)	−121(4)	−178(9)
DGP/calcite 8k[1]						4.7	26.4	42.0	17.8	9.0						−2.4(8)				
DGP/calcite (Avg)																−2.6	85	19	−94	−162
PGA 3k			0.69	2.9	7.8	15.3	18.2	15.6	12.8	10.4	9.16	4.7	2.0	0.57		+3.0(3)	78(4)	12(2)	−81(3)	−126(5)
PGA 5k					2.0	8.2	27.2	29.7	18.7	9.8	3.3	1.1				+2.8(2)	75(2)	15(2)	−81(1)	−126(3)
PGA (Avg)																+2.9	76	14	−81	−126
PGA/calcite 3k				3.2	7.2	14.5	7.3	16.5	30.8	17.1	3.5					+1.7(3)	79(3)	−25(3)	−48(1)	+115(4)
PGA/calcite 5k					1.8	10.2	13.9	36.0	32.1	5.2	0.81					+1.8(2)	84(3)	−39(3)	−39(2)	+123(5)
PGA/calcite 8k						3.7	11.6	65.2	19.5							+1.8(4)				
PGA/calcite (Avg)																+1.8	82	−32	−44	+119
PPA 3k	0.23	0.73	2.0	5.5	8.7	12.8	4.6	13.4	23.3	20.8	6.0	1.4	0.5			+3.6(5)	94(6)	−28(5)	−56(3)	+136(8)
PPA 5k					2.8	12.0	13.4	29.2	34.5	6.9	1.3					+2.9(5)	94(5)	−32(3)	−53(2)	+136(6)
PPA (Avg)																+3.3	94	−30	−54	+136
PPA/calcite 3k			2.1	6.5	8.1	11.4	4.0	13.3	21.4	23.5	8.4	1.6				−2.0(6)	95(4)	−39(5)	−62(2)	+145(7)
PPA/calcite 5k				1.7	3.9	13.7	11.3	23.4	35.2	9.3	1.4					−2.2(7)	99(5)	−42(4)	−63(2)	+152(7)
PPA/calcite (Avg)																−2.1	97	−41	−62	+148

Table 2.5 REDOR proportion of dephasing ($\Delta S/S_0$) for different evolution time (T).
[1]REDOR data of orthophosphate (OthroP) calcite coprecipitates was obtained from a previous study (Kubista, 2011).

	$\Delta S/S_0$ (T)									
T(ms) / Coprecipitate	0.5	1	1.5	2	2.5	3	4	5	6	8
calcite/GPA	0.067	0.135	0.297	0.440		0.698	0.843	0.908		0.980
calcite/LTA		0.0343		0.227		0.282	0.443	0.576		0.816
calcite/DGA		0.0966	0.185	0.318	0.431	0.571	0.724		0.913	0.952
calcite/DGP					0.168					0.619
calcite/PGA		0.203	0.289	0.454	0.519	0.653	0.794		0.931	0.971
calcite/PPA		0.241	0.294	0.458	0.583	0.649	0.798	0.904		0.968
calcite/OrthoP[1]	0.042	0.173	0.269	0.460		0.635	0.840	0.930		

Table 2.6 Summary of peak intensity for first spinning sidebands (SSB) and central band measured from ester/calcite coprecipitate 5 kHz CP spectra. Central and SSB(+/−) represent the value of relative intensity (%) of central bands and first SSBs. (+) and (−) denote SSB with a higher or lower chemical shift than of the central band, respectively.

P monoester				P diester			
	SSB(+)	central	SSB(−)		SSB(+)	central	SSB(−)
DGA/calcite	17.7	43.2	39.0	DGP/calcite	46.4	32.7	20.9
GPA/calcite	17.5	52.2	30.3	LTA/calcite	40.9	36.2	22.9
PGA/calcite	17.0	43.9	39.1				
PPA/calcite	16.2	33.5	50.4				

2.7 Figures

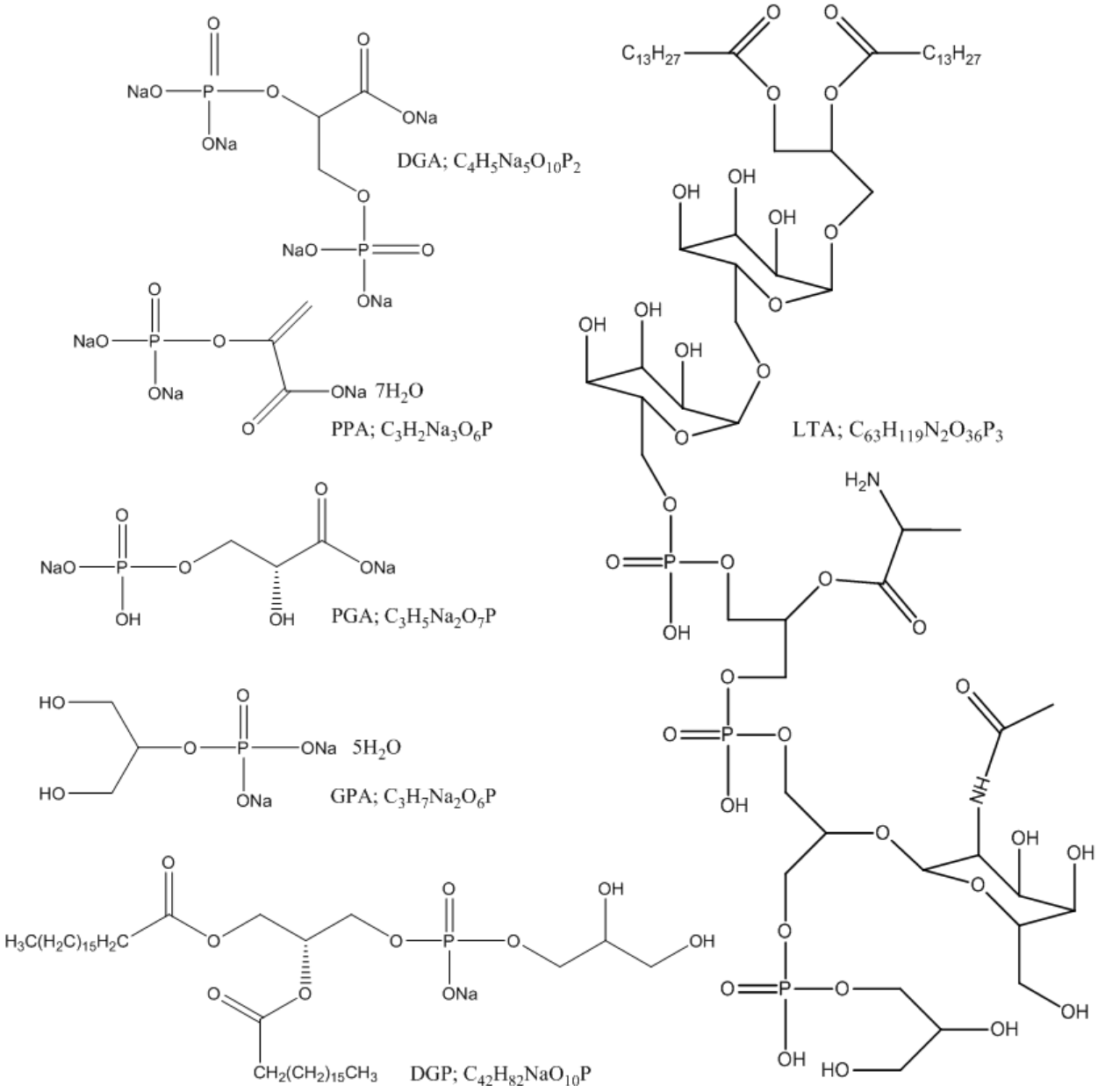

Figure 2.1 Molecular structure and chemical formulae of organic phosphates coprecipitated with calcite and investigated by NMR spectroscopy in this study.

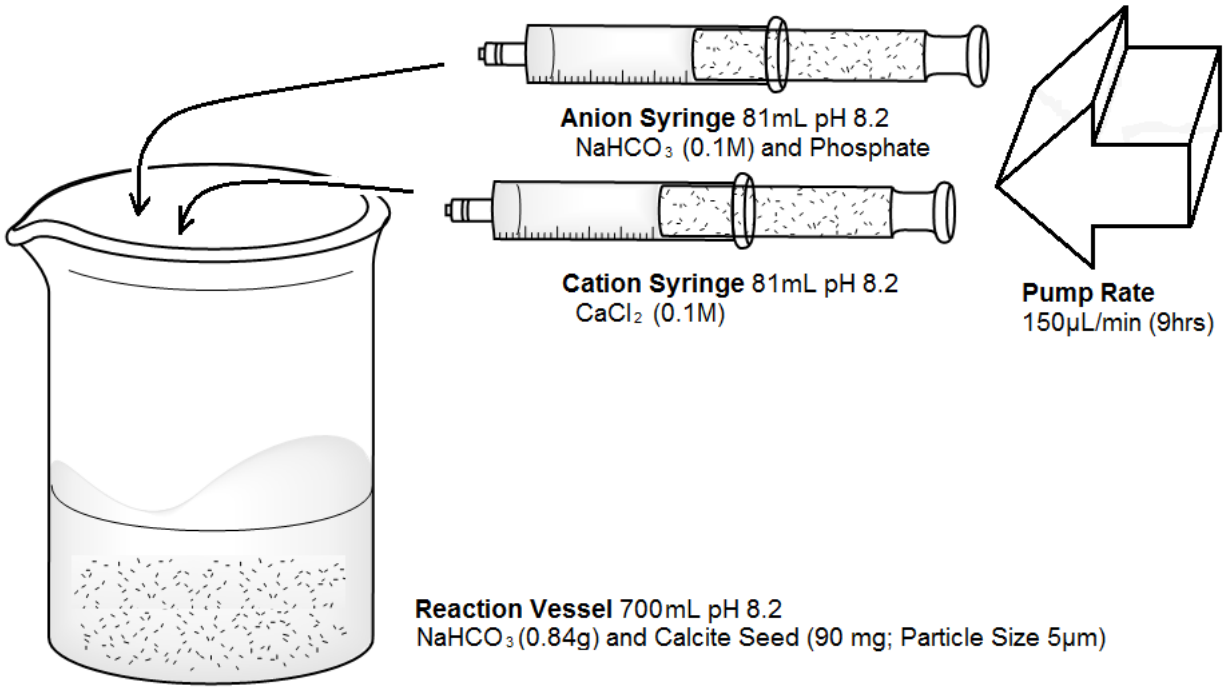

Figure 2.2 Experiment schematic for synthesis of calcite/ organophosphate coprecipitate samples. The synthesis experiment was operated at standard conditions as described in the text. (All solution pH was adjusted to 8.2 by HCl and NaOH.)

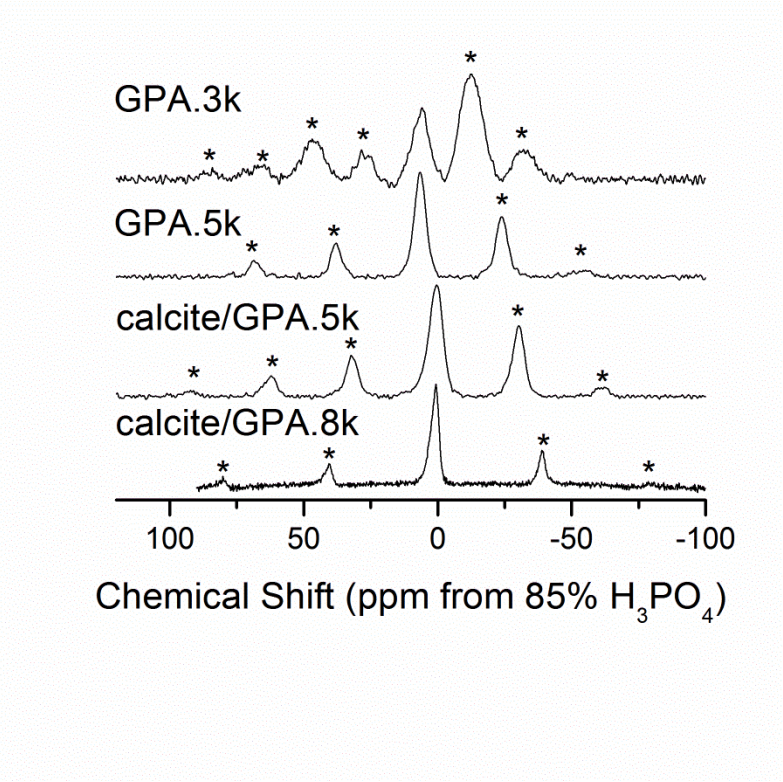

Figure 2.3 ^{31}P {^{1}H} CP/ MAS NMR spectra of the GPA sodium salt and calcite/ GPA coprecipitate, collected with a 2 ms contact time and spinning rates of 3 kHz, 5 kHz, and 8 kHz as indicated. Asterisks denote spinning sidebands.

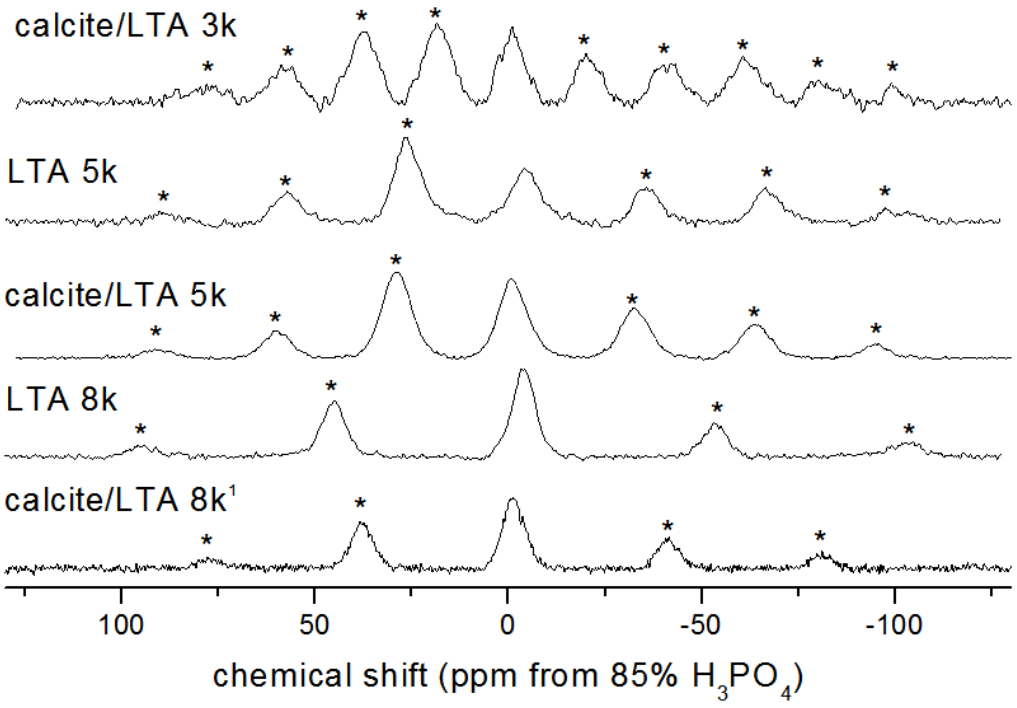

Figure 2.4 ^{31}P {^{1}H} CP/ MAS NMR spectra of LTA and calcite/ LTA coprecipitate, collected with a 2 ms contact time and spinning rates of 3 kHz, 5 kHz, and 8 kHz as indicated. Asterisks denote spinning sidebands.

[1]Spectrum was collected from a 500 MHz spectrometer with a operating frequency 202.3 MHz for ^{31}P, giving a shorter separation between bands than that from 400 MHz spectrometer under the same spinning rate.

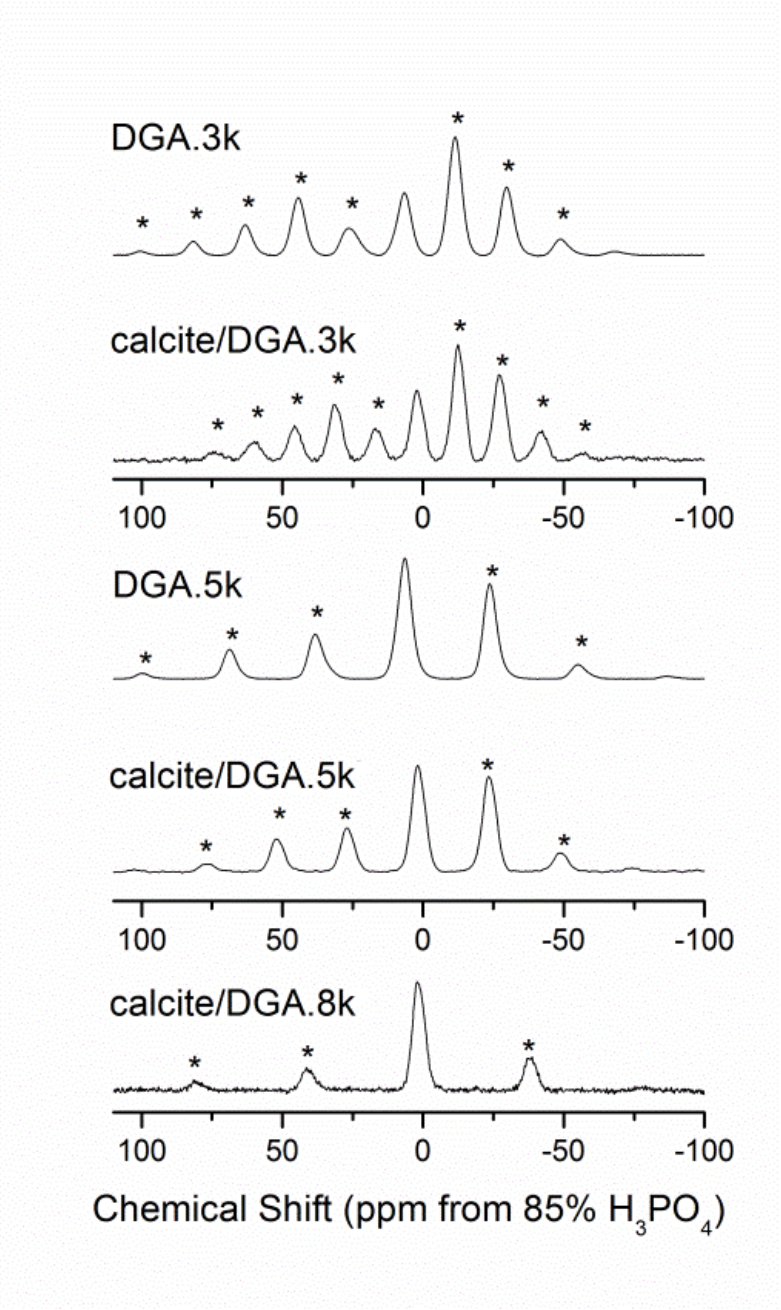

Figure 2.5 ^{31}P {^{1}H} CP/ MAS NMR spectra of DGA and calcite/ DGA coprecipitate, collected with a 2 ms contact time and spinning rates of 3 kHz, 5 kHz and 8 kHz as indicated. Asterisks denote spinning sidebands.

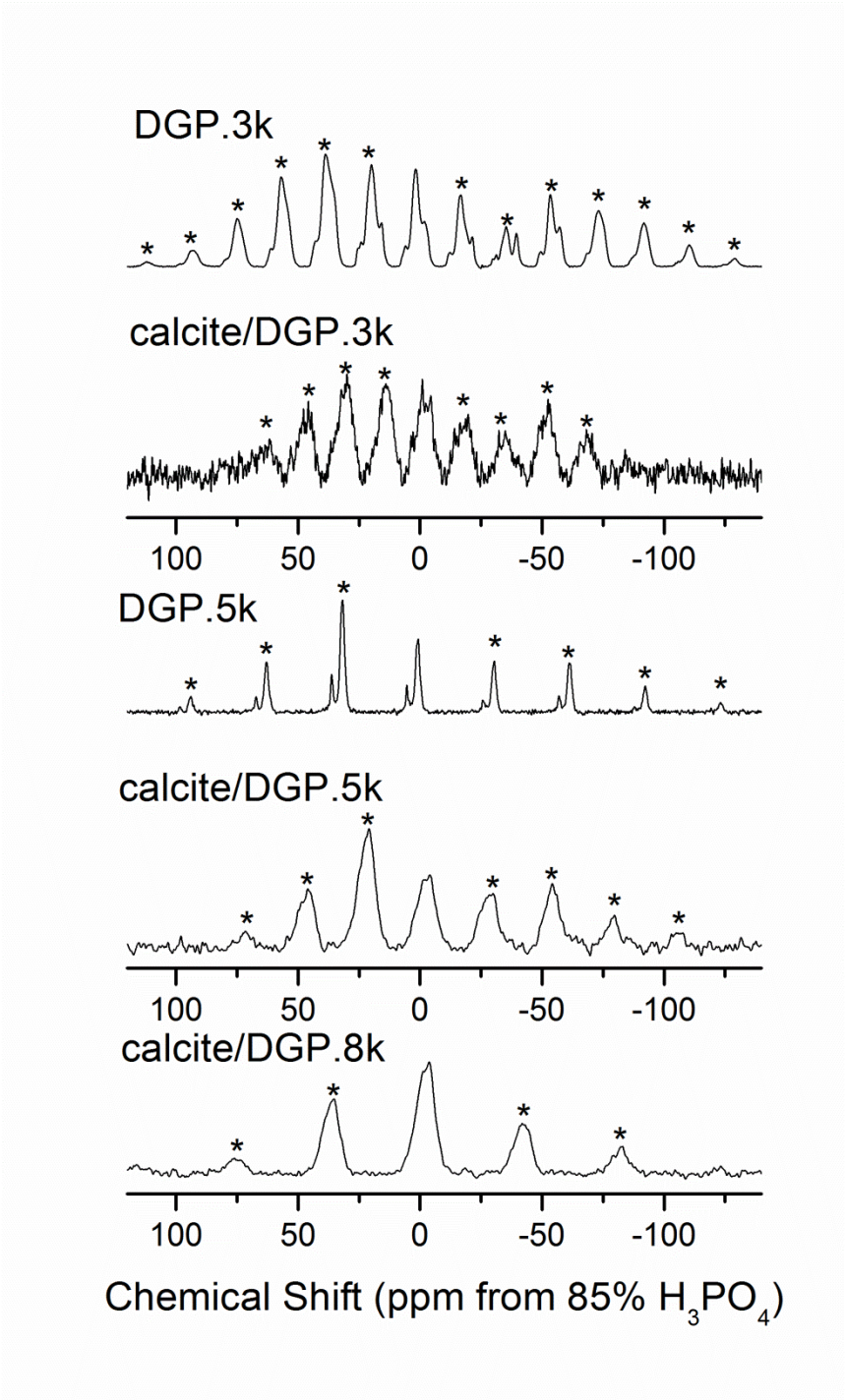

Figure 2.6 ^{31}P {^{1}H} CP/ MAS NMR spectra of the DGP sodium salt and calcite/ DGP coprecipitate, collected with a 2 ms contact time and spinning rates of 3 kHz, 5 kHz and 8 kHz as indicated. Asterisks denote spinning sidebands.

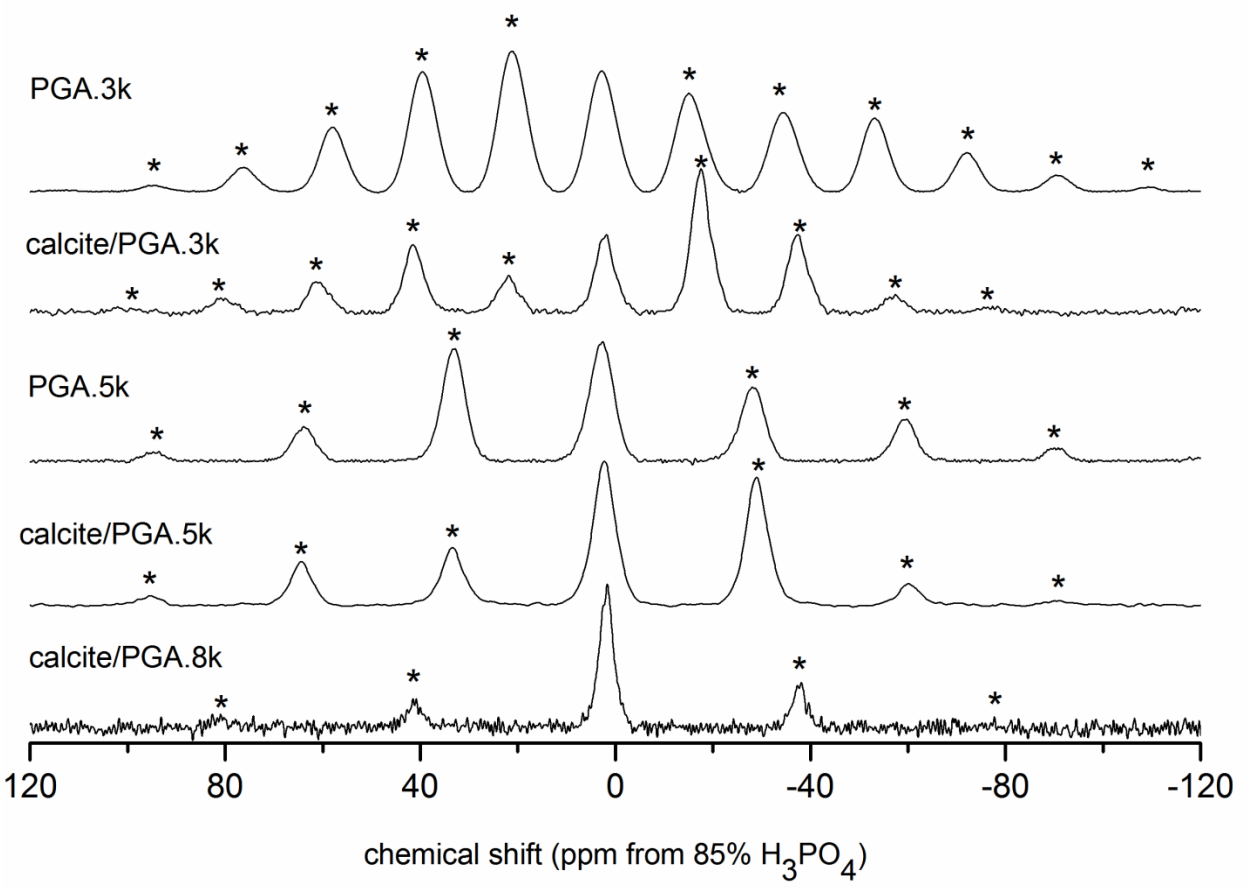

Figure 2.7 ^{31}P {^{1}H} CP/ MAS NMR spectra of the PGA sodium salt and calcite/ PGA coprecipitate, collected with a 2 ms contact time and spinning rates of 3 kHz and 5 kHz as indicated. Asterisks denote spinning sidebands.

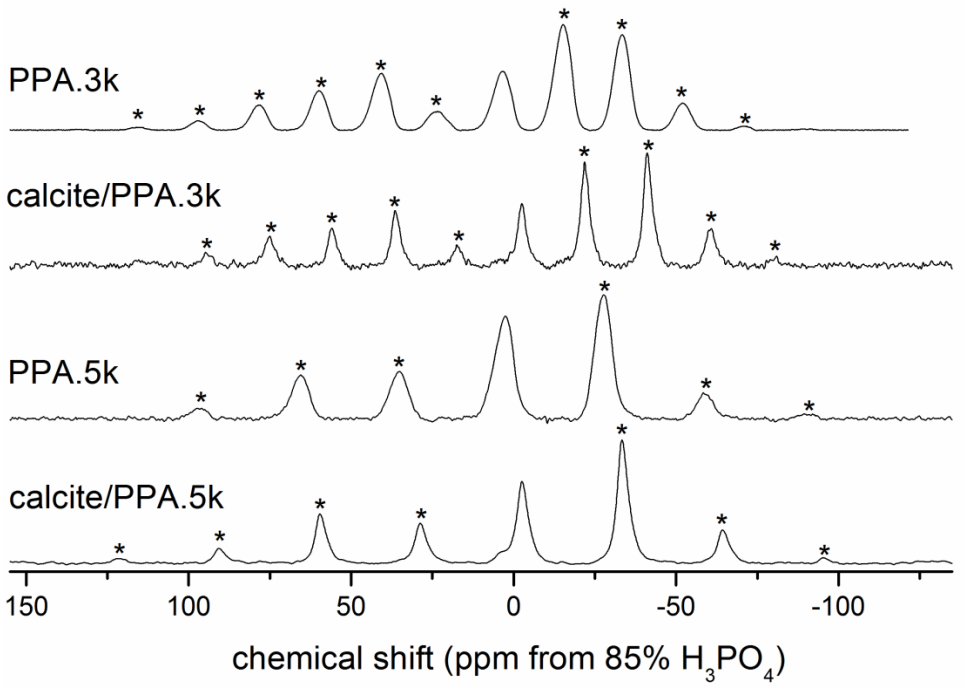

Figure 2.8 ^{31}P {^{1}H} CP/ MAS NMR spectra of the PPA sodium salt and calcite/ PPA coprecipitate, collected with a 2 ms contact time and spinning rates of 3k and 5k as indicated. Asterisks denote spinning sidebands.

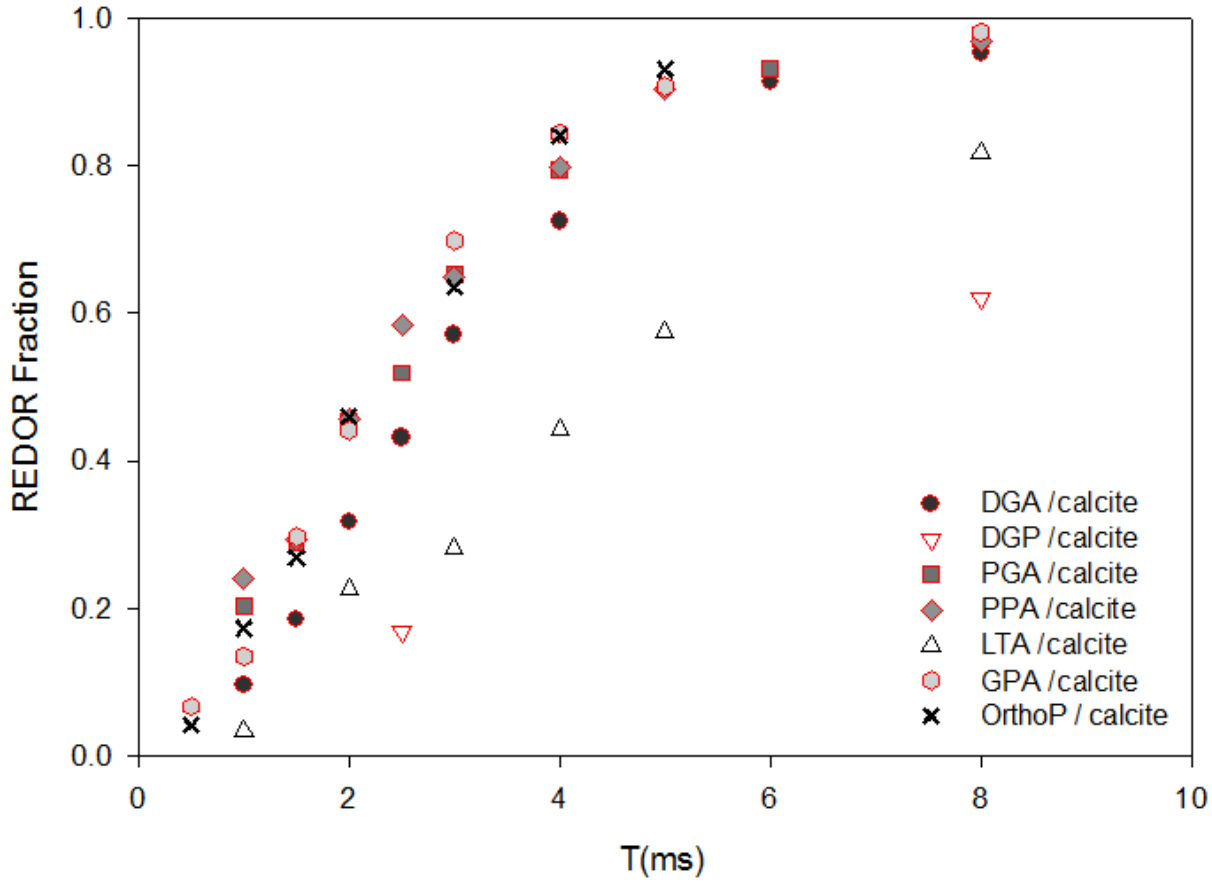

Figure 2.9 ^{31}P {^{13}C} CP/REDOR dephasing curves for coprecipitate samples. Monoester and diester coprecipitate samples are denoted by the filled and hollow symbols, respectively. "X" is for the orthophosphate coprecipitate.

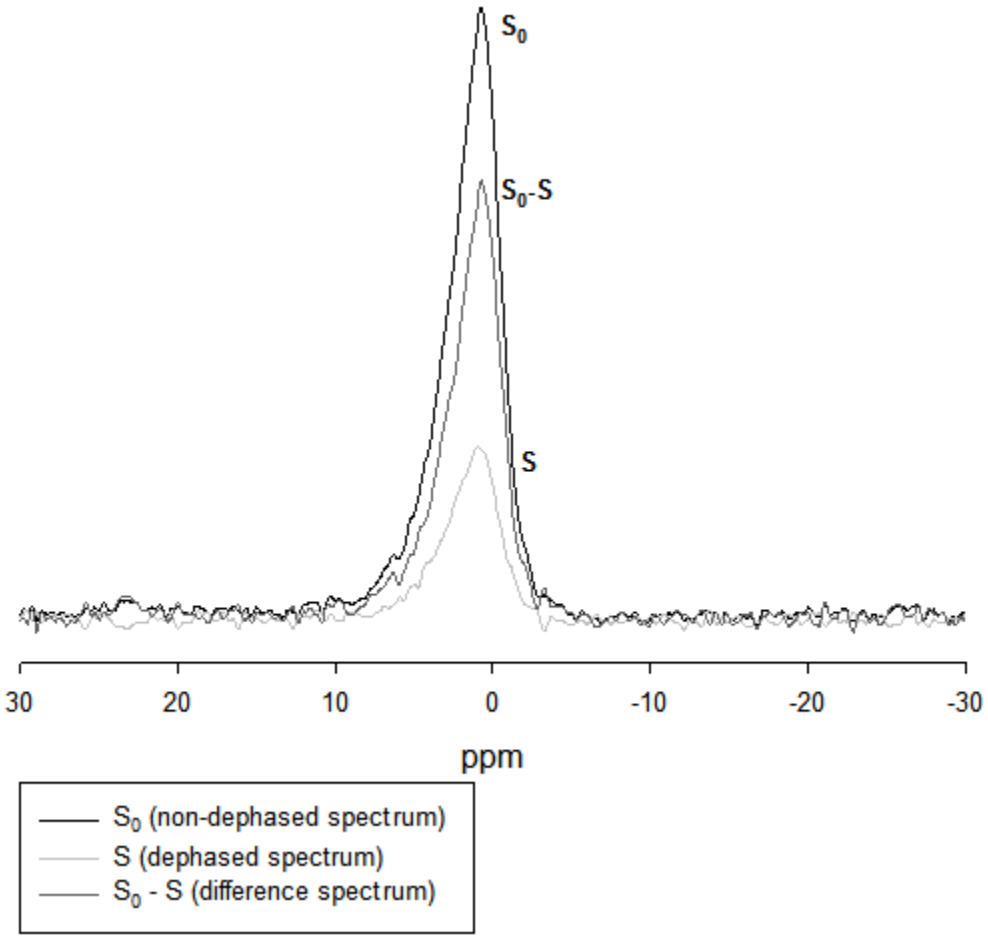

Figure 2.10 REDOR spectra of the calcite/ GPA coprecipitate ($^{31}P\{^{1}H\}$CP/MAS observe, applying ^{13}C dephasing pulses) collected at 8 kHz spinning rate with an evolution period of 24 rotor cycles (3 ms)

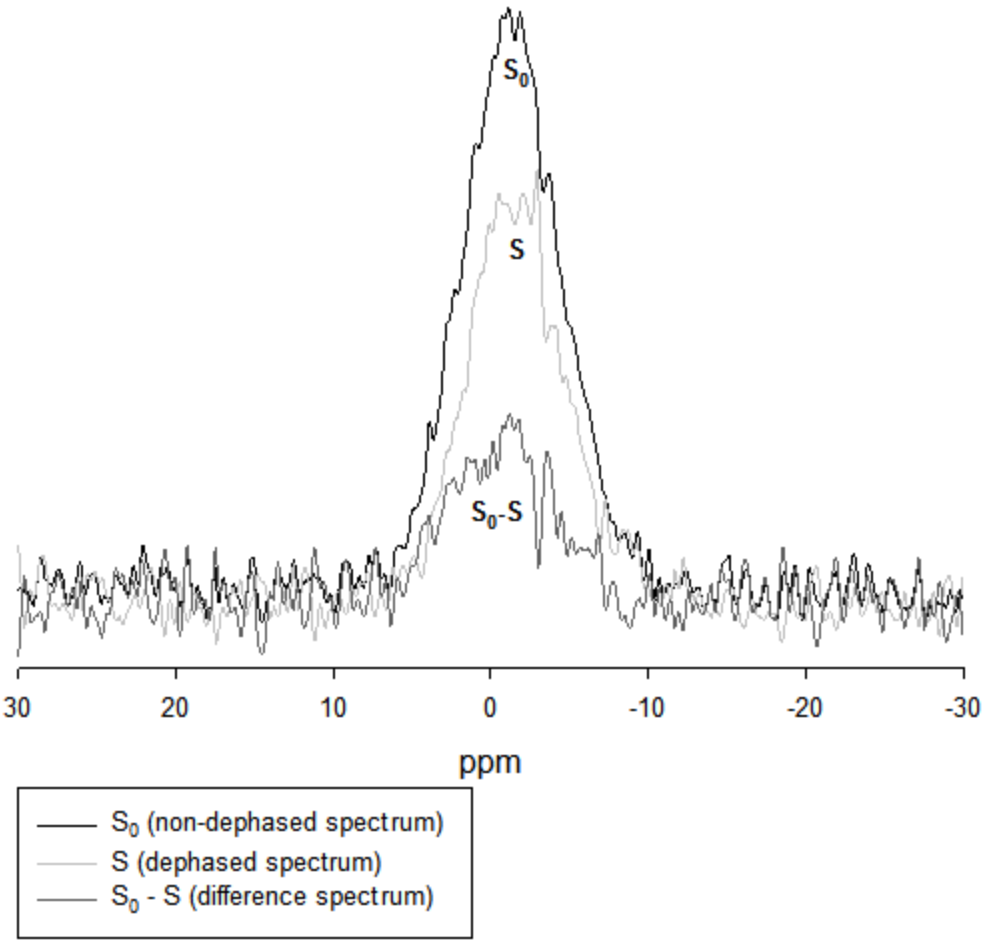

Figure 2.11 REDOR spectra of the calcite/ LTA coprecipitate ($^{31}P\{^{1}H\}$CP/MAS observe, applying ^{13}C dephasing pulses) collected at 8 kHz spinning rate with an evolution period of 24 rotor cycles (3 ms)

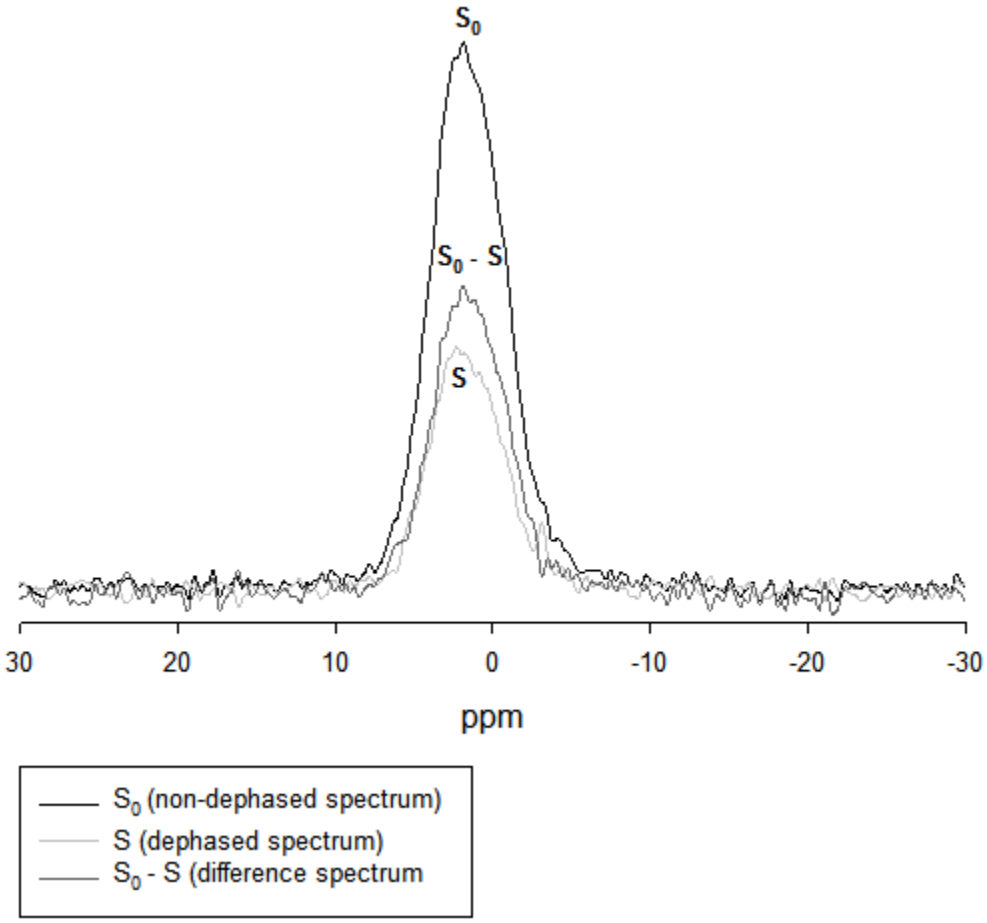

Figure 2.12 REDOR spectra of the calcite/ DGA coprecipitate ($^{31}P\{^{1}H\}$CP/MAS observe, applying ^{13}C dephasing pulses) collected at 8 kHz spinning rate with an evolution period of 24 rotor cycles (3 ms)

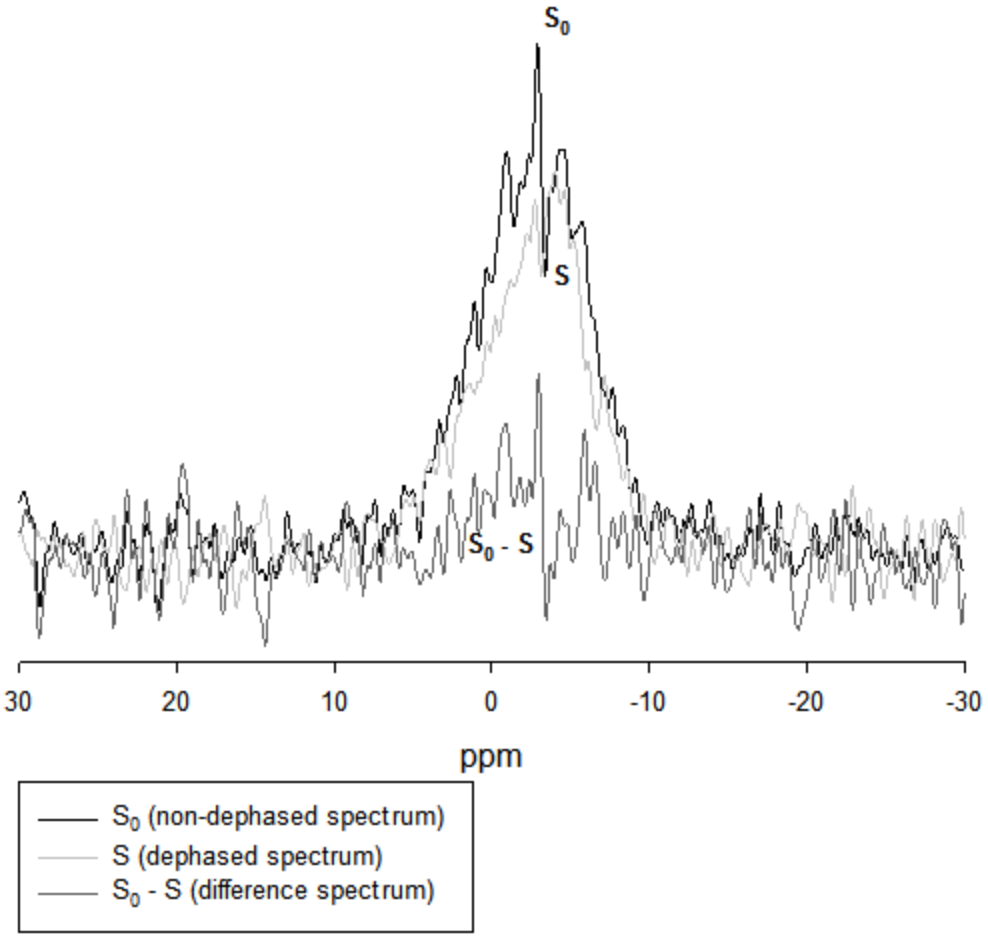

Figure 2.13 REDOR spectra of the calcite/ DGP coprecipitate ($^{31}P\{^{1}H\}$CP/MAS observe, applying ^{13}C dephasing pulses) collected at 8 kHz spinning rate with an evolution period of 20 rotor cycles (2.5 ms)

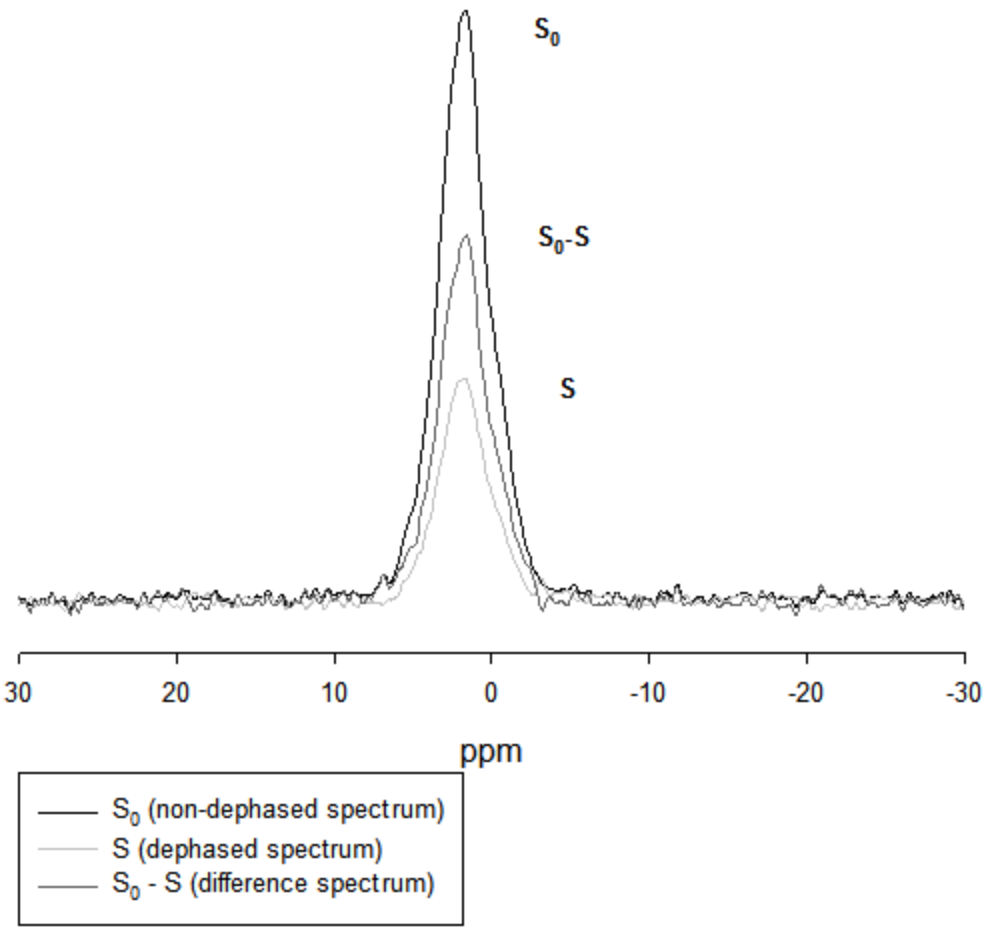

Figure 2.14 REDOR spectra of the calcite/ PGA coprecipitate ($^{31}P\{^{1}H\}$CP/MAS observe, applying ^{13}C dephasing pulses) collected at 8 kHz spinning rate with an evolution period of 24 rotor cycles (3 ms)

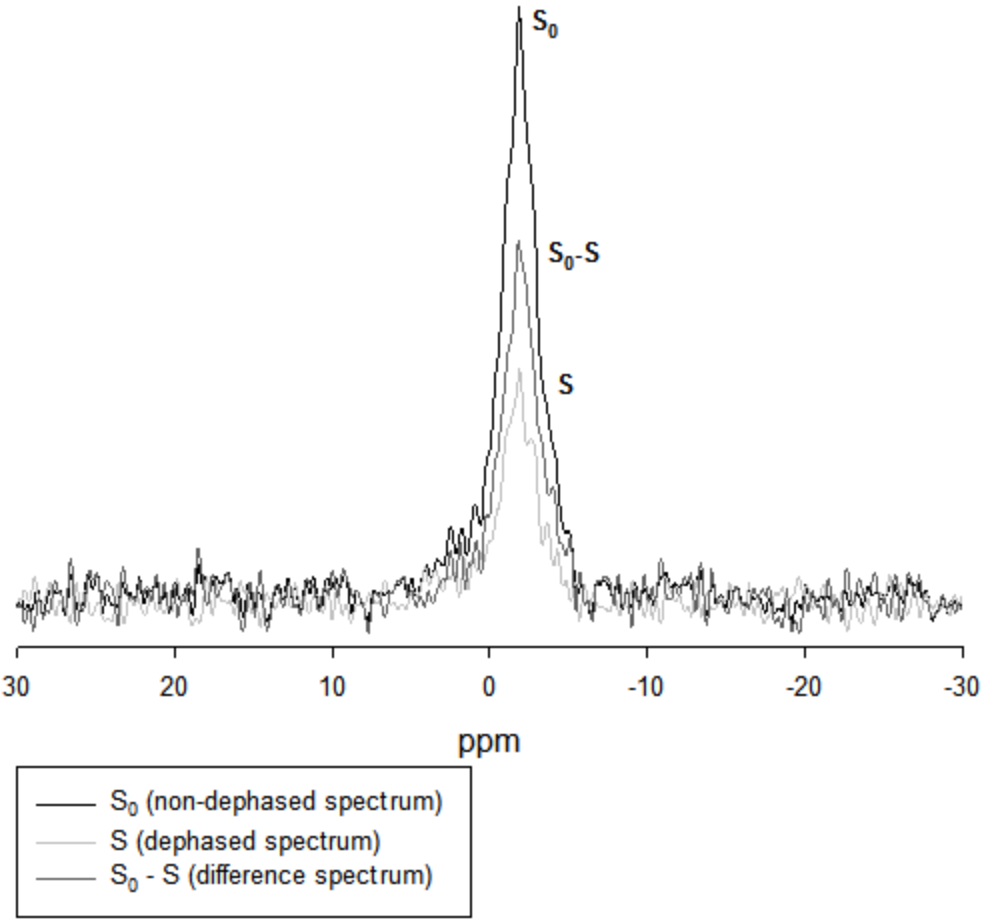

Figure 2.15 REDOR spectra of the calcite/ PPA coprecipitate ($^{31}P\{^{1}H\}$CP/MAS observe, applying ^{13}C dephasing pulses) collected at 8 kHz spinning rate with an evolution period of 24 rotor cycles (3 ms)

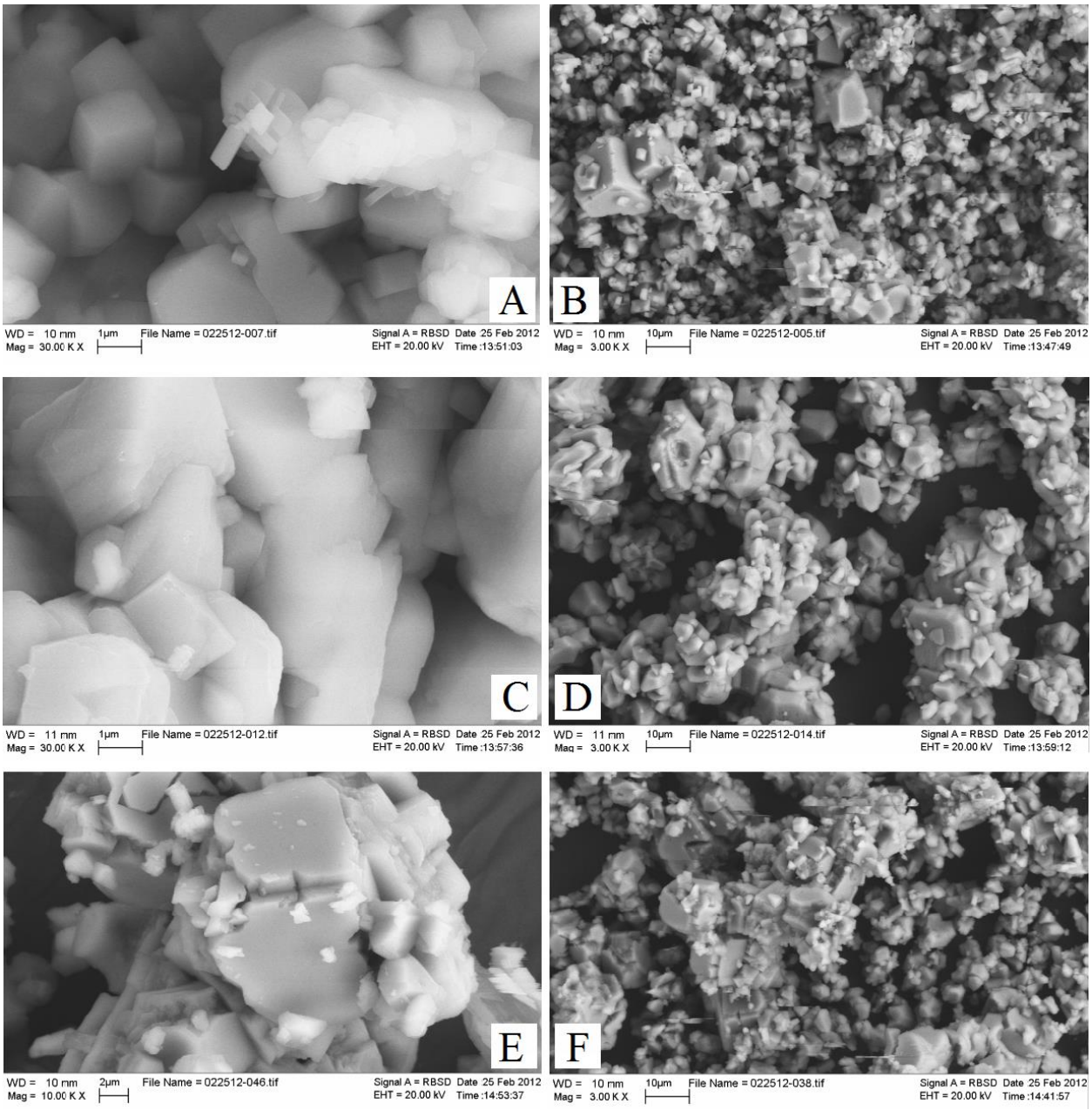

Figure 2.16 SEM micrographs of synthetic samples including calcite/blank precipitate (A, B), calcite/GPA coprecipitate (C, D), and calcite/LTA coprecipitate (E, F).

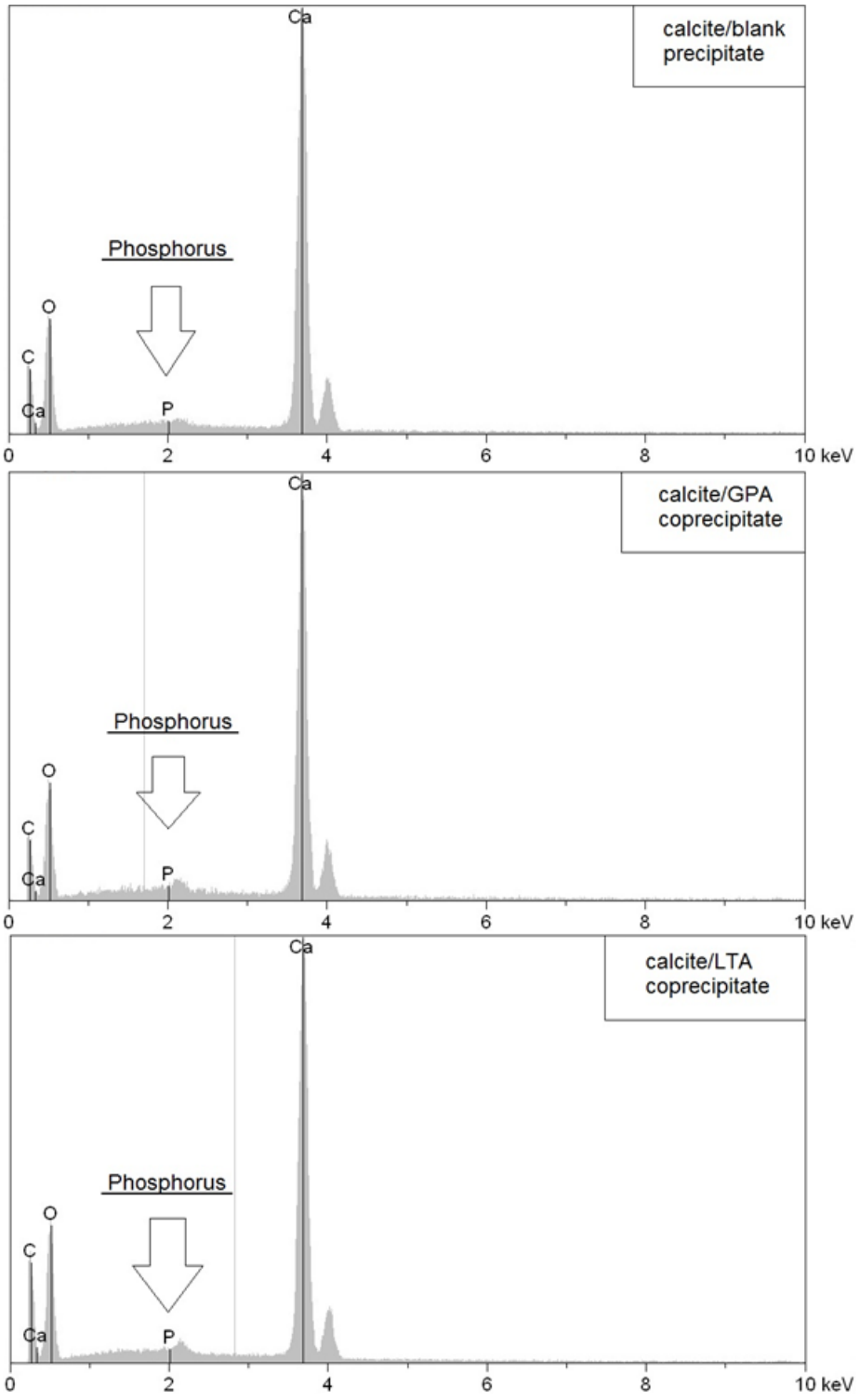

Figure 2.17 EDX spectra of calcite coprecipitated with and without organophosphates: calcite/ blank precipitate (top), calcite/ GPA coprecipitate (middle), and calcite/ LTA coprecipitate (bottom).

2.8 Reference

Abdel-Aal, N. and Sawada, K. (2003) Inhibition of adhesion and precipitation of CaCO3 by aminopolyphosphonate. *J. Cryst. Growth* **256**(1-2), 188-200.

Akiva-Tal, A., Kababya, S., Balazs, Y.S., Glazer, L., Berman, A., Sagi, A. and Schmidt, A. (2011) In situ molecular NMR picture of bioavailable calcium stabilized as amorphous CaCO3 biomineral in crayfish gastroliths. *Proc. Natl. Acad. Sci. U. S. A.* **108**(36), 14763-14768.

Amjad, Z. (1987) Kinetic study of the seeded growth of calcium carbonate in the presence of benzenepolycarboxylic acids. *Langmuir* **3**(2), 224-228.

Amrhein, C. and Suarez, D.L. (1987) Calcite supersaturation in soils as a result of organic matter mineralization. *Soil. Sci. Soc. Am. J.* **51**(4), 932-937.

Banfield, J.F., Javiera, C.-S. and H., N.K. (2005) *Molecular geomicrobiology*. Mineralogical Society of America, Geochemical Society, Chantilly, Va.

Banfield, J.F. and Nealson, K.H. (1997) *Geomicrobiology interactions between microbes and minerals*. Mineralogical Society of America, Washington, D.C.

Benitez-Nelson, C.R. (2000) The biogeochemical cycling of phosphorus in marine systems. *Earth-Sci. Rev.* **51**(1-4), 109-135.

Blyth, A.J., Baker, A., Collins, M.J., Penkman, K.E., Gilmour, M.A., Moss, J.S., Genty, D. and Drysdale, R.N. (2008) Molecular organic matter in speleothems and its potential as an environmental proxy. *Quaternary Sci. Rev.* **27**(9), 905-921.

Cade-Menun, B.J. (2005) Characterizing phosphorus in environmental and agricultural samples by P-31 nuclear magnetic resonance spectroscopy. *Talanta* **66**(2), 359-371.

Celi, L., Lamacchia, S. and Barberis, E. (2000) Interaction of inositol phosphate with calcite. *Nutr. Cycl. Agroecosyst.* **57**(3), 271-277.

Celi, L., Lamacchia, S., Marsan, F.A. and Barberis, E. (1999) Interaction of inositol hexaphosphate on clays: Adsorption and charging phenomena. *Soil. Sci.* **164**(8), 574-585.

Chalmin, E., Perrette, Y., Fanget, B. and Susini, J. (2013) Investigation of Organic Matter Entrapped in Synthetic Carbonates-A Multimethod Approach. *Microsc. microanal.* **19**(1), 132-144.

Collin, R.L. (1966) The Electronic Structure of Phosphate Esters. *J. Am. Chem. Soc.* **88**(14), 3281-3287.

Correll, D.L. (1998) The role of phosphorus in the eutrophication of receiving waters: A review. *J. Environ. Qual.* **27**(2), 261-266.

Cotmore, J.M., Nichols, G. and Wurthier, R.E. (1971) Phospholipid—calcium phosphate complex: enhanced calcium migration in the presence of phosphate. *Science* **172**(3990), 1339-&.

Damle, C., Kumar, A., Sainkar, S.R., Bhagawat, M. and Sastry, M. (2002) Growth of calcium carbonate crystals within fatty acid bilayer stacks. *Langmuir* **18**(16), 6075-6080.

de Vicente, I., Cattaneo, K., Cruz-Pizarro, L., Brauer, A. and Guilizzoni, P. (2006) Sedimentary phosphate fractions related to calcite precipitation in an eutrophic hardwater lake (Lake Alserio, northern Italy). *J. Paleolimnol.* **35**(1), 55-64.

Degroot, C.J. and Golterman, H.L. (1993) On the presence of organic phosphate in some Camargue sediments: evidence for the importance of phytate. *Hydrobiologia* **252**(1), 117-126.

Didymus, J.M., Oliver, P., Mann, S., Devries, A.L., Hauschka, P.V. and Westbroek, P. (1993) Influence of low-molecular-weight and macromolecular organic additives on the morphology of calcium carbonate. *J. Chem. Soc.-Faraday Trans.* **89**(15), 2891-2900.

Dove, P., Yoreo, J.J.D. and Weiner, S. (2003) *Biomineralization*. Mineralogical Society of America, Washington, DC.

Fairchild, I.J., Smith, C.L., Baker, A., Fuller, L., Spötl, C., Mattey, D. and McDermott, F. (2006) Modification and preservation of environmental signals in speleothems. *Earth-Sci. Rev.* **75**(1), 105-153.

Fairchild, I.J. and Treble, P.C. (2009) Trace elements in speleothems as recorders of environmental change. *Quaternary Sci. Rev.* **28**(5-6), 449-468.

Feng, J., Lee, Y.J., Kubicki, J.D., Reeder, R.J. and Phillips, B.L. (2008) NMR spectroscopy of citrate in solids: cross-polarization kinetics in weakly coupled systems. *Magn. Reson. Chem.* **46**(5), 408-417.

Fenter, P., Geissbühler, P., DiMasi, E., Srajer, G., Sorensen, L.B. and Sturchio, N.C. (2000) Surface speciation of calcite observed in situ by high-resolution X-ray reflectivity. *Geochim. Cosmochim. Ac.* **64**(7), 1221-1228.

Filippelli, G.M. (2011) Phosphate rock formation and marine phosphorus geochemistry: The deep time perspective. *Chemosphere* **84**(6), 759-766.

Follmi, K.B. (1996) The phosphorus cycle, phosphogenesis and marine phosphate-rich deposits. *Earth-Sci. Rev.* **40**(1-2), 55-124.
Furrer, G. and Stumm, W. (1986) The Coordination of Weathering .1.Dissolution Kinectics of delta-Al2O3 and BeO. *Geochim. Cosmochim. Ac.* **50**(9), 1847-1860.
Geffroy, C., Foissy, A., Persello, J. and Cabane, B. (1999) Surface complexation of calcite by carboxylates in water. *J. Colloid. Interf. Sci.* **211**(1), 45-53.
Gertman, R., Ben Shir, I., Kababya, S. and Schmidt, A. (2008) In situ observation of the internal structure and composition of biomineralized Emiliania huxleyi calcite by solid-state NMR spectroscopy. *J. Am. Chem. Soc.* **130**(40), 13425-13432.
Griffin, R.G. (1976) Observation of the effect of water on the phosphorus-31 nuclear magnetic resonance spectra of dipalmitoyllecithin. *J. Am. Chem. Soc.* **98**(3), 851-853.
Gröger, C., Lutz, K. and Brunner, E. (2009) NMR studies of biomineralisation. *Prog. Nucl. Mag. Res. Sp.* **54**(1), 54-68.
Gullion, T. and Schaefer, J. (1989) Rotational-echo double-resonance NMR. *J. Magn. Reson.* **81**(1), 196-200.
Henriksen, K., Stipp, S.L.S., Young, J.R. and Marsh, M.E. (2004) Biological control on calcite crystallization: AFM investigation of coccolith polysaccharide function. *Am. Mineral.* **89**(11-12), 1709-1716.
Herzfeld, J. and Berger, A.E. (1980) Sideband intensities in NMR spectra of samples spinning at the magic angle. *J. Chem. Phys.* **73**(6021.
Hinedi, Z.R., Goldberg, S., Chang, A.C. and Yesinowski, J.P. (1992) A ^{31}P and ^{1}H MAS NMR study of phosphate sorption onto calcium carbonate. *J. Colloid. Interf. Sci.* **152**(1), 141-160.
Huang, Y., Fairchild, I.J., Borsato, A., Frisia, S., Cassidy, N.J., McDermott, F. and Hawkesworth, C.J. (2001) Seasonal variations in Sr, Mg and P in modern speleothems (Grotta di Ernesto, Italy). *Chem. Geol.* **175**(3), 429-448.
Iuga, A., Ader, C., Gröger, C. and Brunner, E. (2006) Applications of solid-state ^{31}P NMR spectroscopy, in: Webb, G.A. (Ed.), *Annual Reports on NMR Spectroscopy*. Academic Press, pp. 145-189.
Kubista, L.M. (2011) Solid-State NMR Spectroscopy Investigation of Phosphorus Incorporation In Calcium Carbonate. 1500598 M.S.State University of New York at Stony Brook, Ann Arbor.
Lin, Y.P., Singer, P.C. and Aiken, G.R. (2005) Inhibition of calcite precipitation by natural organic material: Kinetics, mechanism, and thermodynamics. *Environ. Sci. Technol.* **39**(17), 6420-6428.
Lowenstam, H.A. and Weiner, S. (1989) *On biomineralization*. Oxford University Press.
Mason, H.E., Frisia, S., Tang, Y., Reeder, R.J. and Phillips, B.L. (2007) Phosphorus speciation in calcite speleothems determined from solid-state NMR spectroscopy. *Earth. Planet. Sc. Lett.* **254**(3), 313-322.
Mason, H.E., Montagna, P., Kubista, L., Taviani, M., McCulloch, M. and Phillips, B.L. (2011) Phosphate defects and apatite inclusions in coral skeletal aragonite revealed by solid-state NMR spectroscopy. *Geochim. Cosmochim. Acta* **75**(23), 7446-7457.
Matsuya, S., Udoh, K., Nakagawa, M. and Ishikawa, K. (2006) Preparation of carbonate apatite monolith by treatment of the set gypsum containing calcite in trisodium phosphate solution, in: Nakamura, T., Yamashita, K., Neo, M. (Eds.), *Bioceramics 18, Pts 1 and 2*, pp. 125-128.
Meldrum, F.C. and Hyde, S.T. (2001) Morphological influence of magnesium and organic additives on the precipitation of calcite. *J. Cryst. Growth* **231**(4), 544-558.
Merkel, C., Deuschle, J., Griesshaber, E., Enders, S., Steinhauser, E., Hochleitner, R., Brand, U. and Schmahl, W.W. (2009) Mechanical properties of modern calcite- (Mergerlia truncata) and phosphate-shelled brachiopods (Discradisca stella and Lingula anatina) determined by nanoindentation. *J. Struct. Biol.* **168**(3), 396-408.
Meyer, H. (1984) The influence of impurities on the growth rate of calcite. *J. Cryst. Growth* **66**(3), 639-646.
Mirtchi, A.A., Lemaitre, J. and Munting, E. (1990) Calcium phosphate cements: study of the β-tricalcium phosphate - dicalcium phosphate - calcite cements. *Biomaterials* **11**(2), 83-88.
Mirtchi, A.A., Lemaitre, J. and Munting, E. (1991) Calcium phosphate cements: effect of fluorides on the setting and hardening of beta-tricalcium phosphate-dicalcium phosphate-calcite cements. *Biomaterials* **12**(5), 505-510.
Monchau, F., Hivart, P., Genestie, B., Chai, F., Descamps, M. and Hildebrand, H.F. (2013) Calcite as a bone substitute. Comparison with hydroxyapatite and tricalcium phosphate with regard to the osteoblastic activity. *Mater. Sci. Eng. C. Mater. Biol. Appl.* **33**(1), 490-498.
Murphy, T., Hall, K. and Northcote, T. (1988) Lime treatment of a hardwater lake to reduce eutrophication. *Lake. Reserv. Manage.* **4**(2), 51-62.
Orme, C.A., Noy, A., Wierzbicki, A., McBride, M.T., Grantham, M., Teng, H.H., Dove, P.M. and DeYoreo, J.J. (2001) Formation of chiral morphologies through selective binding of amino acids to calcite surface steps. **411**(6839), 775-779.

Pettersson, K. (2001) Phosphorus characteristics of settling and suspended particles in Lake Erken. *Sci. Total. Environ.* **266**(1–3), 79-86.
Phillips, B.L., Lee, Y.J. and Reeder, R.J. (2005) Organic coprecipitates with calcite: NMR spectroscopic evidence. *Eviron. Sci. Technol.* **39**(12), 4533-4539.
Plant, L.J. and House, W.A. (2002) Precipitation of calcite in the presence of inorganic phosphate. *Colloid. Surface. A.* **203**(1–3), 143-153.
Pourpoint, F., Gervais, C., Bonhomme-Coury, L., Azais, T., Coelho, C., Mauri, F., Alonso, B., Babonneau, F. and Bonhomme, C. (2007) Calcium phosphates and hydroxyapatite: Solid-state NMR experiments and first-principles calculations. *Appl. Magn. Reson.* **32**(4), 435-457.
Reddy, M. and Nancollas, G. (1973) Calcite crystal growth inhibition by phosphonates. *Desalination* **12**(1), 61-73.
Reddy, M.M. (1977) Crystallization of calcium carbonate in the presence of trace concentrations of phosphorus-containing anions: I. Inhibition by phosphate and glycerophosphate ions at pH 8.8 and 25 ℃. *J. Cryst. Growth* **41**(2), 287-295.
Reeder, R.J., Nugent, M., Lamble, G.M., Tait, C.D. and Morris, D.E. (2000) Uranyl incorporation into calcite and aragonite: XAFS and luminescence studies. *Environ. Sci. Technol.* **34**(4), 638-644.
Rothwell, W.P., Waugh, J.S. and Yesinowski, J.P. (1980) High-resolution variable-temperature ^{31}P NMR of solid calcium phosphates. *J. Am. Chem. Soc.* **102**(8), 2637-2643.
Ruiz-Agudo, E., Di Tommaso, D., Putnis, C.V., de Leeuw, N.H. and Putnis, A. (2010) Interactions between Organophosphonate-Bearing Solutions and (10(1)over-bar4) Calcite Surfaces: An Atomic Force Microscopy and First-Principles Molecular Dynamics Study. *Cryst. Growth. Des.* **10**(7), 3022-3035.
Ruiz-Agudo, E., Putnis, C.V., Rodriguez-Navarro, C. and Putnis, A. (2011) Effect of pH on calcite growth at constant ratio and supersaturation. *Geochim. Cosmochim. Ac.* **75**(1), 284-296.
Sawada, K., Abdel-Aal, N., Sekino, H. and Satoh, K. (2003) Adsorption of inorganic phosphates and organic polyphosphonate on calcite. *Dalton Trans.*3), 342-347.
Sethmann, I., Putnis, A., Grassmann, O. and Lobmann, P. (2005) Observation of nano-clustered calcite growth via a transient phase mediated by organic polyanions: A close match for biomineralization. *Am. Mineral.* **90**(7), 1213-1217.
Shaojun, Z. and Mucci, A. (1993) Calcite precipitation in seawater using a constant addition technique: A new overall reaction kinetic expression. *Geochim. Cosmochim. Ac.* **57**(7), 1409-1417.
Tas, A.C. (2007) Porous, biphasic CaCO3-calcium phosphate biomedical cement scaffolds from calcite (CaCO3) powder. *Int. J. Appl. Ceram. Tec.* **4**(2), 152-163.
Tas, A.C. (2008) Use of vaterite and calcite in forming calcium phosphate cement scaffolds, in: Brito, M., Case, E., Kriven, W.M. (Eds.), *Developments in Porous, Biological and Geopolymer Ceramics*, pp. 135-150.
Tesoriero, A.J. and Pankow, J.F. (1996) Solid solution partitioning of Sr2+,Ba2+, and Cd2+to calcite. *Geochim. Cosmochim. Ac.* **60**(6), 1053-1063.
Tiano, P. (1995) Stone reinforcement by calcite crystal precipitation induced by organic matrix macromolecules. *Stud. Conserv.* **40**(3), 171-176.
Tsai, T.W.T. and Chan, J.C.C. (2011) Recent Progress in the Solid-State NMR Studies of Biomineralization, in: Webb, G.A. (Ed.), *Annual Reports on Nmr Spectroscopy*, pp. 1-61.
Turner, B.L., Cade-Menun, B.J., Condron, L.M. and Newman, S. (2005) Extraction of soil organic phosphorus. *Talanta* **66**(2), 294-306.
Turner, G.L., Smith, K.A., Kirkpatrick, R.J. and Oldfield, E. (1986) Structure and cation effects on phosphorus-31 NMR chemical shifts and chemical-shift anisotropies of orthophosphates. *J. Magn. Reson.* **70**(3), 408-415.
Ueyama, N., Hosoi, T., Yamada, Y., Doi, M., Okamura, T.-a. and Nakamura, A. (1998) Calcium Complexes of Carboxylate-Containing Polyamide with Sterically Disposed NH ··O Hydrogen Bond: Detection of the Polyamide in Calcium Carbonate by ^{13}C Cross-Polarization/Magic Angle Spinning Spectra. *Macromolecules* **31**(21), 7119-7126.
Verrecchia, E.P. and Verrecchia, K.E. (1994) Needle-fiber calcite: a critical review and a proposed classification. *J. Sediment. Res. Sect. A-Sediment. Petrol. Process.* **64**(3), 650-664.
Wang, S.R., Jin, X.C., Zhao, H.C., Zhou, X.N. and Wu, F.C. (2007) Effect of organic matter on the sorption of dissolved organic and inorganic phosphorus in lake sediments. *Colloid. Surface. A.* **297**(1-3), 154-162.
Watson, E.B. (2004) A conceptual model for near-surface kinetic controls on the trace-element and stable isotope composition of abiogenic calcite crystals. *Geochim. Cosmochim. Ac.* **68**(7), 1473-1488.
Westheimer, F.H. (1987) Why nature chose phosphates. *Science* **235**(4793), 1173-1178.
Wickham, J.R. and Rice, C.V. (2008) Solid-state NMR studies of bacterial lipoteichoic acid adsorption on different surfaces. *Solid State Nucl. Magn. Reson.* **34**(3), 154-161.

Xie, S.C., Huang, J.H., Wang, H.M., Yi, Y., Hu, C.Y., Cai, Y.J. and Cheng, H. (2005) Distributions of fatty acids in a a stalagmite related to paleoclimate change at Qingjiang in Hubei, southern China. *Sci. China. Ser. D.* **48**(9), 1463-1469.

Xie, S.C., Yi, Y., Huang, J.H., Hu, C.Y., Cai, Y.J., Collins, M. and Baker, A. (2003) Lipid distribution in a subtropical southern China stalagmite as a record of soil ecosystem response to paleoclimate change. *Quaternary. Res.* **60**(3), 340-347.

III. Phosphorus Speciation in Calcitic Moonmilk Revealed by Solid-State NMR Spectroscopy

3.1 Introduction

Moonmilk, also known as mondmilch, is a hydrated, spongy to powdery assemblage of microcrystalline carbonate minerals (Hill and Forti, 1997) that resembles toothpaste or marzipan in texture. As a secondary cave deposit, moonmilk is commonly associated with biogenic calcite precipitation (Hill and Forti, 1997), and can also be formed by corrosional process (Northup and Lavoie, 2001). Depending on the structure of the cave where it is deposited, moonmilk can be composed of calcite, aragonite, or hydromagnesite crystals (Hill and Forti, 1997). It can occur in various forms including soft, granular paste, and loosely aggregated powder (Barton and Northup, 2007). Moonmilk usually contains abundant microbial and fungal biomass that may be involved its formation (Blyth and Frisia, 2008; Borsato et al., 2000; Canaveras et al., 2006; Mulec et al., 2002; Northup and Lavoie, 2001).

Although moonmilk has potential to serve as a paleoenvironmental proxy (Borsato et al., 2000), incomplete understanding of the source and control of moonmilk deposition hinders further interpretation. Part of the problem is the limitation of the techniques available for such investigation. The most common approach is microscopic inspection, which aims to identify the microbial features such as calcified cells or filamentous growth. However, this approach cannot always suit the purpose of distinguishing the biogenic and mineralogical structures (Barton et al., 2001). Microbiological techniques like bacteria cultivation have some success (Cacchio et al., 2004; Cacchio et al., 2003), but are limited by the fact that only a portion of bacteria is cultivable in the laboratory (Barton et al., 2001). Recent studies have introduced more sophisticated methodologies such as DNA sequencing and PCR amplification to understand the composition of the microbial communities in cave deposits (Angert et al., 1998; Portillo and Gonzalez, 2011; Sanchez-Moral et al., 2012). Although these techniques are showing increasing success, particularly in characterizing microbial communities in moonmilk deposits, our understanding of the origin of moonmilk is still at an early stage.

As an essential element of all living things, phosphorus is present in many organic compounds (Westheimer, 1987). In karst caves, moonmilk typically is deposited in the presence of microbial and/or fugal species (Braissant et al., 2012; Sanchez-Moral et al., 2012). The metabolically active micro-biota together with diverse organic compounds they produce closely associate with moonmilk formation (Baskar et al., 2011; Canaveras et al., 2006; Rooney et al., 2010). Since many calcium carbonate minerals such as calcite can incorporate organic molecules and phosphate during crystal growth (Chalmin et al., 2013; Geffroy et al., 1999; Montes-Hernandez et al., 2011; Phillips et al., 2005; Reddy, 1977; Ueyama et al., 1998), it is possible that moonmilk mainly made of carbonate minerals can incorporate P in the form of inorganic

phosphates or organophosphates, allowing phosphorus acts as a probe of the conditions present during moonmilk formation.

Although phosphorus is usually present in low concentration at natural environments including cave systems, ^{31}P has 100% abundance naturally, which together with its half integer nuclear spin makes ^{31}P NMR spectroscopy a powerful tool to analyze phosphorus-bearing samples (Cade-Menun, 2005). Nuclear Magnetic Resonance (NMR) spectroscopy takes advantage of NMR phenomena to ascertain local structural information of target nuclei. Since only the magnetic resonance is measured, NMR spectroscopy is non-destructive and non-invasive, allowing samples to be studied without disturbance other than placing them in the measuring container. Carbonate minerals in cave system exhibit a low abundance of paramagnetic ions (Kuczumow et al., 2005). Due to these advantages, ^{31}P NMR has been used to study phosphorus-containing carbonate samples including stalagmite calcite (Mason et al., 2007; Mason et al., 2006), coral aragonite (Mason et al., 2011), and amorphous calcium carbonate (Akiva-Tal et al., 2011; Reeder et al., 2013). Yet it had not been applied to calcitic moonmilk. In this context, ^{31}P NMR spectroscopy can provide structural information about the form of P in the moonmilk, which can be a valuable tool to understand the origin of moonmilk.

In this study, we investigated the nature of phosphorus in moonmilk with solid-state NMR. From the ^{31}P spectral data, the structural information of phosphate is inferred. In addition, ^{13}C NMR was also carried out to study the organic content in the moonmilk crystal. This approach provides a valuable methodology and data that complement previous studies on moonmilk and biomineralization.

3.2 Materials and Methods

3.2.1 Samples and Sites

Two moonmilk samples provided by Dr. Silvia Frisia are examined in this study. Both samples were collected from the top of two active stalactites in cave Coel Zel à, Italy. The first moonmilk sample CZ-3 was collected in a completely dark area which is 80 m away from the cave entrance. The second moonmilk sample CZ-12 was collected in a twilight zone with an enhanced annual fluctuations of temperature and relative humidity, which is 30 m away from the cave entrance. To study the occluded organic matter in crystalline structure, both samples were bleached by suspending in sodium hypochlorite solution to remove extracrystalline organic matter and rinsed.

Cave Coel Zel à(Figure 3.1) is on the eastern side of Canfedin Mountain in the Brenta Dolomites of Italy. It lies at a latitude of 46°06′48″ N and longitude of 11°00′32″ E with an elevation of 1720 meters above sea level. It is essentially a single sub-horizontal gallery 150 m long and from 4 to 8 m wide, which developed along the bedding planes of the Jurassic *Calcari Grigi* (Grey Limestones) formation. The water circulation is currently limited to several slow

drips. Drip flows concentrate especially in the middle part of the cave, which feed moonmilk veils and draperies, some of which are still active as shown in Figure 3.2 a & b. The water is usually near saturation or slightly undersaturated similar to the nearby Cesare Battisti cave (Borsato, 1997; Borsato et al., 2000; Frisia et al., 2000). The cave has a mean temperature around 5.2 ℃ (winter: 4.8 ℃, summer: 5.4 ℃). During the wettest periods, the drippings give rise to small trickles that feed small calcareous tufa flowstones (Borsato et al., 2000). Measured dripwater pH values range from 7.5 to 8.0. Dissolved P concentrations for the drip water range from 1.5 to 2 $\mu g \cdot L^{-1}$, while the total P concentrations range from 2 to 5 $\mu g \cdot L^{-1}$. Other compositions measured for drip water are listed in Table 3.1. The sparitic speleothems, a type of hard and dense speleothem, are all fossil and extremely rare.

In the central part of the cavity, the concentration of CO_2 is usually between 450 and 500 ppm. Relative humidity is between 90 and 98%. The walls are characterized in several areas by water droplets condensed over the rock (Figure 3.2.c).The droplets produce condensation corrosion and enrich the water with the dissolved $CaCO_3$, which is responsible for the formation of the moonmilk coatings and festoons wide and thick up to 20-30 cm. Both fossil and active morphologies have been identified along the cave walls.

3.2.2 XRD

Information of crystal structure about the moonmilk was obtained from X-ray diffraction (XRD) analysis, which was performed by John Vaughn. A Scintag PADX diffractometer was running at 45 kV and 25 ma with Cu Kα radiation (λ = 1.541838Å). Data were collected from 13 to 54 ^{o} 2θ using 0.02 ^{o} 2θ steps and counting rate of 0.5^{o} 2θ · $minute^{-1}$.

3.2.3 NMR

Cross polarization (CP) under the magic-angle spinning (MAS) conditions is an effective technique that is widely used to enhance the signal of observed nuclei by magnetization transfer from ^{1}H, and reduce experiment repetition time to a few seconds. This study exclusively applied CP/MAS to obtain NMR signal of ^{31}P and ^{13}C from moonmilk samples, considering the anticipated low concentration of P in moonmilk and low abundance of ^{13}C in nature. All NMR experiments were carried out on a 400 MHz Varian Inova spectrometer at operating frequencies of 161.8 MHz, 100.6 MHz, and 399.8 MHz for ^{31}P, ^{13}C, and ^{1}H, respectively. Samples were contained in 7.5 mm (o.d.) Si_3N_4 rotors and spun at 3 kHz. All ^{31}P and ^{13}C CP/ MAS experiments were conducted with ^{1}H decoupling. The ^{31}P NMR chemical shifts (δ_{P-31}) are referenced with solid hydroxylapatite (δ_{P-31} = 2.65 ppm), which is a secondary reference for 85% phosphoric acid (δ_{P-31} = 0 ppm).The ^{13}C NMR chemical shifts (δ_{C-13}) are referenced with solid adamantine (δ_{C-13} = 28.46 ppm, 37.85 ppm), which is a secondary reference for tetramethylsilane (δ_{C-13} = 0 ppm). ^{13}C CP/MAS spectra for CZ-3 were obtained with a 1 ms contact time, and 2 s relaxation delay, for 164,058 acquisitions, while for CZ-12 we used a 2 ms contact time and 1 s relaxation delay, for 66,746 acquisitions.

3.3 Results

The X-ray diffraction patterns for moonmilk samples CZ-3 and CZ-12 are reported in Figure 3.3. These patterns are nearly identical to those reported for standard pure calcite powder (Gunasekaran and Anbalagan, 2007; Rahman and Oomori, 2009). Comparison of these crystal reflections with data reported by ICDD (The International Centre for Diffraction Data) show good agreement with reflections of pure calcite powder. As shown in Figure 3.3, all major reflections can be indexed to the reported calcite data as shown in Figure 3.3, including the most typical reflection (104) of calcite with the strongest intensity, and the rest (006), (012), (024), (018), (110), (202), $(11\bar{3})$, and $(11\bar{6})$. This agreement between calcite and moonmilk confirmed that the moonmilk samples are composed dominantly of calcite.

The ^{31}P CP/MAS NMR spectra of both moonmilk samples, illustrated in Figure 3.4, show a dominant peak ($\delta_{P\text{-}31}$=3.45 ppm, FWHM about 5.2 ppm) shouldered by a small peak ($\delta_{P\text{-}31}$ = −2.0 ppm, FWHM around 6.0 ppm) together with several spinning sidebands. The spinning sidebands (SSB) for the two isotropic peaks bear sufficient signal intensity to estimate values of their corresponding chemical shift tensors and consequently chemical shift anisotropy (CSA, $\Delta\delta$). The spectra were fit with a sum of Gaussian curves representing the center band and SSB's by constraining the line width of the SSBs to equal that of the corresponding central band, listed in Table 3.2, and peak positions according to the spinning rates. ^{31}P resonance at 3.45 ppm and −2 ppm yielded CSA values of −41 and 113.3, respectively for CZ-3, and 38.2 for the peak at +3.5 ppm for CZ-12. Detailed analysis of ^{31}P spectra in Table 3.2 shows little difference between the moonmilk samples in terms of P environments. ^{31}P CP spectra of CZ-3 and CZ-12 are remarkably similar in peak position and width to that for calcite/orthophosphate coprecipitate, which gives a main peak near 3 ppm with FWHM around 3 ppm (Kubista, 2011; Mason et al., 2007). The ^{13}C CP/MAS spectra of CZ-3 and CZ-12 in Figure 3.5 show multiple resonances with similar chemical shift positions but slightly different relative intensities. Both CZ-3 and CZ-12 give relatively narrow peaks at 187 ppm and 168 ppm plus broader peaks around 46 ppm and 30 ppm. Detailed analysis from fitting the spectra to a sum of Gaussian curves (Table 3.3) shows close similarities in the chemical shifts and slightly differences in the relative intensities of $\delta_{C\text{-}13}$ resonances between CZ-3 and CZ-12. ^{13}C CP spectral data shows that relative intensities for peaks at 187ppm, 168 ppm, 46 ppm, and 30 ppm represent 28.8%, 5.7%, 42.7%, and 22.7% for CZ-3, and 38.7%, 15.5%, 37.4%, and 8.4% for CZ-12, respectively. However, the ^{13}C peak intensities do not quantitatively represent populations without calibration of the CP dynamical effects, which is impractical for these samples owing to the long acquisition times required. Some of the differences between CZ-3 and CZ-12 could be due to different acquisition parameters (e.g. contact time).

3.4 Discussions

3.4.1 Phosphorus speciation in moonmilk

The XRD patterns for both moonmilk samples are in good agreement with calcite and show the calcitic nature of moonmilk in this study. The signal from ^{31}P CP/MAS NMR shows that most of the P occurs in moonmilk as phosphate in environments similar to the phosphorus in calcite stalagmite speleothems reported by Mason et al. (2007). The main peak ($\delta_{P\text{-}31}$ = 3.45 ppm, 5 ppm FWHM) of moonmilk calcite has a similar chemical shift but is slightly boarder than observed for phosphate in speleothem calcite ($\delta_{P\text{-}31}$ = 3.5ppm, 3 – 4 ppm FWHM) (Mason et al., 2007). Mason et al. (2007) assigned this peak to phosphate defects in the calcite structure based on similarity to the ^{31}P NMR signal from calcite/phosphate coprecipitates. For comparison, a calcite sample coprecipitated with inorganic orthophosphate (OrthoP/calcite) was obtained from Laura (Kubista) Harrington, of which the occurrence of orthophosphate in the calcite structure was confirmed as described in Chapter 2. As shown in Figure 3.4, except for the peak at −0.9 ppm attributed to monetite, ^{31}P CP demonstrates that the main peak from OrthoP/calcite coprecipitate significantly resembles that of moonmilk samples. Therefore, the main peak at 3.45 ppm likely represents the inorganic phosphate occluded in moonmilk calcite.

Phosphate defects in calcite are expected to exhibit a distribution of ^{31}P chemical shifts from a variety of local configurations to accommodate the size and charge difference between carbonate and phosphate groups (Mason et al., 2007). Such distribution gives rise to the large peak widths observed for moonmilk. The SSB intensity of the main peaks at 3.45 ppm in ^{31}P CP spectra are somewhat larger than expected for orthophosphates as structural defects, which is also reflected in the value of the CSA $\Delta\delta$ of around −40 ppm. ^{31}P spectra of unprotonated orthophosphates such as $Ca_3(PO_4)_2$ at $\delta_{P\text{-}31}$ = 3 ppm and $Mg_3(PO_4)_2 \cdot 8H_2O$ at $\delta_{P\text{-}31}$ = 4.6 ppm are dominated by the main isotropic peak, and display small or near-zero intensity of SSB (Turner et al., 1986). ^{31}P NMR spectra of protonated orthophosphates such as brushite ($CaHPO_4 \cdot 2H_2O$; $\delta_{P\text{-}31}$ = 1.6 ppm; $\Delta\delta$ = 94.6) (Hartmann et al., 1994; Pourpoint et al., 2007), monetite ($CaHPO_4$; $\delta_{P\text{-}31}$ = −1.0 ppm; $\Delta\delta < -26.5$) (Rothwell et al., 1980), and hydroxylapatite ($Ca_5(PO4)_3(OH)$; $\delta_{P\text{-}31}$ = 2.7 ppm; $\Delta\delta$ = −26.5) (Pourpoint et al., 2007; Rothwell et al., 1980) exhibit significant sideband pattern and large $\Delta\delta$ values of CSA, as listed in Table 3.4. Phosphate occluded in speleothem calcite from Christmas Island (Australia) gives $\Delta\delta$ = +21.9 of peak $\delta_{P\text{-}31}$ = 3.1 ppm (Kubista, 2011). Hartmann et al. (1994) reported a series of 31P tensor values for mono-protonated orthophosphates, of which $\Delta\delta$ values range from +77 to +107 ppm (Hartmann et al., 1994). He also indicates that Haubenreisser find $\Delta\delta$ values ranging from −60 to −15 ppm for non-protonated phosphates. It is possible that the mixture of unprotonated and protonated phosphates can contribute to a moderate CSA $\Delta\delta$ similar to that for the phosphate in the moonmilk. However, protonation would result in a more negative chemical shifts as indicated by Hartmann et al. (1994). As listed in Table 3.4, non-protonated phosphate groups in tetracalcium phosphate ($Ca_4P_2O_9$) exhibit positive chemical shifts $\delta_{P\text{-}31}$ at 4.0, 5.8, 7.7, and 11.9 ppm, which gives mostly negative CSA values $\Delta\delta$ = −45, −26, +15, and −38, respectively (Pourpoint et al., 2007). Turner et al. (1986) correlated $\Delta\delta$ value with angular distortion of phosphate tetrahedron. Therefore, structural distortion may be involved in the phosphate groups, which gives a moderate CSA value of phosphate in moonmilk samples.

Peak in CP spectra indicates it corresponds to P in close proximity of H. It is possible that signal of unprotonated phosphate can be accommodated by other H-bearing species such as structural H_2O, which was detected in calcite/phosphate coprecipitates (Mason et al., 2007). CP signal requires rigid H species to enable the dipolar coupling. ^{31}P direct excitation NMR, would be helpful to determine protonation of P by revealing all P species regardless of protonation, is not feasible in this study since the P content in moonmilk samples are present at insufficiently low concentration.

Both ^{31}P and ^{13}C CP/MAS NMR spectra confirm the presence of organic matter in moonmilk calcite. ^{31}P resonance with significantly large CSA ($\Delta\delta$ = 113 ppm for CZ-2) at low chemical shifts (near −2 ppm for both CZ-3 and CZ-12) would be expected to be attributed to organic phosphates, since both the value of δ_{iso} and $\Delta\delta$ fall in the range of that for occluded organic P (δ_{iso}: −2.7 to 2.0 ppm; $|\Delta\delta|$: 105 to 178 ppm) as described in Chapter 2. Although the $\Delta\delta$ of the peak near −2 ppm cannot be measured in the spectrum of CZ-12 due to the large uncertainty, an alternative method proposed in Chapter 2 would be helpful to determine the nature of P corresponding to this peak. In Chapter 2, only ^{31}P NMR spectra of calcite/organophosphate coprecipitates exhibit strong SSB manifold in which the intensity of one of the first SSBs is comparable to that of the center band, in clear contrasts to calcite/inorganic P coprecipitate. Detailed analysis on CZ-12 spectrum shows that the relative intensity of the first SSBs are 1.0% and 6.6% for SSB+1 and SSB−1, while the corresponding peak is present 7.3%, comparable to that of SSB−1. ^{31}P spectrum of CZ-3 shows a similar result that the central band and SSB−1 give 7.3% and 6.9%, respectively. Therefore, it is reasonable to ascribe the peaks near −2 ppm to the organic phosphate for both CZ-3 and CZ-12. ^{13}C CP spectra for CZ-3 and CZ-12 display substantial resonances from carbon-bearing groups other than calcite carbonate group, suggesting that only a small fraction of the organic material is organic P. Comparing with reported spectral data, $\delta_{C\text{-}13}$ resonances occurred in moonmilk CP spectra with chemical shifts near 187 ppm, 168 ppm, 46 ppm, and 30 ppm, that can be attributed to carboxyl carbon (C=O), carbonate carbon (CO_3^{2-}), and two different aliphatic carbons, respectively (Chefetz and Xing, 2009; Mathers et al., 2000; Papenguth et al., 1989). The occurrence of a CP peak for carbonate indicates that these carbonate groups are near H. Similar results have previously been observed for calcite coprecipitates with organic molecule (Phillips et al., 2005; Ueyama et al., 1998), but also for synthetic calcite, which was attributed to a small amount of hydrogen carbonate (Feng et al., 2008). The relative peak intensity ascribed to organic ^{13}C for CZ-3 (94.3 %) is somewhat higher than for CZ-12 (84.5%), which suggest a higher concentration of organic molecules and complies with the ^{31}P CP data that CZ-3 has a higher portion of P present as organic phosphate than CZ-12 in terms of P content. ^{13}C CP indicates these moonmilk samples are abundant in organic matter. The dominance of carboxyl and aliphatic carbon in the organic molecules suggest presence mainly of fatty acids, which have been shown to effectively adsorb to calcite surface (Damle et al., 2002; Osman and Suter, 2002), providing a mechanism for incorporation as the crystals grow.

3.4.2 Absence of monetite in moonmilk calcite

Notable in the ^{31}P CP spectrum is the absence of a peak for monetite ($CaHPO_4$, $\delta_{P\text{-}31}$ = −0.9 ppm) in moonmilk samples. A peak for monetite ($\delta_{P\text{-}31}$ = −0.9 ppm) occurs in the ^{31}P CP/MAS of calcite bearing inorganic phosphorus including speleothem calcite and calcite synthesized in the presence of inorganic orthophosphate (Kubista, 2011; Mason et al., 2007). Monetite is a widely recognized as a typical mineral in cave systems. It appears that the absence of monetite in moonmilk differentiates moonmilk calcite from other inorganic phosphorus bearing calcite, suggesting different conditions for moonmilk formation while incorporating phosphate in the crystalline structure. Interestingly, monetite has not been reported in biogenic calcite. One possible exception is the calcite formed from aged lobster gastroliths (Reeder et al., 2013), which was originally composed of hydrated amorphous calcium carbonate (ACC) containing high concentration of phosphate. Calcite and trace amount of monetite were found in the gastroliths which were aged for several days after removal from lobster. In this case, gastrolith ACC partially crystallized to form calcite as well as vaterite; while monetite crystallized from inorganic phosphates (e.g. possibly amorphous calcium phosphate) in the aged lobster gastrolith.

Monetite ($CaHPO_4$) and brushite ($CaHPO_4 \cdot 2H_2O$) are usually formed by the interaction of guano with calcite in caves (Frost and Palmer, 2011; Frost et al., 2013). Guano provides phosphate ions, while the calcium ions originate from the dissolution of calcite at a low pH. It has been found that high concentrations of Ca^{2+} favor brushite formation (Frost and Palmer, 2011). In laboratory studies, monetite and brushite can be synthesized by dissolving powdered natural calcium carbonate minerals (e.g. marine shell aragonite, calcite) in phosphoric acid at certain conditions (Macha et al., 2013; Tamasan et al., 2013). Study of dicalcium phosphate cements (e.g. brushite, monetite ceramics) shows many organic compounds such as carboxylic acids and carboxylates function as retardants (Tamimi et al., 2012).

Clearly, organic compounds can affect phosphorus speciation in moonmilk, considering the absence of monetite. Phosphorus in moonmilk calcite in this study is mainly inorganic and appears similar to the P content reported by Mason et al. (2007) in speleothem calcite (e.g. stalagmite) and calcite synthesized with inorganic orthophosphate. The synthetic calcite samples made by Mason et al. (2007) closely resembled stalagmite calcite in terms of P speciation and were synthesized using a seeded constant-addition method in the presence of inorganic orthophosphate, reproducing the P environment in speleothem in a chemically simple system (Mason et al., 2011).

The absence of monetite indicates a lack of dicalcium phosphate (DCP) during moonmilk formation. It appears the organic compounds prohibit DCP formation perhaps by binding aqueous Ca^{2+} to form complexes or by adsorbing on calcite surfaces to prevent surface dissolution. Organic compounds adsorbed on calcite surface may inhibit calcite growth by blocking kink sites, leaving Ca^{2+} ions to accumulate in the vicinity of calcite surface. According

to the ^{31}P NMR, the P content in moonmilk is mainly inorganic orthophosphate, which indicates presence of aqueous phosphate during calcite growth. Deficiency of DCP indicates Ca^{2+} is insufficient during moonmilk precipitation.

3.4.3 Evidence of moonmilk deposition

XRD and NMR spectra display similar spectroscopic characteristics for both moonmilk samples: purely calcitic and bearing similar impurity in composition (e.g. abundant organic content, minor inorganic phosphate, and trace amount of organic phosphate), indicating similar environment for moonmilk deposition. These moonmilk samples were collected from active stalactites in different zones (dark and twilight) in Cave Coel Zel à, suggesting consistent conditions in the cave for moonmilk precipitating. NMR spectral data for CZ-3 and CZ-12 show only slightly difference in peak intensity for ^{31}P and ^{13}C NMR.

A concept was proposed by Portillo et al. and Sanchez-Moral et al. to understand the formation of moonmilk (Portillo and Gonzalez, 2011; Sanchez-Moral et al., 2012). They suggested a combination of microbial and chemical processes leading to the formation of consolidated moonmilk speleothems. Microbial activity is required to originate the moonmilk precipitation. Progressive accumulation of carbonate leads to an entrapment of bacteria in the minerals, which inhibits microbial metabolism. Slower metabolism rate in CZ-3 sampling site means a longer period for the initial stage to precipitate moonmilk, likewise moonmilk CZ-12 form Microorganisms served as nucleation sites are enclosed in the calcite deposits, which generated a condition that favor carbonate crystal deposition. Speleothem growth can continue abiotically in the absence of further participation, or with minimal contribution of microbial activity. Therefore, organic content incorporates into crystal structures as moonmilk is deposited with minimal influence of microbial activity, which explains the abundance of organic matter in the active moonmilk speleothem. Another theory based on the ecological observation suggests these thick moonmilk depositions act as filters that accumulate the organic matter from the drip water (Papi and Pipan, 2011), therefore organic compounds are mainly from the soil covering the cave. In this scenario, a chemical analysis of drip water and soil leach would be valuable complements. This study contributes to the understanding of the effects of biotic and abiotic process on the deposition of moonmilk speleothem formation in cave.

3.5 Conclusion

Solid-state NMR techniques have proved to be a powerful tool in characterizing organic phosphates in carbonate mineral particular in low phosphorus concentrations. ^{31}P CP/MAS and ^{13}C CP/MAS reveal that rich organic content, minor inorganic phosphate, and trace amount of organophosphate present in the moonmilk calcite as structural defects. Most significantly, even though the phosphorus speciation in moonmilk closely resembles stalagmite calcite, monetite is absent in moonmilk due to the Ca^{2+} deficiency caused by organic compounds. Rich content of structural impurities demonstrate the potential of moonmilk speleothem as an environmental

proxy. The results of this study show that ^{31}P NMR spectroscopy can distinguish inorganic and organophosphate occluded in calcite. However, this is likely to be possible only on the absence of monetite. The ^{31}P NMR peak of monetite overlaps signal from organophosphate, and could effectively obscure the signal in materials such as speleothem calcite that typically contain monetite inclusions.

3.6 Figures

Figure 3.1 Entrance of Cave Coel Zel àhidden at the base of a high limestone cliff. (Photos courtesy of Dr. Andrea Borsato)

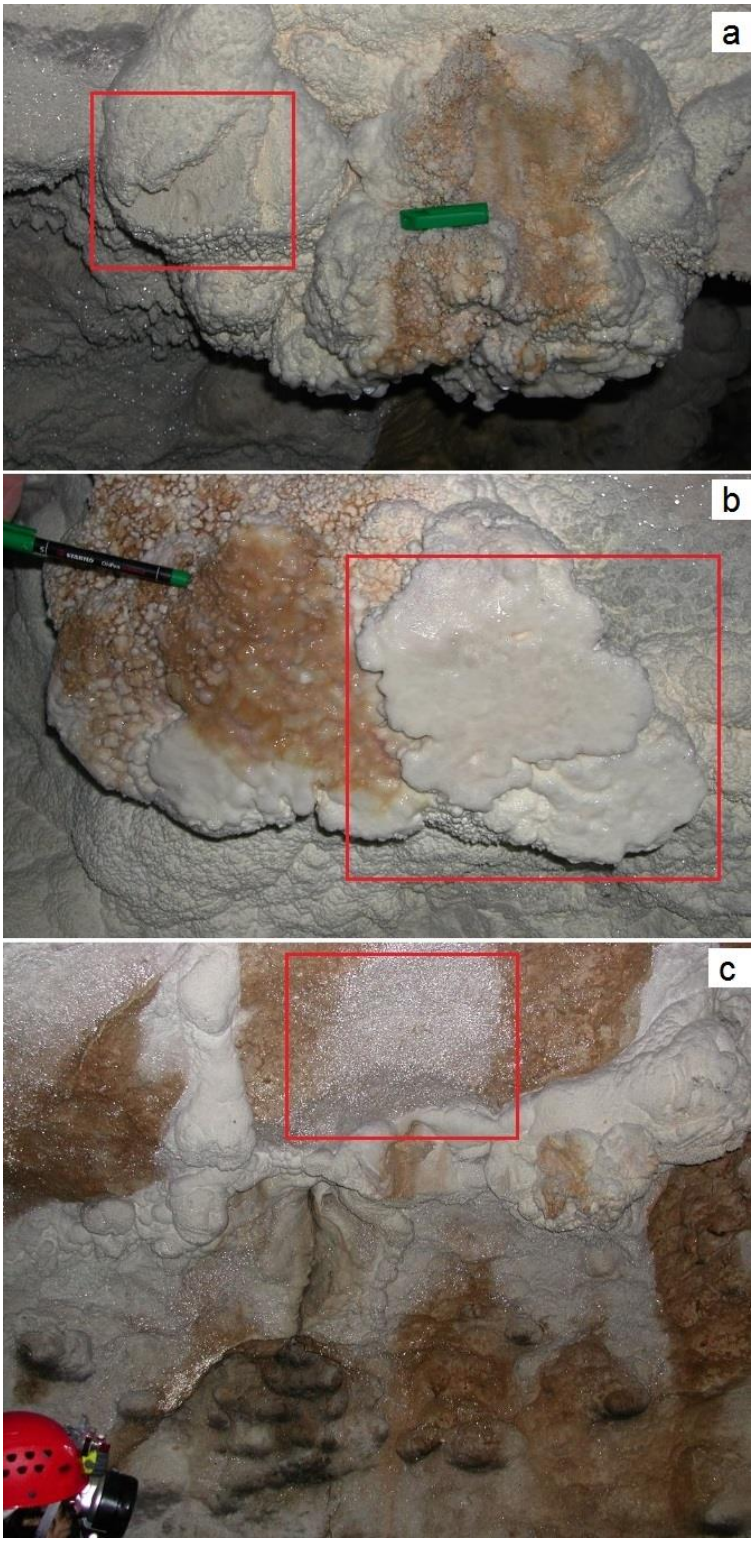

Figure 3.2 a) & b) show large active moonmilk stalagmite. c) clearly shows the condensation water droplets on the rock wall of fossil moonmilk draperies. (Photos courtesy of Dr. Andrea Borsato)

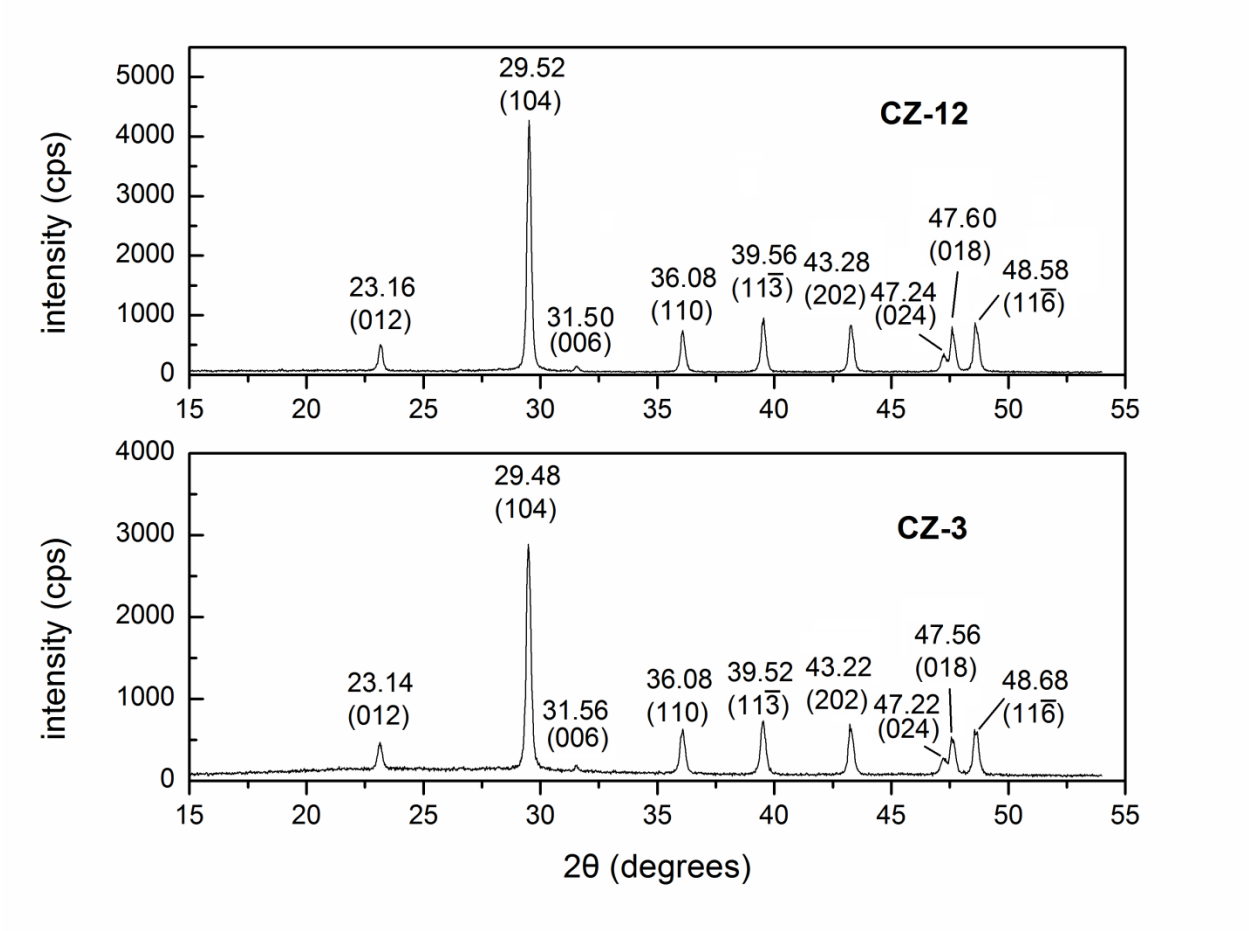

Figure 3.3 X-ray diffraction (XRD) patterns of moonmilk samples CZ-3 and CZ-12. These patterns are almost identical, and both are in a good agreement to those of pure calcite (Gunasekaran and Anbalagan, 2007; Rahman and Oomori, 2009), indicating that only calcite in the moonmilk. Reported calcite reflections are listed under their corresponding peak positions.

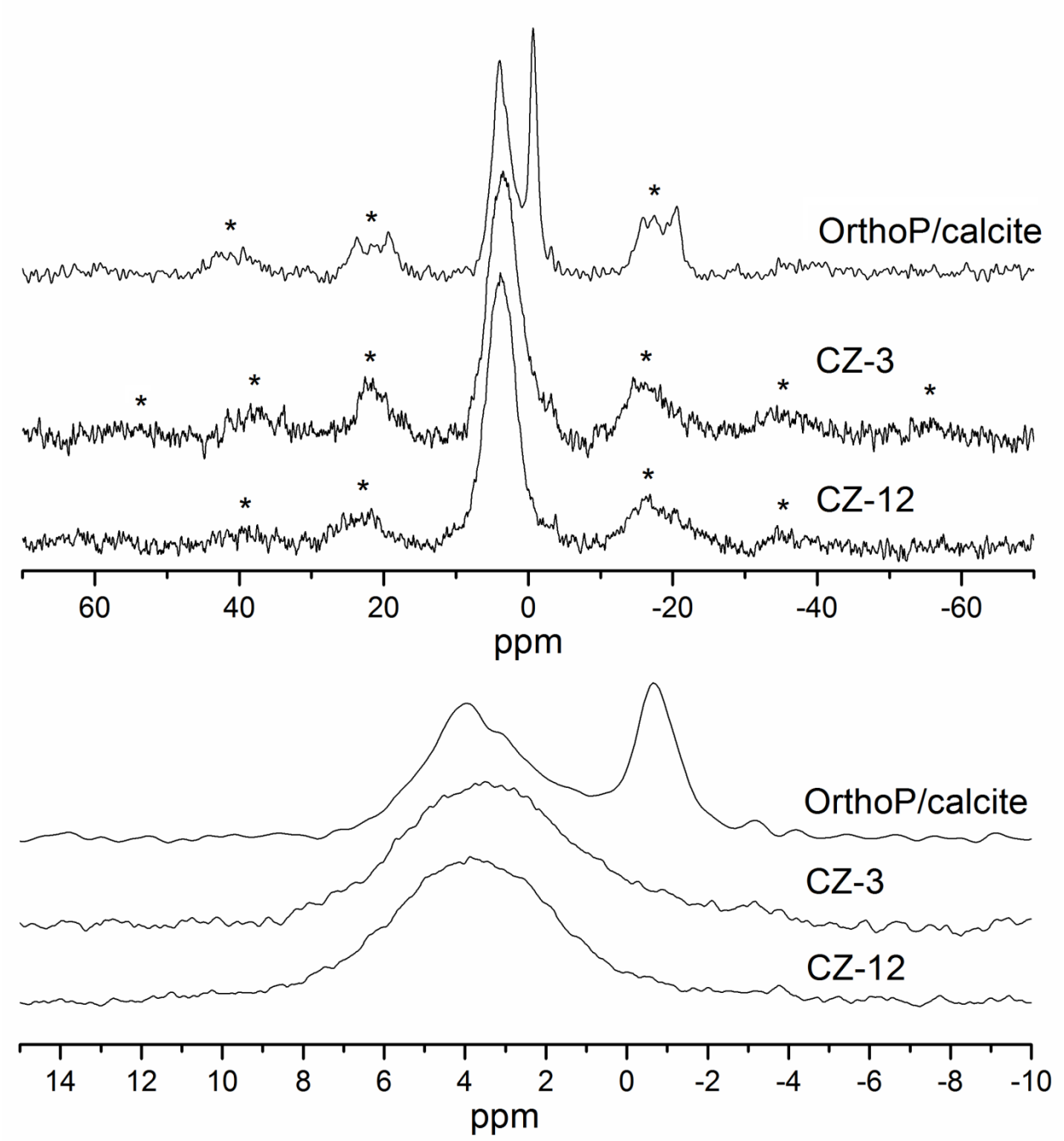

Figure 3.4 $^{31}P\{^{1}H\}$ CP/MAS NMR spectra for a calcite coprecipitate with inorganic orthophosphate (OrthoP/calcite), and bleached moonmilk samples CZ-3 and CZ-12. Spectra were collected at 3kHz spinning rate. Spectra of CZ-3 and CZ-12 represent 637,190 and 403,557 acquisitions, respectively. Asterisks denote spinning sidebands.

Top: full spectrum. Bottom: expanded view of the center band region.

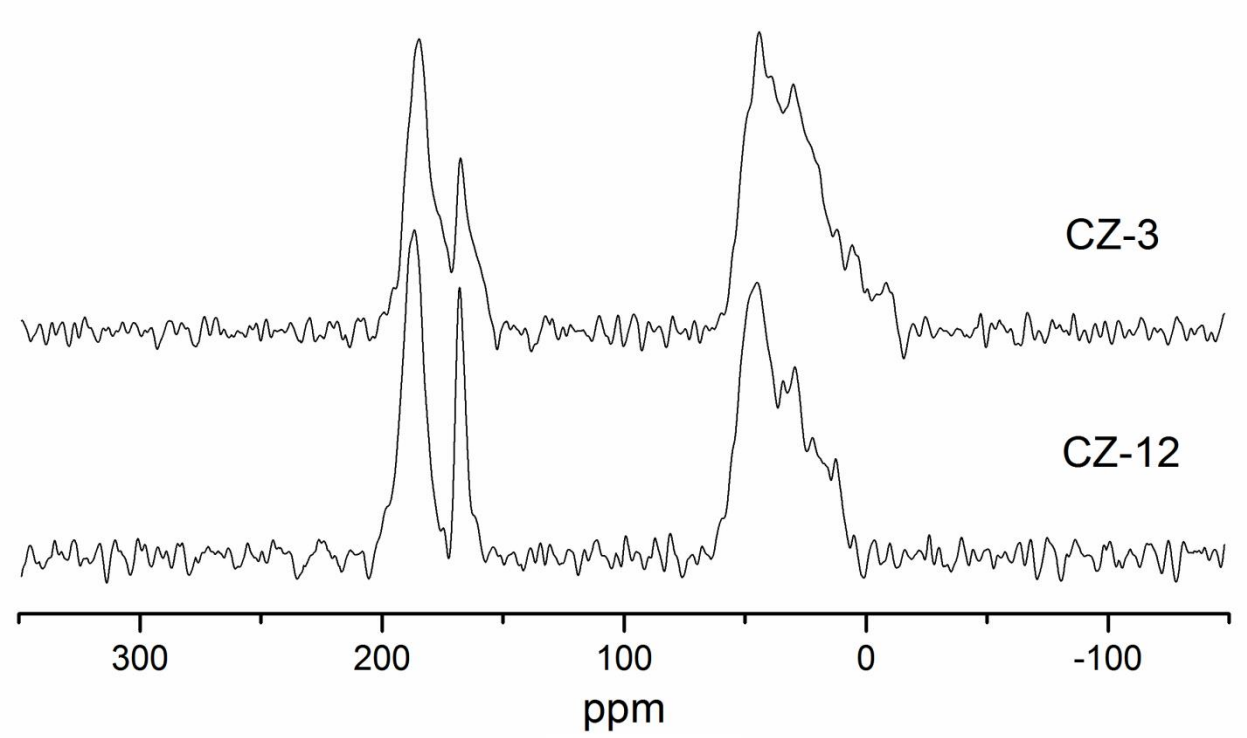

Figure 3.5 $^{13}C\{^{1}H\}$CP/MAS NMR spectra for bleached moonmilk samples CZ-3 and CZ-12 at 3 kHz spinning rate. Spectrum of CZ-3 was collected with 2 s relaxation delay and 1 ms contact time, while spectrum of CZ-12 was collected with 1 s relaxation delay and 2 ms contact time. Spectra of CZ-3 and CZ-12 represent 163,058 and 66,746 acquisitions, respectively.

3.7 Tables

Table 3.1 Composition of drip water that feed moonmilk veils and draperies. (Data provided by Dr. Andrea Borsato)

pH	Ca ($mg \cdot L^{-1}$)	Mg ($mg \cdot L^{-1}$)	NO_3 ($mg \cdot L^{-1}$)	dissolved P ($\mu g \cdot L^{-1}$)	Total P ($\mu g \cdot L^{-1}$)
7.5 – 8.0	40 – 50	0.80 – 1.0	0.8 – 2.0	1.5 – 2	2 – 5

Table 3.2 $^{31}P\{^{1}H\}$CP/MAS NMR spectral characteristics of moonmilk samples including relative band intensity in percentage (%) for SSBs and central bands, isotropic chemical shift and line width (FWHM), and value of chemical shift tensors (e.g. D11, D22, D33) and chemical shift isotropy (Δδ). "R.I." denotes the relative peak intensity in percentage, which is converted from relative band intensity. In addition, relative intensity of first SSBs are also listed for comparision. Uncertanties are given as the last digit.

[a]RI of all bands represents the relative intensity of a single band (e.g. SSB, centerband) in the corresponding spectrum. [b]RI represents the relative intensity among centerband in the corresponding spectrum. [c]Assign represents the peak assignment either inorganic orthophosphate or organic phosphate.

*Values of chemical shift tensor are omitted for peak at −2.1 ppm of CZ-12, since the corresponding SSBs yield insufficient intensities which contribute to a large uncertainty.

	[a]RI of all bands (%)							Isotropic peaks				Chemical shift tensor				Fraction of each peak set
	SSB +3	SSB +2	SSB +1	Central	SSB −1	SSB −2	SSB −3	δ_{iso} (ppm)	FWHM (ppm)	[b]RI (%)	[c]Assign	D11	D22	D33	Δδ	(%)
CZ-3	1.6	3.5	9.6	48.9	8.2	2.4	0.8	+3.45(5)	5.3 (3)	87	Ortho	29.3	4.96	−23.9	−41(3)	75(5)
	0.9	2.2	1.0	7.3	6.9	4.1	2.6	−2.0(2)	6.4 (5)	13	Organic	73.5	−22.3	−57.2	+113(5)	25(5)
CZ-12		1.1	5.9	59.0	9.4	3.5		+3.45(5)	5.0 (3)	89	Ortho	28.9	−9.30	−9.30	−38(3)	79(5)
		2.7	2.0	7.4	6.6	2.4		−2.1(2)	5.7 (4)	11	Organic	*	*	*	*	21(5)

Table 3.3 $^{13}C\{^{1}H\}$CP/MAS NMR spectral characteristics of moonmilk samples. Intensity represents the relative intensity for each peak in percentage (%).

CZ-3			Assignment	CZ-12		
δ_{iso} (ppm)	FWHM	Intensity		δ_{iso} (ppm)	FWHM	Intensity
187.1	12.9	28.8	Organic	187.1	9.4	38.7
167.9	7.0	5.7	Calcite	167.7	4.0	15.5
46.9	17.6	42.7	Organic	46.2	13.2	37.4
29.4	17.1	22.7	Organic	30.7	7.3	8.4

Table 3.4 ^{31}P chemical shift tensor of typical model compounds.

[a]Speleothem sample was collected from Christmas Island (Australia), which contains high phosphorus content. [b]HAp represents Hydroxylapatite.

*Chemical shift tensor for monetite were not measured, but Rothwell et al (1980) suggested that chemical shift anisotropy of monetite is considerably larger than that of HAp considering the stronger SSB pattern exhibited by 31P NMR of Monetite.

Sample	Formula	δ_{P-31} (ppm)	D11	D22	D33	Δδ	Reference
Brushite	$CaHPO_4 \cdot 2H_2O$	+1.6	−54.2	−5.6	64.7	+94.6	(Hartmann et al., 1994; Pourpoint et al., 2007)
Monetite	$CaHPO_4$	−1.0	*	*	*	<−26.5	(Rothwell et al., 1980)
[b]HAp	$Ca_5(PO4)_3(OH)$	+2.7	19	4	-15	−26.5	(Pourpoint et al., 2007; Rothwell et al., 1980)
Tetracalcium phosphate	$Ca_4P_2O_9$	+4.0	27.7	9.9	−25.8	−45	(Pourpoint et al., 2007)
		+5.8	22.3	6.8	−11.6	−26	
		+7.7	17.7	4.1	1.1	+15	
		+11.9	36.4	12.6	−13.4	−38	
[a]Speleothem	PO_4 defect	+3.1	17.0	−3.44	−3.76	+21.9	(Kubista, 2011)
CZ-3		+3.45	29.3	4.96	−23.9	−41	
CZ-12		+3.45	28.9	−9.30	−9.30	−38	

3.9 Reference

Angert, E.R., Northup, D.E., Reysenbach, A.L., Peek, A.S., Goebel, B.M. and Pace, N.R. (1998) Molecular phylogenetic analysis of a bacterial community in Sulphur River, Parker Cave, Kentucky. *Am. Miner.* **83**(11-12), 1583-1592.

Barton, H.A. and Northup, D.E. (2007) Geomicrobiology in cave environments: Past, current and future perspectives. *J. Cave Karst Stud.* **69**(1), 163-178.

Barton, H.A., Spear, J.R. and Pace, N.R. (2001) Microbial life in the underworld: Biogenicity in secondary mineral formations. *Geomicrobiol. J.* **18**(3), 359-368.

Baskar, S., Baskar, R. and Routh, J. (2011) Biogenic evidences of moonmilk deposition in the Mawmluh Cave, Meghalaya, India. *Geomicrobiol. J.* **28**(3), 252-265.

Blyth, A.J. and Frisia, S. (2008) Molecular evidence for bacterial mediation of calcite formation in cold high-altitude caves. *Geomicrobiol. J.* **25**(2), 101-111.

Borsato, A. (1997) Late-glacial to Holocene biogenic moonmilk and calcareous tufa deposits from caves in Trentino (NE-Italy): environment of precipitation and paleoclimatic significance. **9**(2), 8.

Borsato, A., Frisia, S., Jones, B., Van der Borg, K., Space, Space and Space (2000) Calcite moonmilk: Crystal morphology and environment of formation in caves in the Italian Alps. *J. Sediment. Res.* **70**(5), 1171-1182.

Braissant, O., Bindschedler, S., Daniels, A.U., Verrecchia, E.P. and Cailleau, G. (2012) Microbiological activities in moonmilk monitored using isothermal microcalorimetry (cave of Vers chez le Brandt, Neuchatel, Switzerland). *J. Cave Karst Stud.* **74**(1), 116-126.

Cacchio, P., Contento, R., Ercole, C., Cappuccio, G., Martinez, M.P. and Lepidi, A. (2004) Involvement of microorganisms in the formation of carbonate speleothems in the Cervo Cave (L'Aquila-Italy). *Geomicrobiol. J.* **21**(8), 497-509.

Cacchio, P., Ercole, C., Cappuccio, G. and Lepidi, A. (2003) Calcium carbonate precipitation by bacterial strains isolated from a limestone cave and from a loamy soil. *Geomicrobiol. J.* **20**(2), 85-98.

Cade-Menun, B.J. (2005) Characterizing phosphorus in environmental and agricultural samples by P-31 nuclear magnetic resonance spectroscopy. *Talanta* **66**(2), 359-371.

Canaveras, J.C., Cuezva, S., Sanchez-Moral, S., Lario, J., Laiz, L., Gonzalez, J.M. and Saiz-Jimenez, C. (2006) On the origin of fiber calcite crystals in moonmilk deposits. *Naturwissenschaften* **93**(1), 27-32.

Chalmin, E., Perrette, Y., Fanget, B. and Susini, J. (2013) Investigation of Organic Matter Entrapped in Synthetic Carbonates-A Multimethod Approach. *Microsc. microanal.* **19**(1), 132-144.

Chefetz, B. and Xing, B.S. (2009) Relative Role of Aliphatic and Aromatic Moieties as Sorption Domains for Organic Compounds: A Review. *Environ. Sci. Technol.* **43**(6), 1680-1688.

Damle, C., Kumar, A., Sainkar, S.R., Bhagawat, M. and Sastry, M. (2002) Growth of calcium carbonate crystals within fatty acid bilayer stacks. *Langmuir* **18**(16), 6075-6080.

Feng, J., Lee, Y.J., Kubicki, J.D., Reeder, R.J. and Phillips, B.L. (2008) NMR spectroscopy of citrate in solids: cross-polarization kinetics in weakly coupled systems. *Magn. Reson. Chem.* **46**(5), 408-417.

Frisia, S., Borsato, A., Fairchild, I.J. and McDermott, F. (2000) Calcite fabrics, growth mechanisms, and environments of formation in speleothems from the Italian Alps and southwestern Ireland. *J. Sediment. Res.* **70**(5), 1183-1196.

Frost, R.L. and Palmer, S.J. (2011) Thermal stability of the 'cave' mineral brushite CaHPO4 center dot 2H(2)O - Mechanism of formation and decomposition. *Thermochim. Acta* **521**(1-2), 14-17.

Frost, R.L., Xi, Y.F., Millar, G., Tan, K.Q. and Palmer, S.J. (2013) Vibrational Spectroscopy of Natural Cave Mineral Monetite CaHPO4 and the Synthetic Analog. *Spectr. Lett.* **46**(1), 54-59.

Geffroy, C., Foissy, A., Persello, J. and Cabane, B. (1999) Surface complexation of calcite by carboxylates in water. *J. Colloid. Interf. Sci.* **211**(1), 45-53.

Gunasekaran, S. and Anbalagan, G. (2007) Spectroscopic characterization of natural calcite minerals. *Spectroc. Acta. A.* **68**(3), 656-664.

Hartmann, P., Vogel, J. and Schnabel, B. (1994) The Influence of Short-Range Geometry on the ^{31}P Chemical-Shift Tensor in Protonated Phosphates. *J. Magn. Reson. Ser. A* **111**(1), 110-114.

Hill, C.A. and Forti, P. (1997) *Cave minerals of the world*. National Speleological Society, Huntsville, Ala.

Kubista, L.M. (2011) Solid-State NMR Spectroscopy Investigation of Phosphorus Incorporation In Calcium Carbonate. 1500598 M.S.State University of New York at Stony Brook, Ann Arbor.

Kuczumow, A., Genty, D., Chevallier, P., Nowak, J., Florek, M. and Buczynska, A. (2005) X-ray and electron microprobe investigation of the speleothems from Godarville tunnel. *X-Ray Spectrom.* **34**(6), 502-508.

Macha, I.J., Ozyegin, L.S., Chou, J., Samur, R., Oktar, F.N. and Ben-Nissan, B. (2013) An Alternative Synthesis Method for Di Calcium Phosphate (Monetite) Powders from Mediterranean Mussel (Mytilus galloprovincialis) Shells. *J. Aust. Ceram. Soc.* **49**(2), 122-128.

Mason, H.E., Frisia, S., Tang, Y., Reeder, R.J. and Phillips, B.L. (2007) Phosphorus speciation in calcite speleothems determined from solid-state NMR spectroscopy. *Earth Planet. Sci. Lett.* **254**(3-4), 313-322.

Mason, H.E., Hausner, D., Frisia, S., Tang, Y., Reeder, R.J., Strongin, D.R. and Phillips, B.L. (2006) Phosphorus distribution in calcite speleothems from solid-state NMR and AFM. *Geochim. Cosmochim. Acta* **70**(18), A399-A399.

Mason, H.E., Montagna, P., Kubista, L., Taviani, M., McCulloch, M. and Phillips, B.L. (2011) Phosphate defects and apatite inclusions in coral skeletal aragonite revealed by solid-state NMR spectroscopy. **75**(23), 7446-7457.

Mathers, N.J., Mao, X.A., Xu, Z.H., Saffigna, P.G., Berners-Price, S.J. and Perera, M.C.S. (2000) Recent advances in the application of C-13 and N-15 NMR spectroscopy to soil organic matter studies. *Aust. J. Soil Res.* **38**(4), 769-787.

Montes-Hernandez, G., Sarret, G., Hellmann, R., Menguy, N., Testemale, D., Charlet, L. and Renard, F. (2011) Nanostructured calcite precipitated under hydrothermal conditions in the presence of organic and inorganic selenium. *Chem. Geol.* **290**(3-4), 109-120.

Mulec, J., Zalar, P., Hajna, N.Z. and Rupnik, M. (2002) *Screening for culturable microorganisms from cave environments (Slovenia)*. Slovenska akademija znanosti in umetnosti.

Northup, D.E. and Lavoie, K.H. (2001) Geomicrobiology of caves: A review. *Geomicrobiol. J.* **18**(3), 199-222.

Osman, M.A. and Suter, U.W. (2002) Surface treatment of calcite with fatty acids: Structure and properties of the organic monolayer. *Chem. Mat.* **14**(10), 4408-4415.

Papenguth, H.W., Kirkpatrick, R.J., Montez, B. and Sandberg, P.A. (1989) C-13 MAS NMR-spectroscopy of inorganic and biogenic carbonates. *Am. Miner.* **74**(9-10), 1152-1158.

Papi, F. and Pipan, T. (2011) Ecological studies of an epikarst community in Snežna jama na planini Arto – an ice cave in north central Slovenia. *Acta Carsologica.* **40**(3), 505-513.

Phillips, B.L., Lee, Y.J. and Reeder, R.J. (2005) Organic coprecipitates with calcite: NMR spectroscopic evidence. *Environ. Sci. Technol.* **39**(12), 4533-4539.

Portillo, M.C. and Gonzalez, J.M. (2011) Moonmilk Deposits Originate from Specific Bacterial Communities in Altamira Cave (Spain). *Microb. Ecol.* **61**(1), 182-189.

Pourpoint, F., Gervais, C., Bonhomme-Coury, L., Azais, T., Coelho, C., Mauri, F., Alonso, B., Babonneau, F. and Bonhomme, C. (2007) Calcium phosphates and hydroxyapatite: Solid-state NMR experiments and first-principles calculations. *Appl. Magn. Reson.* **32**(4), 435-457.

Rahman, M.A. and Oomori, T. (2009) In Vitro Regulation of CaCO3 Crystal Growth by the Highly Acidic Proteins of Calcitic Sclerites in Soft Coral, Sinularia Polydactyla. *Connect. Tissue Res.* **50**(5), 285-293.

Reddy, M.M. (1977) Crystallization of calcium carbonate in the presence of trace concentrations of phosphorus-containing anions: I. Inhibition by phosphate and glycerophosphate ions at pH 8.8 and 25 ℃. *J. Cryst. Growth* **41**(2), 287-295.

Reeder, R.J., Tang, Y., Schmidt, M.P., Kubista, L.M., Cowan, D.F. and Phillips, B.L. (2013) Characterization of Structure in Biogenic Amorphous Calcium Carbonate: Pair Distribution Function and Nuclear Magnetic Resonance Studies of Lobster Gastrolith. *Cryst. Growth. Des.* **13**(5), 1905-1914.

Rooney, D.C., Hutchens, E., Clipson, N., Baldini, J. and McDermott, F. (2010) Microbial Community Diversity of Moonmilk Deposits at Ballynamintra Cave, Co. Waterford, Ireland. *Microb. Ecol.* **60**(4), 753-761.

Rothwell, W.P., Waugh, J.S. and Yesinowski, J.P. (1980) High-resolution variable-temperature ^{31}P NMR of solid calcium phosphates. *J. Am. Chem. Soc.* **102**(8), 2637-2643.

Sanchez-Moral, S., Portillo, M.C., Janices, I., Cuezva, S., Fernandez-Cortes, A., Canaveras, J.C. and Gonzalez, J.M. (2012) The role of microorganisms in the formation of calcitic moonmilk deposits and speleothems in Altamira Cave. *Geomorphology* **139**(285-292.

Tamasan, M., Ozyegin, L.S., Oktar, F.N. and Simon, V. (2013) Characterization of calcium phosphate powders originating from Phyllacanthus imperialis and Trochidae Infundibulum concavus marine shells. *Mater. Sci. Eng. C Mater. Biol. Appl.* **33**(5), 2569-2577.

Tamimi, F., Sheikh, Z. and Barralet, J. (2012) Dicalcium phosphate cements: Brushite and monetite. *Acta Biomater.* **8**(2), 474-487.

Turner, G.L., Smith, K.A., Kirkpatrick, R.J. and Oldfield, E. (1986) Structure and cation effects on phosphorus-31 NMR chemical shifts and chemical-shift anisotropies of orthophosphates. *J. Magn. Reson.* **70**(3), 408-415.

Ueyama, N., Hosoi, T., Yamada, Y., Doi, M., Okamura, T.-a. and Nakamura, A. (1998) Calcium Complexes of Carboxylate-Containing Polyamide with Sterically Disposed NH ··O Hydrogen Bond: Detection of the

Polyamide in Calcium Carbonate by ^{13}C Cross-Polarization/Magic Angle Spinning Spectra. *Macromolecules* **31**(21), 7119-7126.
Westheimer, F.H. (1987) Why nature chose phosphates. *Science* **235**(4793), 1173-1178.

Bibliography

Abdel-Aal, N. and Sawada, K. (2003) Inhibition of adhesion and precipitation of CaCO3 by aminopolyphosphonate. *J. Cryst. Growth* **256**(1-2), 188-200.

Akiva-Tal, A., Kababya, S., Balazs, Y.S., Glazer, L., Berman, A., Sagi, A. and Schmidt, A. (2011) In situ molecular NMR picture of bioavailable calcium stabilized as amorphous CaCO3 biomineral in crayfish gastroliths. *Proc. Natl. Acad. Sci. U. S. A.* **108**(36), 14763-14768.

Al-Thawadi, S.M. (2011) Ureolytic bacteria and calcium carbonate formation as a mechanism of strength enhancement of sand. *J. Adv. Sci. Eng. Res.* **1**(1), 98-114.

Amjad, Z. (1987) Kinetic study of the seeded growth of calcium carbonate in the presence of benzenepolycarboxylic acids. *Langmuir* **3**(2), 224-228.

Amrhein, C. and Suarez, D.L. (1987) Calcite supersaturation in soils as a result of organic matter mineralization. *Soil. Sci. Soc. Am. J.* **51**(4), 932-937.

Angert, E.R., Northup, D.E., Reysenbach, A.L., Peek, A.S., Goebel, B.M. and Pace, N.R. (1998) Molecular phylogenetic analysis of a bacterial community in Sulphur River, Parker Cave, Kentucky. *Am. Miner.* **83**(11-12), 1583-1592.

Astilleros, J.M., Pina, C.M., Fernández-Díaz, L. and Putnis, A. (2000) The effect of barium on calcite {1014} surfaces during growth. *Geochim. Cosmochim. Ac.* **64**(17), 2965-2972.

Baldini, J.U.L., McDermott, F. and Fairchild, I.J. (2007) Structure of the 8200-year cold event revealed by a speleothem trace element record (Retraction of vol 296, pg 2203, 2002). *Science* **317**(5839), 748-748.

Banfield, J.F., Javiera, C.-S. and H., N.K. (2005) *Molecular geomicrobiology*. Mineralogical Society of America, Geochemical Society, Chantilly, Va.

Banfield, J.F. and Nealson, K.H. (1997) *Geomicrobiology interactions between microbes and minerals*. Mineralogical Society of America, Washington, D.C.

Barkouki, T., Martinez, B., Mortensen, B., Weathers, T., De Jong, J., Ginn, T., Spycher, N., Smith, R. and Fujita, Y. (2011) Forward and inverse bio-geochemical modeling of microbially induced calcite precipitation in half-meter column experiments. *Transport. Porous Med.* **90**(1), 23-39.

Barton, H.A. and Northup, D.E. (2007) Geomicrobiology in cave environments: Past, current and future perspectives. *J. Cave Karst Stud.* **69**(1), 163-178.

Barton, H.A., Spear, J.R. and Pace, N.R. (2001) Microbial life in the underworld: Biogenicity in secondary mineral formations. *Geomicrobiol. J.* **18**(3), 359-368.

Baskar, S., Baskar, R. and Routh, J. (2011) Biogenic evidences of moonmilk deposition in the Mawmluh Cave, Meghalaya, India. *Geomicrobiol. J.* **28**(3), 252-265.

Becker, A., Ziegler, A. and Epple, M. (2005) The mineral phase in the cuticles of two species of Crustacea consists of magnesium calcite, amorphous calcium carbonate, and amorphous calcium phosphate. *Dalton Trans.*10), 1814-1820.

Benitez-Nelson, C.R. (2000) The biogeochemical cycling of phosphorus in marine systems. *Earth-Sci. Rev.* **51**(1-4), 109-135.

Blyth, A.J., Baker, A., Collins, M.J., Penkman, K.E., Gilmour, M.A., Moss, J.S., Genty, D. and Drysdale, R.N. (2008) Molecular organic matter in speleothems and its potential as an environmental proxy. *Quaternary Sci. Rev.* **27**(9), 905-921.

Blyth, A.J. and Frisia, S. (2008) Molecular evidence for bacterial mediation of calcite formation in cold high-altitude caves. *Geomicrobiol. J.* **25**(2), 101-111.

Borsato, A. (1997) Late-glacial to Holocene biogenic moonmilk and calcareous tufa deposits from caves in Trentino (NE-Italy): environment of precipitation and paleoclimatic significance. **9**(2), 8.

Borsato, A., Frisia, S., Fairchild, I.J., Somogyi, A. and Susini, J. (2007) Trace element distribution in annual stalagmite laminae mapped by micrometer-resolution X-ray fluorescence: Implications for incorporation of environmentally significant species. *Geochim. Cosmochim. Ac.* **71**(6), 1494-1512.

Borsato, A., Frisia, S., Jones, B. and Van der Borg, K. (2000) Calcite moonmilk: Crystal morphology and environment of formation in caves in the Italian Alps. *J. Sediment. Res.* **70**(5), 1171-1182.

Braissant, O., Bindschedler, S., Daniels, A.U., Verrecchia, E.P. and Cailleau, G. (2012) Microbiological activities in moonmilk monitored using isothermal microcalorimetry (cave of Vers chez le Brandt, Neuchatel, Switzerland). *J. Cave Karst Stud.* **74**(1), 116-126.

Cacchio, P., Contento, R., Ercole, C., Cappuccio, G., Martinez, M.P. and Lepidi, A. (2004) Involvement of microorganisms in the formation of carbonate speleothems in the Cervo Cave (L'Aquila-Italy). *Geomicrobiol. J.* **21**(8), 497-509.

Cacchio, P., Ercole, C., Cappuccio, G. and Lepidi, A. (2003) Calcium carbonate precipitation by bacterial strains isolated from a limestone cave and from a loamy soil. *Geomicrobiol. J.* **20**(2), 85-98.

Cade-Menun, B.J. (2005) Characterizing phosphorus in environmental and agricultural samples by P-31 nuclear magnetic resonance spectroscopy. *Talanta* **66**(2), 359-371.

Canaveras, J.C., Cuezva, S., Sanchez-Moral, S., Lario, J., Laiz, L., Gonzalez, J.M. and Saiz-Jimenez, C. (2006) On the origin of fiber calcite crystals in moonmilk deposits. *Naturwissenschaften* **93**(1), 27-32.

Celi, L., Lamacchia, S. and Barberis, E. (2000) Interaction of inositol phosphate with calcite. *Nutr. Cycl. Agroecosys.* **57**(3), 271-277.

Celi, L., Lamacchia, S., Marsan, F.A. and Barberis, E. (1999) Interaction of inositol hexaphosphate on clays: Adsorption and charging phenomena. *Soil. Sci.* **164**(8), 574-585.

Chalmin, E., Perrette, Y., Fanget, B. and Susini, J. (2013) Investigation of Organic Matter Entrapped in Synthetic Carbonates-A Multimethod Approach. *Microsc. microanal.* **19**(1), 132-144.

Chefetz, B. and Xing, B.S. (2009) Relative Role of Aliphatic and Aromatic Moieties as Sorption Domains for Organic Compounds: A Review. *Environ. Sci. Technol.* **43**(6), 1680-1688.

Chou, C.-W., Seagren, E.A., Aydilek, A.H. and Lai, M. (2011) Biocalcification of sand through ureolysis. *J. Geotech. Geoenviron.* **137**(12), 1179-1189.

Collin, R.L. (1966) The Electronic Structure of Phosphate Esters. *J. Am. Chem. Soc.* **88**(14), 3281-3287.

Correll, D.L. (1998) The role of phosphorus in the eutrophication of receiving waters: A review. *J. Environ. Qual.* **27**(2), 261-266.

Cotmore, J.M., Nichols, G. and Wurthier, R.E. (1971) Phospholipid—calcium phosphate complex: enhanced calcium migration in the presence of phosphate. *Science* **172**(3990), 1339-&.

Cross, A.F. and Schlesinger, W.H. (1995) A literature review and evaluation of the. Hedley fractionation: Applications to the biogeochemical cycle of soil phosphorus in natural ecosystems. **64**(3-4), 197-214.

Curti, E. (1999) Coprecipitation of radionuclides with calcite: estimation of partition coefficients based on a review of laboratory investigations and geochemical data. *Appl. Geochem.* **14**(4), 433-445.

Damle, C., Kumar, A., Sainkar, S.R., Bhagawat, M. and Sastry, M. (2002) Growth of calcium carbonate crystals within fatty acid bilayer stacks. *Langmuir* **18**(16), 6075-6080.

Davis, K.J., Dove, P.M., Wasylenki, L.E. and De Yoreo, J.J. (2004) Morphological consequences of differential Mg2+ incorporation at structurally distinct steps on calcite. *Am. Mineral.* **89**(5-6), 714-720.

De Reggi, M., Gharib, B., Patard, L. and Stoven, V. (1998) Lithostathine, the presumed pancreatic stone inhibitor, does not interact specifically with calcium carbonate crystals. *J. Biol. Chem.* **273**(9), 4967-4971.

de Vicente, I., Cattaneo, K., Cruz-Pizarro, L., Brauer, A. and Guilizzoni, P. (2006) Sedimentary phosphate fractions related to calcite precipitation in an eutrophic hardwater lake (Lake Alserio, northern Italy). *J. Paleolimnol.* **35**(1), 55-64.

Degroot, C.J. and Golterman, H.L. (1993) On the presence of organic phosphate in some Camargue sediments: evidence for the importance of phytate. *Hydrobiologia* **252**(1), 117-126.

DeJong, J.T., Fritzges, M.B. and Nüsslein, K. (2006) Microbially induced cementation to control sand response to undrained shear. *J. Geotech. Geoenviron.* **132**(11), 1381-1392.

DeJong, J.T., Mortensen, B.M., Martinez, B.C. and Nelson, D.C. (2010) Bio-mediated soil improvement. *Ecol. Eng.* **36**(2), 197-210.

Dekanel, J. and Morse, J.W. (1978) The chemistry of orthophosphate uptake from seawater on to calcite and aragonite. *Geochim. Cosmochim. Ac.* **42**(9), 1335-1340.

Didymus, J.M., Oliver, P., Mann, S., Devries, A.L., Hauschka, P.V. and Westbroek, P. (1993) Influence of low-molecular-weight and macromolecular organic additives on the morphology of calcium carbonate. *J. Chem. Soc.-Faraday Trans.* **89**(15), 2891-2900.

Dove, P., Yoreo, J.J.D. and Weiner, S. (2003) *Biomineralization*. Mineralogical Society of America, Washington, DC.

Dove, P.M.D.Y.J.W.S.M.S.o.A. (2003) *Biomineralization*. Mineralogical Society of America, Washington, DC.

Fairchild, I.J., Baker, A., Borsato, A., Frisia, S., Hinton, R.W., McDermott, F. and Tooth, A.F. (2001) Annual to sub-annual resolution of multiple trace-element trends in speleothems. *J. Geol. Soc. London* **158**(831-841.

Fairchild, I.J., Smith, C.L., Baker, A., Fuller, L., Spötl, C., Mattey, D. and McDermott, F. (2006) Modification and preservation of environmental signals in speleothems. *Earth-Sci. Rev.* **75**(1), 105-153.

Fairchild, I.J. and Treble, P.C. (2009) Trace elements in speleothems as recorders of environmental change. *Quaternary Sci. Rev.* **28**(5-6), 449-468.

Feng, J., Lee, Y.J., Kubicki, J.D., Reeder, R.J. and Phillips, B.L. (2008) NMR spectroscopy of citrate in solids: cross-polarization kinetics in weakly coupled systems. *Magn. Reson. Chem.* **46**(5), 408-417.

Fenter, P., Geissbühler, P., DiMasi, E., Srajer, G., Sorensen, L.B. and Sturchio, N.C. (2000) Surface speciation of calcite observed in situ by high-resolution X-ray reflectivity. *Geochim. Cosmochim. Ac.* **64**(7), 1221-1228.

Filippelli, G.M. (2011) Phosphate rock formation and marine phosphorus geochemistry: The deep time perspective. *Chemosphere* **84**(6), 759-766.

Follmi, K.B. (1996) The phosphorus cycle, phosphogenesis and marine phosphate-rich deposits. *Earth-Sci. Rev.* **40**(1-2), 55-124.

Freeman, J.S. and Rowell, D.L. (1981) The adsorption and precipitation of phosphate onto calcite. *J. Soil Sci.* **32**(1), 75-84.

Frisia, S., Borsato, A., Drysdale, R.N., Paul, B., Greig, A. and Cotte, M. (2012) A re-evaluation of the palaeoclimatic significance of phosphorus variability in speleothems revealed by high-resolution synchrotron micro XRF mapping. *Clim. Past.* **8**(6), 2039-2051.

Frisia, S., Borsato, A., Fairchild, I.J. and McDermott, F. (2000) Calcite fabrics, growth mechanisms, and environments of formation in speleothems from the Italian Alps and southwestern Ireland. *J. Sediment. Res.* **70**(5), 1183-1196.

Frost, R.L. and Palmer, S.J. (2011) Thermal stability of the 'cave' mineral brushite CaHPO4 center dot 2H(2)O - Mechanism of formation and decomposition. *Thermochim. Acta* **521**(1-2), 14-17.

Frost, R.L., Xi, Y.F., Millar, G., Tan, K.Q. and Palmer, S.J. (2013) Vibrational Spectroscopy of Natural Cave Mineral Monetite CaHPO4 and the Synthetic Analog. *Spectr. Lett.* **46**(1), 54-59.

Fujita, Y., Redden, G.D., Ingram, J.C., Cortez, M.M., Ferris, F.G. and Smith, R.W. (2004) Strontium incorporation into calcite generated by bacterial ureolysis. *Geochim. Cosmochim. Ac.* **68**(15), 3261-3270.

Furrer, G. and Stumm, W. (1986) The Coordination of Weathering .1.Dissolution Kinectics of delta-Al2O3 and BeO. *Geochim. Cosmochim. Ac.* **50**(9), 1847-1860.

Garcia-Anton, E., Cuezva, S., Fernandez-Cortes, A., Cuevas-Gonzalez, J., Munoz-Cervera, M.C., Benavente, D., Sanchez-Moral, S. and Canaveras, J.C. (2011) Mineral-Variations Study of Canelobre Cave Phosphate Stalactites by Raman and Luminescence Methods. *Spectr. Lett.* **44**(7-8), 539-542.

Geffroy, C., Foissy, A., Persello, J. and Cabane, B. (1999) Surface complexation of calcite by carboxylates in water. *J. Colloid. Interf. Sci.* **211**(1), 45-53.

Gertman, R., Ben Shir, I., Kababya, S. and Schmidt, A. (2008) In situ observation of the internal structure and composition of biomineralized Emiliania huxleyi calcite by solid-state NMR spectroscopy. *J. Am. Chem. Soc.* **130**(40), 13425-13432.

Giannimaras, E.K. and Koutsoukos, P.G. (1987) The crystallization of calcite in the precence of orthophosphate. *J. Colloid. Interf. Sci.* **116**(2), 423-430.

Godelitsas, A., Astilleros, J.M., Hallam, K., Harissopoulos, S. and Putnis, A. (2003) Interaction of Calcium Carbonates with Lead in Aqueous Solutions. *Environ. Sci. Technol.* **37**(15), 3351-3360.

Griffin, R.A. and Jurinak, J.J. (1974) Kinetics of the Phosphate Interaction with Calcite. *Soil Sci. Soc. Am. J.* **38**(1), 75-79.

Griffin, R.G. (1976) Observation of the effect of water on the phosphorus-31 nuclear magnetic resonance spectra of dipalmitoyllecithin. *J. Am. Chem. Soc.* **98**(3), 851-853.

Gröger, C., Lutz, K. and Brunner, E. (2009) NMR studies of biomineralisation. *Prog. Nucl. Mag. Res. Sp.* **54**(1), 54-68.

Gullion, T. and Schaefer, J. (1989) Rotational-echo double-resonance NMR. *J. Magn. Reson.* **81**(1), 196-200.

Gunasekaran, S. and Anbalagan, G. (2007) Spectroscopic characterization of natural calcite minerals. *Spectroc. Acta. A.* **68**(3), 656-664.

Gunawan, E.K., Warmadewanthi and Liu, J.C. (2010) Removal of phosphate and fluoride from optoelectronic wastewater by calcite. *Int. J. Environ. Tech. Manag.* **12**(2-4), 308-321.

Harris, R.K., Becker, E.D., Cabral de Menezes, S.M., Goodfellow, R. and Granger, P. (2002) NMR nomenclature: nuclear spin properties and conventions for chemical shifts. IUPAC Recommendations 2001. International Union of Pure and Applied Chemistry. Physical Chemistry Division. Commission on Molecular Structure and Spectroscopy. *Magn. Reson. Chem.* **40**(7), 489-505.

Hartmann, P., Vogel, J. and Schnabel, B. (1994) The Influence of Short-Range Geometry on the ^{31}P Chemical-Shift Tensor in Protonated Phosphates. *J. Magn. Reson. Ser. A* **111**(1), 110-114.

Henriksen, K., Stipp, S.L.S., Young, J.R. and Marsh, M.E. (2004) Biological control on calcite crystallization: AFM investigation of coccolith polysaccharide function. *Am. Mineral.* **89**(11-12), 1709-1716.

Herzfeld, J. and Berger, A.E. (1980) Sideband intensities in NMR spectra of samples spinning at the magic angle. *J. Chem. Phys.* **73**(6021.

Hill, C.A. and Forti, P. (1997) *Cave minerals of the world*. National Speleological Society, Huntsville, Ala.

Hinedi, Z.R., Goldberg, S., Chang, A.C. and Yesinowski, J.P. (1992) A ^{31}P and ^{1}H MAS NMR study of phosphate sorption onto calcium carbonate. *J. Colloid. Interf. Sci.* **152**(1), 141-160.

Hoch, A.R., Reddy, M.M. and Aiken, G.R. (2000) Calcite crystal growth inhibition by humic substances with emphasis on hydrophobic acids from the Florida Everglades. *Geochim. Cosmochim. Ac.* **64**(1), 61-72.

House, W.A. and Donaldson, L. (1986) Adsorption and coprecipitation of phosphate on calcite. *J. Colloid. Interf. Sci.* **112**(2), 309-324.

Huang, Y., Fairchild, I.J., Borsato, A., Frisia, S., Cassidy, N.J., McDermott, F. and Hawkesworth, C.J. (2001) Seasonal variations in Sr, Mg and P in modern speleothems (Grotta di Ernesto, Italy). *Chem. Geol.* **175**(3), 429-448.

Iuga, A., Ader, C., Gr öger, C. and Brunner, E. (2006) Applications of solid-state ^{31}P NMR spectroscopy, in: Webb, G.A. (Ed.), *Annu. Rep. NMR Spectrosc.* Academic Press, pp. 145-189.

Kamiya, M., Hatta, J., Shimada, E., Ikuma, Y., Yoshimura, M. and Monma, H. (2004) AFM analysis of initial stage of reaction between calcite and phosphate. *Mat. Sci. Eng. B-solid.* **111**(2-3), 226-231.

Karageorgiou, K., Paschalis, M. and Anastassakis, G.N. (2007) Removal of phosphate species from solution by adsorption onto calcite used as natural adsorbent. *J. Hazard. Mater.* **139**(3), 447-452.

Keeler, J. (2010) *Understanding NMR spectroscopy*. John Wiley and Sons, Chichester, U.K.

Khasawneh, F.E., Sample, E. and Kamprath, E. (1980) *The role of phosphorus in agriculture*. American Society of Agronomy, Crop Science Society of America, Soil Science Society of America.

Kitano, Y. and Hood, D.W. (1965) The influence of organic material on the polymorphic crystallization of calcium carbonate. *Geochim. Cosmochim. Ac.* **29**(1), 29-41.

Klein, C., Hurlbut, C.S. and Dana, J.D. (1993) *Manual of mineralogy*. Wiley New York.

Kolodziejski, W. (2005) Solid-state NMR studies of bone, in: Klinowski, J. (Ed.), *New Techniques in Solid-State Nmr*. Springer-Verlag Berlin, Berlin, pp. 235-270.

Kolodziejski, W. and Klinowski, J. (2002) Kinetics of cross-polarization in solid-state NMR: A guide for chemists. *Chem. Rev.* **102**(3), 613-628.

Kubista, L.M. (2011) Solid-State NMR Spectroscopy Investigation of Phosphorus Incorporation In Calcium Carbonate. 1500598 M.S.State University of New York at Stony Brook, Ann Arbor.

Kuczumow, A., Genty, D., Chevallier, P., Nowak, J., Florek, M. and Buczynska, A. (2005) X-ray and electron microprobe investigation of the speleothems from Godarville tunnel. *X-Ray Spectrom.* **34**(6), 502-508.

Lee, A.P., Klinowski, J. and Marseglia, E.A. (1995) Application of nuclear magnetic resonance spectroscopy to bone diagenesis. *J. Archaeol. Sci.* **22**(2), 257-262.

Levitt, M.H. (2001) *Spin dynamics : basics of nuclear magnetic resonance*. John Wiley & Sons, Chichester; New York.

Lin, Y.P., Singer, P.C. and Aiken, G.R. (2005) Inhibition of calcite precipitation by natural organic material: Kinetics, mechanism, and thermodynamics. *Environ. Sci. Technol.* **39**(17), 6420-6428.

Liu, Y., Sheng, X., Dong, Y.H. and Ma, Y.J. (2012) Removal of high-concentration phosphate by calcite: Effect of sulfate and pH. *Desalination* **289**(66-71.

Lowenstam, H.A. and Weiner, S. (1989) *On biomineralization*. Oxford University Press.

Macha, I.J., Ozyegin, L.S., Chou, J., Samur, R., Oktar, F.N. and Ben-Nissan, B. (2013) An Alternative Synthesis Method for Di Calcium Phosphate (Monetite) Powders from Mediterranean Mussel (Mytilus galloprovincialis) Shells. *J. Aust. Ceram. Soc.* **49**(2), 122-128.

Mason, H.E., Frisia, S., Tang, Y., Reeder, R.J. and Phillips, B.L. (2007) Phosphorus speciation in calcite speleothems determined from solid-state NMR spectroscopy. *Earth. Planet. Sc. Lett.* **254**(3), 313-322.

Mason, H.E., Hausner, D., Frisia, S., Tang, Y., Reeder, R.J., Strongin, D.R. and Phillips, B.L. (2006) Phosphorus distribution in calcite speleothems from solid-state NMR and AFM. *Geochim. Cosmochim. Ac.* **70**(18), A399-A399.

Mason, H.E., Montagna, P., Kubista, L., Taviani, M., McCulloch, M. and Phillips, B.L. (2011) Phosphate defects and apatite inclusions in coral skeletal aragonite revealed by solid-state NMR spectroscopy. *Geochim. Cosmochim. Acta* **75**(23), 7446-7457.

Mathers, N.J., Mao, X.A., Xu, Z.H., Saffigna, P.G., Berners-Price, S.J. and Perera, M.C.S. (2000) Recent advances in the application of C-13 and N-15 NMR spectroscopy to soil organic matter studies. *Aust. J. Soil Res.* **38**(4), 769-787.

Matsuya, S., Udoh, K., Nakagawa, M. and Ishikawa, K. (2006) Preparation of carbonate apatite monolith by treatment of the set gypsum containing calcite in trisodium phosphate solution, in: Nakamura, T., Yamashita, K., Neo, M. (Eds.), *Bioceramics 18, Pts 1 and 2*, pp. 125-128.

Meldrum, F.C. and Hyde, S.T. (2001) Morphological influence of magnesium and organic additives on the precipitation of calcite. *J. Cryst. Growth* **231**(4), 544-558.

Merkel, C., Deuschle, J., Griesshaber, E., Enders, S., Steinhauser, E., Hochleitner, R., Brand, U. and Schmahl, W.W. (2009) Mechanical properties of modern calcite- (Mergerlia truncata) and phosphate-shelled brachiopods (Discradisca stella and Lingula anatina) determined by nanoindentation. *J. Struct. Biol.* **168**(3), 396-408.

Meyer, H. (1984) The influence of impurities on the growth rate of calcite. *J. Cryst. Growth* **66**(3), 639-646.

Mirtchi, A.A., Lemaitre, J. and Munting, E. (1990) Calcium phosphate cements: study of the β-tricalcium phosphate - dicalcium phosphate - calcite cements. *Biomaterials* **11**(2), 83-88.

Mirtchi, A.A., Lemaitre, J. and Munting, E. (1991) Calcium phosphate cements: effect of fluorides on the setting and hardening of beta-tricalcium phosphate-dicalcium phosphate-calcite cements. *Biomaterials* **12**(5), 505-510.

Monchau, F., Hivart, P., Genestie, B., Chai, F., Descamps, M. and Hildebrand, H.F. (2013) Calcite as a bone substitute. Comparison with hydroxyapatite and tricalcium phosphate with regard to the osteoblastic activity. *Mater. Sci. Eng. C. Mater. Biol. Appl.* **33**(1), 490-498.

Montes-Hernandez, G., Sarret, G., Hellmann, R., Menguy, N., Testemale, D., Charlet, L. and Renard, F. (2011) Nanostructured calcite precipitated under hydrothermal conditions in the presence of organic and inorganic selenium. *Chem. Geol.* **290**(3-4), 109-120.

Mortensen, B., Haber, M., DeJong, J., Caslake, L. and Nelson, D. (2011) Effects of environmental factors on microbial induced calcium carbonate precipitation. *J. Appl. Microbiol.* **111**(2), 338-349.

Mulec, J., Zalar, P., Hajna, N.Z. and Rupnik, M. (2002) *Screening for culturable microorganisms from cave environments (Slovenia)*. Slovenska akademija znanosti in umetnosti.

Murphy, T., Hall, K. and Northcote, T. (1988) Lime treatment of a hardwater lake to reduce eutrophication. *Lake. Reserv. Manage.* **4**(2), 51-62.

Northup, D.E. and Lavoie, K.H. (2001) Geomicrobiology of caves: A review. *Geomicrobiol. J.* **18**(3), 199-222.

Orme, C.A., Noy, A., Wierzbicki, A., McBride, M.T., Grantham, M., Teng, H.H., Dove, P.M. and DeYoreo, J.J. (2001) Formation of chiral morphologies through selective binding of amino acids to calcite surface steps. **411**(6839), 775-779.

Osman, M.A. and Suter, U.W. (2002) Surface treatment of calcite with fatty acids: Structure and properties of the organic monolayer. *Chem. Mat.* **14**(10), 4408-4415.

Otsuki, A. and Wetzel, R.G. (1972) Coprecipitation of phosphate with carbonates in a marl-lake. *Limnol. Oceanogr.* **17**(5), 763-767.

Papenguth, H.W., Kirkpatrick, R.J., Montez, B. and Sandberg, P.A. (1989) C-13 MAS NMR-spectroscopy of inorganic and biogenic carbonates. *Am. Miner.* **74**(9-10), 1152-1158.

Papi, F. and Pipan, T. (2011) Ecological studies of an epikarst community in Snežna jama na planini Arto – an ice cave in north central Slovenia. *Acta Carsologica* **40**(3), 505-513.

Pettersson, K. (2001) Phosphorus characteristics of settling and suspended particles in Lake Erken. *Sci. Total. Environ.* **266**(1–3), 79-86.

Phillips, B.L., Lee, Y.J. and Reeder, R.J. (2005) Organic coprecipitates with calcite: NMR spectroscopic evidence. *Environ. Sci. Technol.* **39**(12), 4533-4539.

Pingitore, N.E. and Eastman, M.P. (1986) The coprecipitation of Sr2+ with calcite at 25 ℃ and 1 atm. *Geochim. Cosmochim. Ac.* **50**(10), 2195-2203.

Plant, L.J. and House, W.A. (2002) Precipitation of calcite in the presence of inorganic phosphate. *Colloid. Surface. A.* **203**(1–3), 143-153.

Pogson, R.E., Osborne, R.A.L., Colchester, D.M. and Cendon, D.I. (2011) Sulfate and phosphate speleothem at Jenolan caves, New South Wales, Australia. *Acta Carsologica* **40**(2), 239-254.

Portillo, M.C. and Gonzalez, J.M. (2011) Moonmilk Deposits Originate from Specific Bacterial Communities in Altamira Cave (Spain). *Microb. Ecol.* **61**(1), 182-189.

Pourpoint, F., Gervais, C., Bonhomme-Coury, L., Azais, T., Coelho, C., Mauri, F., Alonso, B., Babonneau, F. and Bonhomme, C. (2007) Calcium phosphates and hydroxyapatite: Solid-state NMR experiments and first-principles calculations. *Appl. Magn. Reson.* **32**(4), 435-457.

Rahman, M.A. and Oomori, T. (2009) In Vitro Regulation of CaCO3 Crystal Growth by the Highly Acidic Proteins of Calcitic Sclerites in Soft Coral, Sinularia Polydactyla. *Connect. Tissue Res.* **50**(5), 285-293.

Reddy, M. and Nancollas, G. (1973) Calcite crystal growth inhibition by phosphonates. *Desalination* **12**(1), 61-73.

Reddy, M.M. (1977) Crystallization of calcium carbonate in the presence of trace concentrations of phosphorus-containing anions: I. Inhibition by phosphate and glycerophosphate ions at pH 8.8 and 25 ℃. *J. Cryst. Growth* **41**(2), 287-295.

Reddy, M.M. and Hoch, A.R. (2001) Calcite Crystal Growth Rate Inhibition by Polycarboxylic Acids. *J. Colloid. Interf. Sci.* **235**(2), 365-370.

Reeder, R.J., Nugent, M., Lamble, G.M., Tait, C.D. and Morris, D.E. (2000) Uranyl incorporation into calcite and aragonite: XAFS and luminescence studies. *Environ. Sci. Technol.* **34**(4), 638-644.

Reeder, R.J., Tang, Y., Schmidt, M.P., Kubista, L.M., Cowan, D.F. and Phillips, B.L. (2013) Characterization of Structure in Biogenic Amorphous Calcium Carbonate: Pair Distribution Function and Nuclear Magnetic Resonance Studies of Lobster Gastrolith. *Cryst. Growth. Des.* **13**(5), 1905-1914.

Rong, H., Qian, C. and Wang, R. (2011) A cementation method of loose particles based on microbe-based cement. *Sci. China Ser. E.* **54**(7), 1722-1729.

Rooney, D.C., Hutchens, E., Clipson, N., Baldini, J. and McDermott, F. (2010) Microbial Community Diversity of Moonmilk Deposits at Ballynamintra Cave, Co. Waterford, Ireland. *Microb. Ecol.* **60**(4), 753-761.

Rothwell, W.P., Waugh, J.S. and Yesinowski, J.P. (1980) High-resolution variable-temperature ^{31}P NMR of solid calcium phosphates. *J. Am. Chem. Soc.* **102**(8), 2637-2643.

Ruiz-Agudo, E., Di Tommaso, D., Putnis, C.V., de Leeuw, N.H. and Putnis, A. (2010) Interactions between Organophosphonate-Bearing Solutions and (10(1)over-bar4) Calcite Surfaces: An Atomic Force Microscopy and First-Principles Molecular Dynamics Study. *Cryst. Growth. Des.* **10**(7), 3022-3035.

Ruiz-Agudo, E., Putnis, C.V., Rodriguez-Navarro, C. and Putnis, A. (2011) Effect of pH on calcite growth at constant ratio and supersaturation. *Geochim. Cosmochim. Ac.* **75**(1), 284-296.

Sanchez-Moral, S., Portillo, M.C., Janices, I., Cuezva, S., Fernandez-Cortes, A., Canaveras, J.C. and Gonzalez, J.M. (2012) The role of microorganisms in the formation of calcitic moonmilk deposits and speleothems in Altamira Cave. *Geomorphology* **139**(285-292.

Sawada, K., Abdel-Aal, N., Sekino, H. and Satoh, K. (2003) Adsorption of inorganic phosphates and organic polyphosphonate on calcite. *Dalton Trans.*3), 342-347.

Schiller, J. and Arnold, K. (2002) Application of high resolution ^{31}P NMR spectroscopy to the characterization of the phospholipid composition of tissues and body fluids - a methodological review. *Med. Sci. Monitor* **8**(11), 205-222.

Schmahl, W.W., Griesshaber, E., Kelm, K., Goetz, A., Jordan, G., Ball, A., Xu, D.Y., Merkel, C. and Brand, U. (2012) Hierarchical structure of marine shell biomaterials: biomechanical functionalization of calcite by brachiopods. *Z. Kristall.* **227**(11), 793-804.

Sethmann, I., Putnis, A., Grassmann, O. and Lobmann, P. (2005) Observation of nano-clustered calcite growth via a transient phase mediated by organic polyanions: A close match for biomineralization. *Am. Mineral.* **90**(7), 1213-1217.

Shaojun, Z. and Mucci, A. (1993) Calcite precipitation in seawater using a constant addition technique: A new overall reaction kinetic expression. *Geochim. Cosmochim. Ac.* **57**(7), 1409-1417.

Smil, V. (2000) Phosphorus in the environment: Natural flows and human interferences. *Annu. Rev. Energy. Environ.* **25**(53-88.

So, H.U., Postma, D., Jakobsen, R. and Larsen, F. (2011) Sorption of phosphate onto calcite; results from batch experiments and surface complexation modeling. *Geochim. Cosmochim. Ac.* **75**(10), 2911-2923.

So, H.U., Postma, D., Jakobsen, R. and Larsen, F. (2012) Competitive adsorption of arsenate and phosphate onto calcite; experimental results and modeling with CCM and CD-MUSIC. *Geochim. Cosmochim. Ac.* **93**(1-13.

Song, Y.H., Weidler, P.G., Berg, U., Nuesch, R. and Donnert, D. (2006) Calcite-seeded crystallization of calcium phosphate for phosphorus recovery. *Chemosphere* **63**(2), 236-243.

Suzuki, T., Inomata, S. and Sawada, K. (1986) Adsorption of phosphate on calcite. *J. Chem. Soc. Faraday T. 1* **82**(1733-1743.

Tamasan, M., Ozyegin, L.S., Oktar, F.N. and Simon, V. (2013) Characterization of calcium phosphate powders originating from Phyllacanthus imperialis and Trochidae Infundibulum concavus marine shells. *Mater. Sci. Eng. C Mater. Biol. Appl.* **33**(5), 2569-2577.

Tamimi, F., Sheikh, Z. and Barralet, J. (2012) Dicalcium phosphate cements: Brushite and monetite. *Acta Biomater.* **8**(2), 474-487.

Tas, A.C. (2007) Porous, biphasic CaCO3-calcium phosphate biomedical cement scaffolds from calcite (CaCO3) powder. *Int. J. Appl. Ceram. Tec.* **4**(2), 152-163.

Tas, A.C. (2008) Use of vaterite and calcite in forming calcium phosphate cement scaffolds, in: Brito, M., Case, E., Kriven, W.M. (Eds.), *Developments in Porous, Biological and Geopolymer Ceramics*, pp. 135-150.

Tesoriero, A.J. and Pankow, J.F. (1996) Solid solution partitioning of Sr2+,Ba2+, and Cd2+to calcite. *Geochim. Cosmochim. Ac.* **60**(6), 1053-1063.

Tiano, P. (1995) Stone reinforcement by calcite crystal precipitation induced by organic matrix macromolecules. *Stud. Conserv.* **40**(3), 171-176.

Treble, P.C., Chappell, J. and Shelley, J.M.G. (2005) Complex speleothem growth processes revealed by trace element mapping and scanning electron microscopy of annual layers. *Geochim. Cosmochim. Ac.* **69**(20), 4855-4863.

Tsai, T.W.T. and Chan, J.C.C. (2011) Recent Progress in the Solid-State NMR Studies of Biomineralization. *Annu. Rep. NMR Spectrosc.* **73**, 1-61.

Turner, B.L., Cade-Menun, B.J., Condron, L.M. and Newman, S. (2005) Extraction of soil organic phosphorus. *Talanta* **66**(2), 294-306.

Turner, G.L., Smith, K.A., Kirkpatrick, R.J. and Oldfield, E. (1986) Structure and cation effects on phosphorus-31 NMR chemical shifts and chemical-shift anisotropies of orthophosphates. *J. Magn. Reson.* **70**(3), 408-415.

Ueyama, N., Hosoi, T., Yamada, Y., Doi, M., Okamura, T.-a. and Nakamura, A. (1998) Calcium Complexes of Carboxylate-Containing Polyamide with Sterically Disposed NH ··O Hydrogen Bond: Detection of the Polyamide in Calcium Carbonate by ^{13}C Cross-Polarization/Magic Angle Spinning Spectra. *Macromolecules* **31**(21), 7119-7126.

van Meer, G., Voelker, D.R. and Feigenson, G.W. (2008) Membrane lipids: where they are and how they behave. *Nat. Rev. Mol. Cell Biol.* **9**(2), 112-124.

van Paassen, L.A., Ghose, R., van der Linden, T.J., van der Star, W.R. and van Loosdrecht, M.C. (2010) Quantifying biomediated ground improvement by ureolysis: large-scale biogrout experiment. *J. Geotech. Geoenviron.* **136**(12), 1721-1728.

Verrecchia, E.P. and Verrecchia, K.E. (1994) Needle-fiber calcite: a critical review and a proposed classification. *J. Sediment. Res. Sect. A-Sediment. Petrol. Process.* **64**(3), 650-664.

Wang, S.R., Jin, X.C., Zhao, H.C., Zhou, X.N. and Wu, F.C. (2007) Effect of organic matter on the sorption of dissolved organic and inorganic phosphorus in lake sediments. *Colloid. Surface. A.* **297**(1-3), 154-162.

Watson, E.B. (2004) A conceptual model for near-surface kinetic controls on the trace-element and stable isotope composition of abiogenic calcite crystals. *Geochim. Cosmochim. Ac.* **68**(7), 1473-1488.

Weiner, S. and Dove, P.M. (2003) An overview of biomineralization processes and the problem of the vital effect, in: Dove, P.M., DeYoreo, J.J., Weiner, S. (Eds.), *Biomineralization*. Mineralogical Soc America, Washington, pp. 1-29.

Westheimer, F.H. (1987) Why nature chose phosphates. *Science* **235**(4793), 1173-1178.

Whiffin, V.S., van Paassen, L.A. and Harkes, M.P. (2007) Microbial carbonate precipitation as a soil improvement technique. *Geomicrobiol. J.* **24**(5), 417-423.

Wickham, J.R. and Rice, C.V. (2008) Solid-state NMR studies of bacterial lipoteichoic acid adsorption on different surfaces. *Solid State Nucl. Magn. Reson.* **34**(3), 154-161.

Xie, S.C., Huang, J.H., Wang, H.M., Yi, Y., Hu, C.Y., Cai, Y.J. and Cheng, H. (2005) Distributions of fatty acids in a a stalagmite related to paleoclimate change at Qingjiang in Hubei, southern China. *Sci. China. Ser. D.* **48**(9), 1463-1469.

Xie, S.C., Yi, Y., Huang, J.H., Hu, C.Y., Cai, Y.J., Collins, M. and Baker, A. (2003) Lipid distribution in a subtropical southern China stalagmite as a record of soil ecosystem response to paleoclimate change. *Quaternary. Res.* **60**(3), 340-347.

Yesinowski, J.P. and Mobley, M.J. (1983) Fluorine-19 MAS-NMR of fluoridated hydroxyapatite surfaces. *J. Am. Chem. Soc.* **105**(19), 6191-6193.

Young, J.R. and Henriksen, K. (2003) Biomineralization within vesicles: The calcite of coccoliths, in: Dove, P.M., DeYoreo, J.J., Weiner, S. (Eds.), *Biomineralization*. Mineralogical Soc Amer, Chantilly, pp. 189-215.

Zachara, J., Cowan, C. and Resch, C. (1991) Sorption of divalent metals on calcite. *Geochim. Cosmochim. Ac.* **55**(6), 1549-1562.